UNIVERSITY OF TURKU

Master's thesis

Student: Nelson Nnamdi Nwaenie

Supervisor: Xiang-Guo Li, Assistant Professor, PhD

Co-supervisor: Tuomas Karskela, PhD

Chemo- and regioselective ^{18}F-labelling of peptides bearing free amino- and sulfhydryl-groups

Turku PET CENTRE

ACKNOWLEDGEMNTS

My supervisor, Xiang-Guo Li, has my deepest gratitude. As a mentor and educator, you have my deepest gratitude. From the first time we discussed the thesis to now, I am grateful for all the lessons learnt. Tuomas Karskela, my co-supervisor, thanks for being there when I needed you and paying close enough attention to detail to make sure I understood everything and could teach others what I had learnt. Some of the things I learnt in the project were a new venture for me, but you made it all easy to understand. Once again, a big thank you.

Pyry, you were my best motivator the whole time and pretty much carried this project as much as I did; therefore, I want to thank you from the bottom of my heart. This project was completed on time in large part due to your encouragement and assistance whenever required. Your contributions to this thesis are much appreciated, and I am at a loss for words.

To everyone at the Aurum Lab and Turku PET Centre: Dominika, Petter, Jonne, Jesse, Andrianna, Sami, David, Emel, Xiaoxing, and Dr. Risto. You are all amazing. Whether it was in the lab or at a conference, we had a wonderful time chatting about chemistry and life in general. Everything about the structure and our time together was fantastic.

And to my parent, sisters, and VSBSB, my family. Your kindness and support mean the world to me, for the endless love. I say a big thank you to all. My biggest fans.

This brings me to my last point, my partner Mea: You have been an incredible source of support during this long but thrilling process, and I am at a loss for words to describe how grateful I am. You made sure I didn't lose my composure and that I did everything by the book. Your affection is greatly valued.

Abstract

The radioactive prosthetic group 6-[^{18}F]fluoronicotinic acid ([^{18}F]FNA) has been conjugated with numerous biomolecules using its activated esters. All reported conjugations had resulted in *N*-acylated products, except the conjugation with peptide ACooP (H-ACGLSGLGVA-NH_2) in 2024, as reported by Dillemuth et al. ACooP is a variant of the nonapeptide CooP (H-CGLSGLGVA-NH_2), which has been seen in recent studies to be a brain tumor-homing peptide that targets fatty acid-binding protein 3 (FABP3), which is also known as a heart-type fatty acid-binding protein or a mammary-derived growth inhibitor.

Of the many challenges posed by synthetic chemistry, the achievement of both high-level chemo- and regioselectivity in various biomolecules such as proteins, peptides, and some macromolecules serves as one of the toughest challenges posed to the study. Lately, Dillemuth and coworkers synthesised radiolabelled CooP and ACooP using the prosthetic chemical [^{18}F]FNA 4-nitrophenyl ester to develop radiotracers for positron emission tomography (PET). The conjugation yielded the products [^{18}F]FNA-*N*-CooP and [^{18}F]FNA-*S*-ACooP. The disparity in acylation prompted the notion that intramolecular transfer or acyl migration transpired in CooP rather than ACooP, owing to unfavourable circumstances in the transition state of conjugation with ACooP. To verify this hypothesis, studies were conducted utilising FNA and four new peptides C@1-K (H-CGLSGLGVAK-NH_2), C@3 (H-AGCLSGLGVA-NH_2), C@4 (H-AGLCSGLGVA-NH_2), and C@5 (H-AGLSCGLGVA-NH_2).

The aim of this study was to radiosynthesize and understand the mechanism underlying the chemoselectivity and regioselectivity of the [^{18}F]FNA with the variants of the ACooP peptides, in this case four new peptides. The radiosynthesis was carried out using two of the peptides C@5 and C@1-K. In the radiosynthesis of C@5, a radiochemical purity of 98.5 % ± 1.3 (n=3) and a decay-corrected radiochemical yield of 14.4 ± 7.4% were obtained. Two syntheses were carried out for C@1-K, with an average radiochemical purity of 98.6% (n = 2) and a decay-corrected radiochemical yield of 6.4% (n = 2).

The non-radioactive products of the four peptides were analysed with liquid chromatography-mass spectroscopy (LC-MS)/MS for confirmation of the products and side products. We proceeded with characterisation and structural confirmation of the conjugated product of the four products (C@1-K, C@3, C@4, and C@5)

In the LC-MS/MS study for two of the peptides, specifically C@1-K and C@3, certain side products were identified with additional modifications at various other sites. These were also observed during high-performance liquid chromatography purification. The side products were isolated during purification; however, upon drying for nuclear magnetic resonance (NMR) analysis, they yielded minimal to nearly negligible quantities of products that did not allow accurate analysis. The NMR results after analysing the four peptides confirmed the following: C@3, C@4, and C@5 were *S-acylated,* while C@1-K was *N-acylated* at the cysteine residue. The regioselectivity was also confirmed with the NMR, with conjugation occurring at the cysteine site. Both commercial and in-house prepared FNA-*N*-C@1-K were found to be impure. Still, we found that *N*-acylation of cysteine was observed in the product, so the other part of the product that makes it impure is a question that needs investigating.

The results confirmed the hypothesis proposed. Further study would be essential to aid the synthesis of *S-acylated* tracers when needed.

Table of Contents

List of abbreviations

AEC	Anion exchange cartridge
A_m	Molar activity
FNA	6-Fluoronicotinic acid
HPLC	High performance liquid chromatography
NMR	Nuclear magnetic resonance
PET	Positron emission tomography
QC	Quality control
RCC	Radiochemical conversion
RCP	Radiochemical purity
RCY	Radiochemical yield
TFA	Trifluoroacetic acid
TOCSY	Total correlation spectroscopy
HMBC	Heteronuclear multiple bond correlation
HSQC	Heteronuclear Single Quantum Coherence
MS	Microsoft

Peptide Panels

ACooP: H-A**C**GLSGLGVA-NH_2

CooP: H-**C**GLSGLGVA-NH_2

C@3: H-AG**C**LSGLGVA-NH_2

C@4: H-AGL**C**SGLGVA-NH_2

C@5: H-AGLS**C**GLGVA-NH_2

C@1-K: H-**C**GLSGLGVAK-NH_2

1.0 INTRODUCTION

The favoured reaction of a chemical substance with two or more actively different functional groups is called "chemoselectivity".[1] Of the many challenges posed by synthetic chemistry, the achievement of both high-level chemo- and regioselectivity in various biomolecules such as proteins, peptides, and some macromolecules serves as one of the toughest posed to the study. Regardless of this daunting challenge, chemists have continually worked on developing methods, including chemical ligation practices that aid in high selectivity. [2,3]

In organic and medicinal chemistry, the formation of amide bonds through chemoselectivity is important and imperative in biology for mechanisms such as post-translational modification of proteins (PTMs).[4,5] *S- to N-acyl* migration arises as a result of the exclusive reactivity of thioesters, which makes them suitable (in some cases) for acyl transfer in the chemoselectivity process. The recent development in synthetic and biosynthetic ligation methods is due to the use of thioesters as intermediates for some complex ligation, which is owed to their reactivity and efficiency in an aqueous environment under neutral conditions. [6-9]

Siva et al. studied the acyl migration of *S-acylated* cysteine peptide through several cyclic transition states. For the case study, the possibility of acyl migrations occurring in a 5-membered ring to a 19-membered ring was exhibited. The *S-to-N-acyl* transfer was discovered to vary according to the size of the macrocyclic transition state. [10-12]

In this thesis, the experimental work is based on the confirmation of the hypothesis of *S-to-N-acyl migration* that occurs in the conjugation of [^{18}F]FNA 4-nitrophenyl ester with the peptide CooP (H-**C**GLSGLGVA-NH_2), which is a brain tumor-homing peptide that shows affinity with FABP3 and its variant ACooP (H-A**C**GLSGLGVA-NH_2) [53-54]. Four new peptides were studied; all peptides were variants of the peptide sequence of ACooP. This thesis includes the radiosynthesis of two of these peptides C@5 (H-AGLS**C**GLGVA-NH_2)and C@1-K (H-**C**GLSGLGVAK-NH_2), the cold conjugation, purification, structural confirmation, MS, and NMR analysis of the four peptides (C@1-K, C@3 (H-AGCLSGLGVA-NH_2), C@4 (H-AGLCSGLGVA-NH_2), and C@5) conjugated with [^{19}F]FNA.

2.0 LITERATURE REVIEW

2.1 POSITRON EMISSION TOMOGRAPHY

Positron emission tomography (PET) is an imaging technique in nuclear medicine that provides information on the physiological and pathological attributes according to the detection of radiation, dispersal of radioactive labelled compounds (radiotracers) that have been introduced into a human or animal through the instillation of radiotracers. Amongst all tomographic imaging techniques, one of the techniques that offers the highest qualities of sensitivity and quantitative accuracy is PET. The characteristics that PET possesses make it important for both use in research and in diagnostics [13]. For biological comparisons, PET is usually used alongside other imaging modalities like a magnetic resonance imaging or a computed tomography scan of the studied body or subject, to produce the best results that would give the most imperative information and data needed for a complete analysis.

In PET, the main principle behind it is simply the emission or the release of positrons by a radioisotope that is neutron deficient. Radionuclides that decay through the release of positrons are rich in protons, which causes them to move towards stability as they give off a positive charge. A new nuclide is formed when radionuclides release positrons or undergo positron decay; this phenomenon results in the formation of a new nuclide that has one less proton and an additional neutron, also producing the emission of a positron and a neutrino [14].

Annihilation occurs when the radionuclide in the tracer decays to stable states (Figure 1). As a result of decay, the positron that is emitted from this decay travels a short distance (it is key to note that this varies for different isotopes and the substances in which the radionuclides present) and then collides with an electron; this process produces two different photons that possess high energy (511 keV each). These photons move in contrasting directions but along a straight line that a PET scanner outside the body can sense or detect.

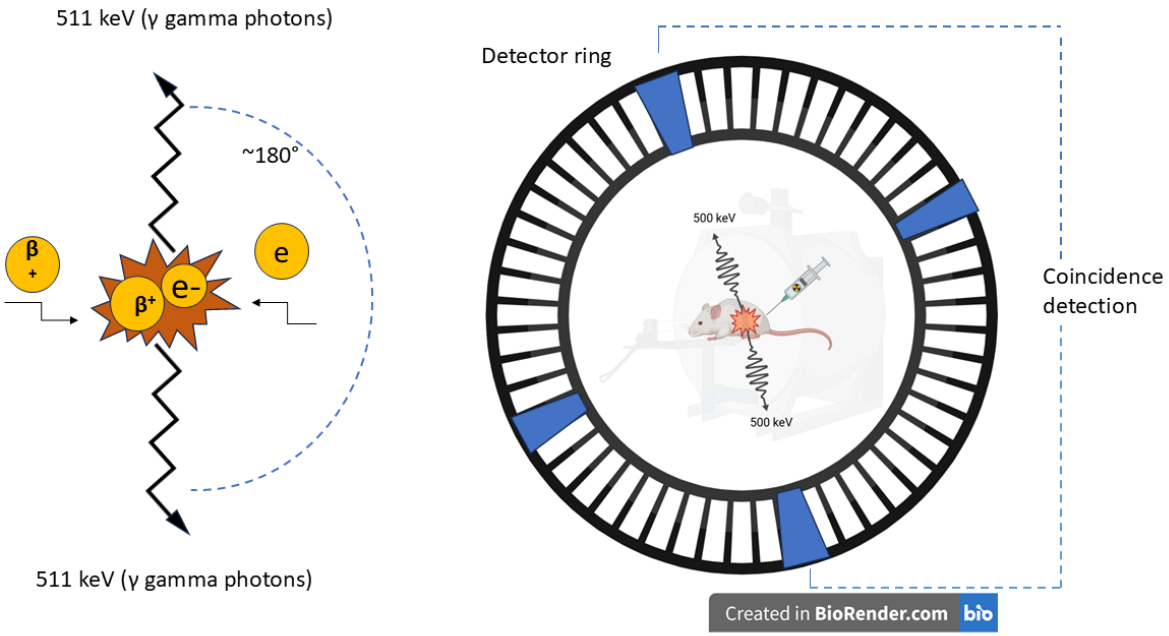

Figure 1. Basic principle of PET imaging. The Figure is adapted from [14] and created with BioRender.com.

The scanner in PET detects the gamma rays through scintillator materials. The scintillator materials have changed over time, with new age scintillators made of lutetium oxyorthosilicate (LSO) and lutetium yttrium oxyorthosilicate (LYSO) compared to the older scintillator made of bismuth germanate (BGO), all of which are integrated with highly sensitive photosensors[13]. The emission of the two photons (511 keV) happens concurrently in adjacent directions (roughly 180 degrees in opposite directions), and that produces the images through coincidence detection. The detectors show that annihilation has indeed occurred along the conduit of the detectors. Line of Response (LOR) describes the route between the detectors, [14.] Figure 1 above shows a clear representation.

The energy captured by the detectors allows the fabrication of a 3-dimensional PET image, which indicates the concentration of cumulative radioactivity in the scanned subject as a function of time.[1]

2.1.1 ADVANTAGES AND DRAWBACKS OF PET IMAGING

There are numerous advantages to PET imaging; the few that are important are sensitivity, quantitative attributes, and the signal possessing an indefinite penetration depth. The highly sensitive feature owes to the principle of the detection; this allows for only the detection of annihilation that has released gamma rays and not scattered photons. Concentrations in trace amounts are detectable because of high sensitivity[16]. The study of subjects (organisms) in vivo, devoid of interfering with their physiological state, is possible because of the use of minuscule amounts of radiotracers, which is known as "microdose" [17]. When choosing a radionuclide intended for PET imaging, the availability, suitable half-life in correlation with the biological half-life of the tracer, and the amount of time needed to transport said tracers are all taken into consideration [18]. Suitably high molar activity is essential to the produced PET image because of its effects on the signal-to-noise ratio [19].

In the detection of the 511 keV gamma rays generated from the annihilation event, three possible coincidences can occur. These three coincidences are known as true coincidence, random coincidence, and scattered coincidence. The preferred detection is true coincidence, which emanates from the two particles interacting to form annihilation, which leads to the 511 keV gamma rays that get to the parallel side of the detectors in the required time frame. Random coincidence happens when photons from two different annihilation processes reach the detectors simultaneously, and scattered coincidence is because of photons that have been scattered in their path to the detector. The energy level of the detector is adjusted to allow only 511 keV photons, with the sole purpose of reducing the effects of scattered and random coincidence on the detector [20]. One other feature that impairs the quality of the produced PET images is "Attenuation". Attenuation occurs when coincidences are reduced, and also in the case where photons interact with media like a tissue (soft) in the subject [21]. Attenuation can be corrected by doing calculated attenuation correction or measured attenuation correction[14]. Irrespective of the numerous advantages of PET, some drawbacks include a limited capacity for anatomical information and an inadequate spatial resolution (4–5 mm). PET imaging necessitates the rapid and efficient on-site radiolabelling and quality control of radionuclides with short half-lives

2.2 PET RADIOCHEMISTRY

2.2.1 POSITRON EMITTERS CHEMISTRY

These radioisotopes, ^{11}C, ^{15}O, and ^{18}F, are frequently used in PET imaging and for research; they all possess significant branching ratios (β^+ decay) and half-lives that are short [21]. Amongst the shortlist of PET radionuclides used for imaging, gallium-68 is usually produced using a $^{68}Ge/^{68}Ga$ generator. Cyclotrons are used to create the other radionuclides in the list (Table 1) [22]. The table below shows the emitters and how they are being made, and some physical properties [23,32-35].

Table 1. Positron emitters and some of their attributes

Nuclide	Half-life	Production	Mean Positron Energy (keV)	Maximal Positron Energy (MeV)	β^+ intensity
^{11}C	20.3 (min)	Cyclotron	385.70	0.96	99.77%
^{13}N	9.97 (min)	Cyclotron	492.21	1.19	99.80%
^{15}O	2.04 (min)	Cyclotron	735.28	1.73	99.90%
^{18}F	109.7 (min)	Cyclotron	249.8	0.63	96.73%
^{64}Cu	12.7 (h)	Cyclotron	278	0.65	61.50%
^{89}Zr	78.4 (h)	Cyclotron	391	0.89	1.53%
^{124}I	4.18 (d)	Cyclotron	188	2.1	22.70%
^{68}Ga	67.8 (min)	$^{68}Ge/^{68}Ga$ Generator	829.5	1.89	88.91%

Free form fluorinated compounds are not abundant in nature compared to many other elements, but in PET imaging, fluorine-18 is one of the most important radionuclides. The characteristics that make fluorine-18 the topmost pick are the quantitative dependability and the resolution quality that it gives in PET imaging. Also, the viability, the time frame of the half-life, which is almost few minutes short of 2 hours (109.8 min), It is an excellent option for radiosynthesis because of the time factor, which means a radiotracer can be administered later compared to radiotracers with shorter half-life radionuclides[24]. Radiochemical protocols for carbon-11, nitrogen-13, and oxygen-15 have been challenging to develop, which is owed to the relatively short half-life of these isotopes, which are 20.3 minutes, 9.97 minutes, and 2.04 minutes, respectively [25]. Although they are still used often because of the presence of these elements in biomolecules, which makes isotopic radiolabelling, an example is the of nitrogen-13 in the diagnosis of coronary artery disease [26,29]. Copper-64, fluorine-18, and gallium-68 are favoured for the labelling of peptides or antibody fragments, including low-molecular-weight nanobodies and affibodies. Whilst PET radionuclides iodine-124 (Half-life = 4.18 days) and zirconium-89 (Half-life= 78.4 h) provide an adequate imaging window for investigating processes with slower kinetics, including the biodistribution and targeting efficacy of intact antibodies [27-28,30].

2.2.2 MOLAR ACTIVITY IN PET RADIOCHEMISTRY

The importance of molar activity cannot be understated in PET radiochemistry and PET imaging; Even though the imaging quality of PET is not directly correlated to molar activity, it remains a factor, as it affects the signal-to-noise ratio and, in turn, the quality of images produced [35-36]. Molar activity is the radioactivity measured in each mole of a compound (in Bq/mol or GBq/μmol). The molar activity is represented by A_m[37]. A high molar activity is usually needed for radiopharmaceuticals as the unlabelled species might compete for target binding [38,39]. The variation in A_m values achieved during the production of PET tracers is primarily determined by the nuclear and radiochemical techniques employed, in addition to the potential for contamination by non-radioactive isotopes.

Representation of the comparison between high and low molar activity is shown below in Figure 2.

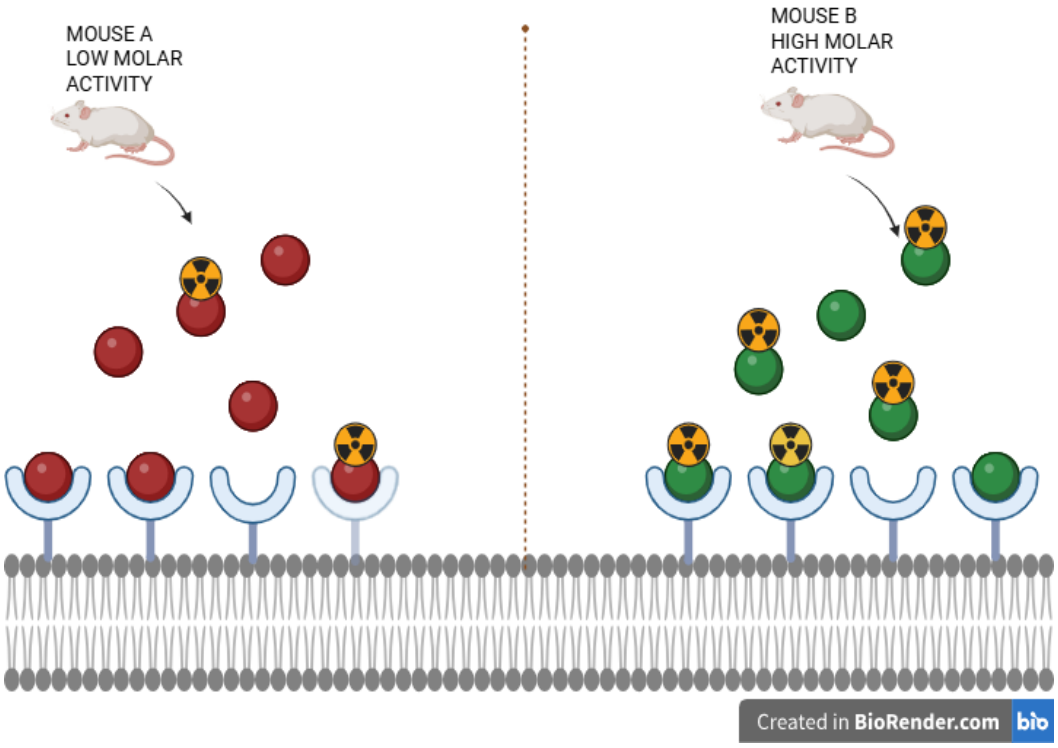

Figure 2. Representation of the comparison of low molar activity and high molar activity. The balls with the radioactivity warning sign represent radioactive tracer, and the balls without the radioactivity warning sign represent non-radioactive tracer. In general, in the case of low molar activity, poor quality images are produced, and in high molar activity, good imaging quality is achieved. Receptors are represented by wine-glass-like shapes. Created with Biorender.com.

2.3 PEPTIDE-BASED PET RADIOPHARMACEUTICALS

A PET radiopharmaceutical is a pharmacophore conjugated with a positron-emitting radionuclide. Pharmacophores incorporate small molecules, amino acids, peptides, antibodies, and nanoparticles, among others. These molecules can identify cancer biomarkers (e.g., enzymes) or biological processes (e.g., energy metabolism)[66]. For the past forty years, there has been a development in nuclear medicine with the introduction and use of radiolabelled bioactive large molecules in imaging. Especially in positron emission tomography, where radiolabelled proteins and peptides have been important for use in preclinical and clinical research, as diagnosing medicine has evolved to be referred to as "real" medicine.[40] Peptides have been continually researched for their biological actions and correspondence with several receptors. These receptors of interest are

mostly populated in cancers of distinct types, with little or no density in the other tissues under physiological conditions. The development of these kinds of research led to the recognition of radiolabelled peptides as radiopharmaceuticals, with this serving as the molecular basis for further development, such as radiotherapy as well as radioimaging [41]

Many radiolabelled peptides are in various stages of development, and these stages of development are universal for a radiolabelled peptide to be certified as a radiopharmaceutical that can be used widely. Some of these radiolabelled peptides are in research to see if they will be used for or show any potential for clinical use or application. A few of these peptides have shown promise for imaging of infection, and tumors.[42] The development stages of radiolabelled peptides can be put together in six (6) stages: (1) Molecular target identification; this is done with the use of specific receptors for immunohistochemistry or autoradiography. This is done to know the incidence, homogeneity, and density of the receptor which would in turn be useful for in vivo targeting. (2) Peptide synthesis; the synthesis is always done based on the structure of the natural peptide putting into account the required affinity with the receptors. The natural peptide is mostly altered in several ways to create a metabolically stabilized peptide that has preserved the most important biological activity that the original peptide possesses. (3) Radiolabelling; in typical cases peptide is conjugated with a prosthetic group that possesses the radioactive element of choice for the said study. This conjugation takes place in specific conditions that would aid a good conjugation. The labelling conjugation is expected to allow for good radiochemical yield, suitably high molar activity, and high radiochemical purity as well as the high affinity between the radiopeptide and the receptor. (4) In vitro classification; The binding of the radioligand studies in several cells or cell membrane studies enables the evaluation and screening of radiopeptides in terms of their receptor affinity, dissociation from tumour cells, and other relevant factors. (5) In vivo evaluation; this is done by evaluating the imaging and biodistribution in appropriate animal models. Several factors must be considered for future development, this includes the uptake of the radiopeptide in both the desired tissues and the undesired issues, the elimination from the body, and the route by which it is excreted. The stability in the body (in vivo) is also considered. (6) Radiolabelled peptides that have gone through all these processes successfully are then taken through toxicological studies before they are approved for clinical studies (first-in-human testing). The journey from designing a new peptide to its use in the clinic is extensive, and out of the numerous

created radiopeptides, only a small fraction meets the criteria to be considered a radiopharmaceutical suitable for clinical application.[41]

In PET examinations, we currently have numerous ^{18}F-labelled tracers available for use. The effect of the high molar activity enhances the possibility to quantify receptors and visualize them in vivo. The study of these tracers focuses on many pathologies, including degenerative disorders (Alzheimer's and Parkinson's), and gene therapy. PET, a molecular imaging technology, provides unique insights into physiopathology and metabolism.[46]

Oligonucleotides, antibodies, peptides, and proteins are all examples of biomolecules that can be labelled with fluorine-18 and then assessed to check for suitability in diagnostics. The time considered as the appropriate time for imaging when using fluorine-18 in a biological system is recorded as up to 4 hours, which is about two half-lives of the isotope. Thus, when fluorine-18 is used for labelling a biomolecule, the labelled molecule has a fast clearance from the biological system, blood, and high accumulation in the site targeted by the radiopharmaceutical. Over time, it has been discovered through many experiments that peptides are best suited for fluorine-18 labelling because of rapid clearance from the biological system including the blood and the target tissue. Also, peptides can be readily synthesized in numerous laboratory settings, owing to their small sizes, with occasional chemical modifications as required. In general, peptides are also known to be able to withstand relatively harsher environments better than large proteins. It also adds a significant importance to peptides as they are known to be able to penetrate tumors due to their low non-specific binding, leading to high accumulation in target tissue.[47]

2.3.1 ^{18}F-LABELING OF PEPTIDES AND PROTEINS

The main use for fluorine–18 radiopharmaceutical opens the conversation about PET, as this is the technology that uses this element and its radionuclide and its radiopharmaceutical. The technology of PET in nuclear medicine gives clear images and moderate spatial resolution of the radiopharmaceutical in vivo evaluation[43]. The technology has the required speed of accretion, which allows for pharmacokinetics of the radiopharmaceutical uptake determination and biodistribution. When an approved radiopharmaceutical is combined with PET imaging, this gives the information through images attained that shows the biological function and aids in the diagnosis of the disease.[43,47] The future of PET can be maximized by improving approved radiopharmaceuticals with efficient preparation techniques. PET involves the administering of

radiolabelled pharmaceuticals that contain positron-emitting nuclides, which include ^{15}O, ^{11}C, ^{13}N, and ^{18}F [44].

In comparison with other radionuclides, ^{18}F is frequently used when developing radiotracers that would be used for PET imaging because of its half-life of 109.7 min and significant positron abundance of over 97%. Also, stable chemical bonds can be formed with ^{18}F in the chemical structures of tracers, which aids in the multiple steps that can be used in labelling reactions and delayed imaging. Today, we have four distinctive categories in which ^{18}F- labelling can be attained with the different classes being isotope exchange labelling, A1[^{18}F]F-complex labelling, nucleophilic, and electrophilic fluorination.[6] Many prosthetic groups labelled with ^{18}F have already been developed, and many more are in development using some of the labelling steps above to conjugate with peptides and proteins successfully. Some coupling reactions and systems have been studied with different formations such as oxime coupling, acylation, *S*-alkylation, and lately the introduction of copper (I)- catalyzed azide-alkyne cycloaddition (CuAAC).[40]

In theory, a prosthetic group can circumvent the difficulty of radiolabeling specific compounds with ^{18}F in 1-2 stages via fast nucleophilic substitution of a leaving group with ^{18}F and other ^{18}F-flourination methods. A prosthetic group in radiopharmaceutical chemistry is a secondary operative that is connected to a precursor molecule analogy to current conjugation-chemistry procedures (triazole, dihydropyrazine, oxime formations, etc.) or ^{11}C-labeling techniques (alkylation, acylation, amination, etc.). For numerous biomolecules they are unstable in harsh conditions or environments. It is also noted that in many peptides as well as proteins a few interfering nucleophilic groups that can cause crosslinking reactions are also present. Due to the reasons above, it is difficult to directly label with no-carrier added fluoride with many biomolecules. To solve this problem, the conjugation with biomolecules with fluorine-18 is commonly done using several steps, which includes the use of prosthetic groups for the radiosynthesis which can link to the biomolecules through the thiol-reactive or amino-reactive groups via oxime, amidation, acylation, imidation, acylation and alkylation.[45]

When choosing a prosthetic group for radiolabelling, note the yield produced with the labelling (highest yield possible) and the difficulty of the radiosynthesis. It must also be considered the in vivo stability of the prosthetic group. In principle, when conjugating a specifically functionalized biomolecule with a ^{18}F-prosthetic group the chemoselectivity and regioselectivity are considered.

Certain peptides and proteins may only be labelled using a limited number of techniques; furthermore, the labelled peptide may not have high enough molar activity; post-labelling purification may be required; and defluorination can lead to low in vivo stability. For ^{18}F-labeling biomolecules, many prosthetic groups have been created.[45,51]

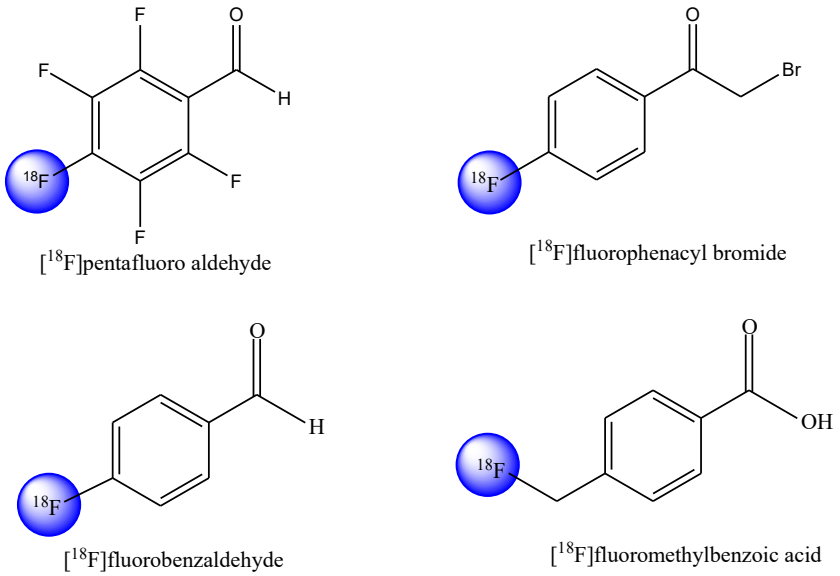

Figure 3 Fluorine-18 prosthetic groups

2.3.2 ACTIVATED ESTERS OF NICOTINIC ACID AS ^{18}F-PROSTHETIC GROUPS

Amongst the extensive list of prosthetic groups currently available *N*-succinimidyl-4-[^{18}F]fluorobenzoate ([^{18}F]SFB) is one of the most used for amino functionalities conjugation.[48]

However, the radiosynthesis of [^{18}F]SFB is rather challenging in the setting of radiopharmaceutical preparation compliant with Good Manufacturing Practice (GMP). Accordingly, researchers have developed similar structures to [^{18}F]SFB but with straightforward synthesis protocols. For example, the activated esters of 6-fluoronicotinic acid (FNA, also known as FPy) are conveniently prepared, and their conjugates have shown great promise in preclinical and clinical PET imaging. The chemical structures of those prosthetic compounds are shown in Figure 3, and some of the published studies are summarized in Table 1. Some of these conjugations will be highlighted in sections 2.3.2.1─2.3.2.5. with specifics on how they have been achieved.

Table 2. Examples of using activated esters of 6-fluoronicotinic acid as prosthetic groups.

Prosthetic group	**Biomolecules**	**Conjugation conditions**	**Radiochemical yield**	**Disease models**
[^{18}F]c(RGDfK) (Fpy-TFP)	Peptide (RGD)	sodium bicarbonate (10–15 mg) in1 mL water, 10 mins at 50°C	10–35 %	Human serum[48]
[^{18}F]TFPFN-2Rs15d (FPy-TFP)	single domain antibody fragments (sdAbs) + Antibody (HER 2 * 2Rs15d)	0.1 M borate buffer, pH 8.5, 20°C for 20 min	5.7 ± 3.6 %	MICE (Human Ovarian cancer cells (SKOV-3) and Human Breast cancer cells (BT474))[49]
[^{18}F]TFPFN- 5F7 (FPy-TFP)	single domain antibody fragments (sdAbs) + Antibody (HER 2 * 5F7)	0.1 M borate buffer, pH 8.5, 20°C for 20 min	4.0 ± 2.0 %	MICE (Human Ovarian cancer cells (SKOV-3) and Human Breast cancer cells (BT474))[49]
^{18}F-labeled tetrazine. [^{18}F]T2 and [^{18}F]T3 (Fpy-TFP)	Antibody (RmAb158-scFv8D3 and Tribody A2) infused with protein (amyloid-β (Aβ))	10 % PBS 10x, pH 7.4	[^{18}F]T2 18 ± 6 % and [^{18}F]T3 16 ± 3 %	Alzheimer's disease and Control (mice)[50]
[^{18}F]-siRNA/PAHOleic (FPy-TFP)	Protein (siRNA)	50 mM borate buffer pH 8.5, rt at 20 mins	Not mentioned	Healthy rodents and A549 tumour bearing mice[52]
[^{18}F]PSMA -1007 (FPy-TFP)	Peptide (PSMA)	phosphate buffer (0.2 M; pH 9.0), 60 °C for 20 min	1.5 %–6.0 %	Healthy human and Humans with high-risk prostate cancer[51]

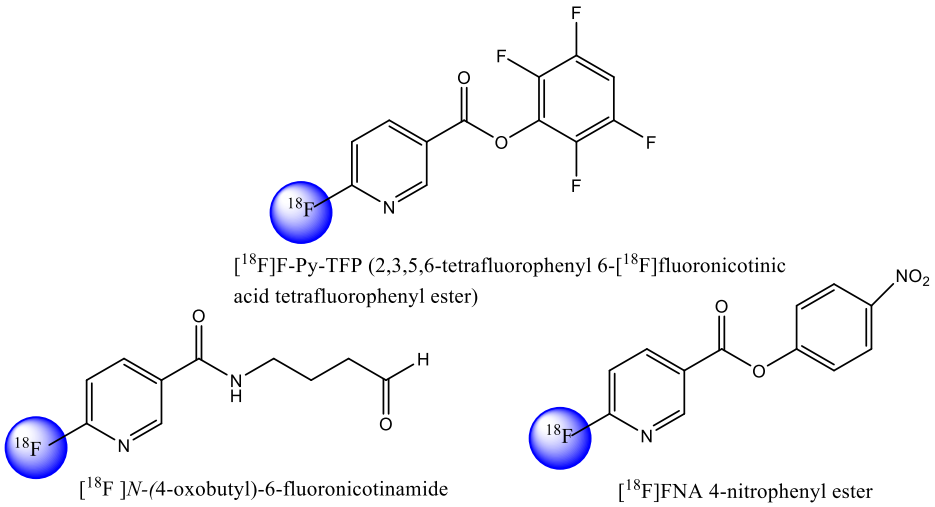

Figure 4 Chemical structure of the activated esters of 6-fluoronicotinic acid

2.3.2.1 [^{18}F]FPy-TFP conjugation with FVIIA protein.

Of the few experiments and conjugations that have been made and will be discussed in this work. It is to be pointed out that this experiment is the only experiment carried out for the essence of the applicability of the proven method, as oxime coupling was carried out in this research.

Jepsen et al. (2021) devised two methodologies to generate reactive ^{18}F-aldehydes that are appropriate for oxime coupling on chemically sensitive proteins. An alternative method involves beginning with the established synthesis of [^{18}F]FPy-TFP, but without the use of azeotropic distillation. The process of drying, specifically at a temperature of 16 degrees, can be employed as a method like that used in many experiments, resulting in the production of [^{18}F]fluornicotinamide aldehyde. The alternative method, which begins with a spirocyclic iodonium (III) ylide precursor, has fewer stages and is therefore more suitable for labelling a single item. This method produces three distinct ^{18}F-aldehydes, one of which is ^{18}F-fluorinated butyraldehyde. The compound ^{18}F-fluorinated butyraldehyde exhibited higher reactivity towards O-Bn-ONH$_2$ compared to the compound synthesized from [^{18}F]SFB. Additionally, the synthesis time for ^{18}F-fluorinated butyraldehyde was reduced to around 60 minutes, whereas it took 150 minutes (about 2 and a half hours) to synthesize ^{18}F-fluorinated butyraldehyde from [^{18}F]SFB. The coupling of the ^{18}F-fluorinated butyraldehyde with FVIIai-ONH$_2$ lead to in a modest yield of 11%, high purity of over

98%, and a molar activity of 27 GBq/μmol, which is considered acceptable. This method is therefore appropriate for coupling oximes with delicate proteins that have been modified with amino-oxy groups. It was also recorded that the [^{18}F]fluoronicotinamide aldehyde made from the [^{18}F]FPy-TFP had comparable results to what was achieved with ^{18}F-fluorinated butyraldehyde during this experiment. [47]

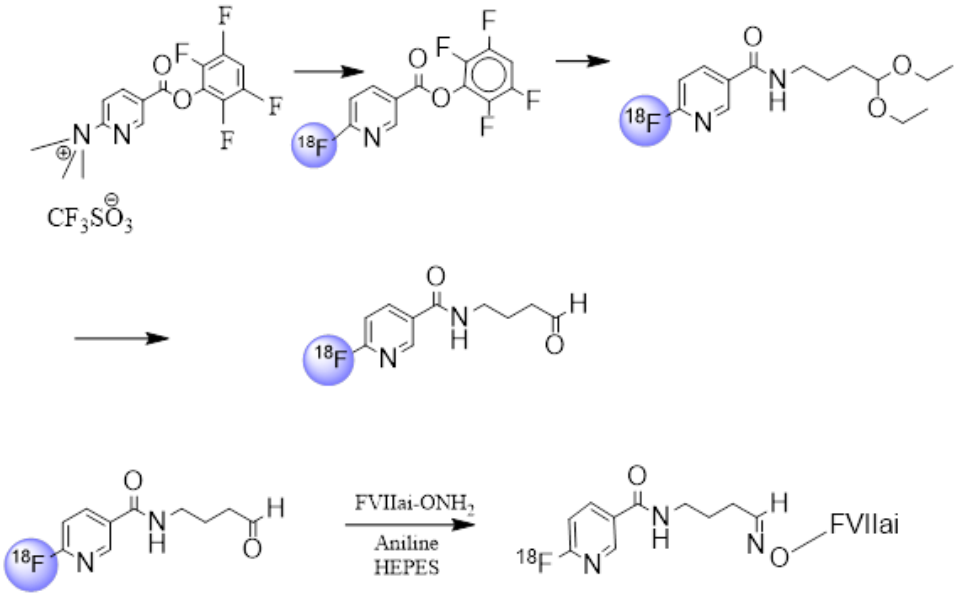

Figure 5 Synthesis of [^{18}F]fluoronicotinamide aldehyde from [^{18}F]FPy-TFP and conjugation of [^{18}F]FPy-TFP and protein.

2.3.2.2 [^{18}F]FPy-TFP conjugation with cyclic RGD peptide c(RGDfK)

As an image tracer for integrin αvβ3, the tripeptide molecule Arg-Gly-Asp (RGD) is often used because it binds well and is very specific. There are also tracers built on RGD that have a C-^{18}F link. It takes an extended period to make the tracer because they are prepared in multiple phases and then processed with High Performance Liquid Chromatography (HPLC).

Basuli et al. followed the technique precisely in their experiment. In 1 mL of water, 1.5 mL of [^{18}F] FPy-TFP solution was mixed with 3–5 mg of c(RGDfK) and 10–15 mg of sodium bicarbonate. The result was cleaned with HPLC. Before the solution was put through a tC18 environmental filter for HPLC purification, a total of 30 mL of water was added to it. Semi-preparative HPLC purification involved mixing the reaction mixture with 2 mL of HPLC buffer and adding it to the HPLC apparatus. The HPLC setup utilised a Phenomenex Luna (2) C18 column (10 × 250 mm)

with a particle size of 5 µm. A 4 mL/min mobile phase of 25% ethanol in 50 mM o-phosphoric acid was used. Analytical HPLC verified product purity. For a stability check, 0.074 Gbq of [^{18}F]c(RGDfK) was added to two millilitres of human serum. For different time points (0, 60, 120, and 240 minutes), 20 µL of the sample that had been stored was put directly into the HPLC without any additional measures being taken. HPLC showed that [18F]FPy-TFP and c(RGDfK) in the presence of sodium carbonate as a base converted over 80% to the product. After Sep-Pak purification, the compound was radiochemical pure with over 98% purity and 37000-81400 GBq/mmol specific activity. Twelve replicates were used for this purification stage after synthesis. The recorded radiochemical yield is 32-43% and the total synthesis time of 0.5 hours. A 3ml radiosynthesis product with 103 mCi(3811 GBq) of [^{18}F]F- has 7 micrograms per milliliter of impurities. The product was spiked with a non-radioactive compound to confirm that the product's radioactive and non-radioactive compounds eluted at the same time. The product [18F]c(RGDfK) was serum stable for up to 4 hours after production.[48]

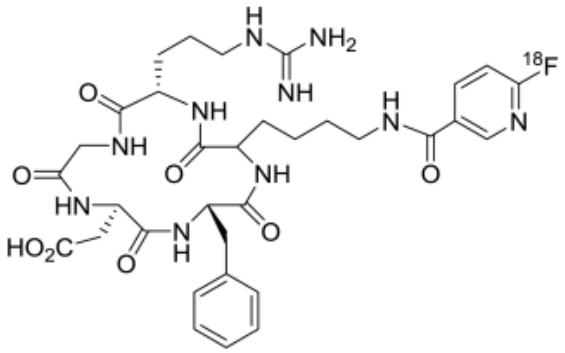

[^{18}F]c(RGDfK)

Figure 6 Structure of [^{18}F]c(RGDfK

2.3.2.3 [^{18}F]FPy-TFP conjugation with single domain antibody fragments (sdAbs)

Two anti-HER2 single domain antibody fragments were labelled with ^{18}F by Zhou et al. (2019), who used a substitute agent called [^{18}F]TFPFN, which contains fluoropyridine. The HER2-reactive single-domain antibodies (sdAbs) that were labelled kept their ability to bind and respond to the target antigen. This labelling method works much better at getting into the kidneys than the RL-I and RL-II residualizing prosthetic agents that were previously created for 18F labelling. When [^{18}F]TFPFN was used with the sdAb, the tumour uptake levels went up because the sdAb was

better at entering the cell after binding to its receptor. The amount of tumour uptake for the sdAb 2Rs15d that does not go inside the cell as well was the same as what was seen for [^{18}F]SFB-2Rs15d. There was a minor improvement, though, in that the radioactivity was now absent in the kidneys. Because making [^{18}F]TFPFN by hand is easier than making [^{18}F]SFB and because it hasn't been fully improved yet, results suggest that [^{18}F]TFPFN should be looked into more as a way to label sdAbs and other low molecular weight proteins. DCC-mediated coupling between 6-fluoronicotinic acid and 2,3,5,6-tetrafluorophenol was used in the preparation. The pure yield of the product that was made was 41%. The structure matched the data from the NMR and mass spectral tests. The radiochemical yield that took into account radioactive decay for making [18F]FPy-TFP, which included HPLC processing, was found to be 23.4 ± 11.2% (n = 15). When radioactive decay was taken into account, the yield for making [18F] TFPFN-2Rs15d was 5.7 ± 3.6% and for making [^{18}F]TFPFN-5F7 it was 4.0 ± 2.0%.[49]

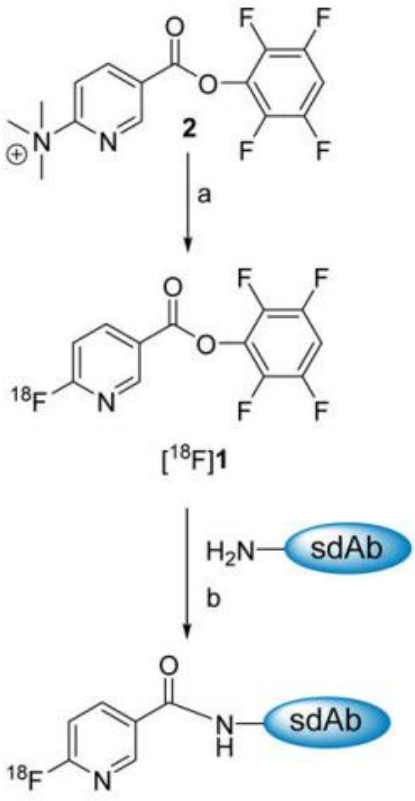

a) [^{18}F]fluoride, *tert*-butanol, acetonitrile, on cartridge labeling
b) Borate buffer, pH 8.5

Figure 7: Conjugation conditions for [^{18}F]FPy-TFP with single domain antibody fragments (sdAbs)

2.3.2.4 [^{18}F]FPy-TFP conjugation with RmAb158-scFv8D3 and Tribody A2

It is not possible for antibodies to target the central nervous system (CNS) because they cannot typically breach the blood-brain barrier (BBB). This limitation makes them less desirable as radioligands, even if they are very specific and have a strong affinity. They were mixed with a portion of a transferrin receptor (TfR) antibody to help the amyloid-β (Aβ) antibodies get to more places in the brain. The combination made it possible for transfer across the BBB using methods that depend on receptors. The goal of the study by Syvänen et al. (2020) was to attach fluorine-18 to these two types of antibodies so that they could be used for Aβ PET imaging. The researchers changed two types of antibody ligands RmAb158-scFv8D3 and Tribody A2 by adding trans-cyclooctene (TCO) groups. These were then connected to 18F-labelled tetrazines using a special chemical reaction that occurred at room temperature. In a controlled lab setting, ^{18}F-labelling did not change how the antibody bound in any way. It was also found that the first time the antibody was absorbed in the brain was important. The first tetrazine variation ([^{18}F]T1) had a strong affinity for bone, which suggested that it defluorinated a lot. The next two tetrazine variations ([^{18}F]T2 and [^{18}F]T3) were able to successfully address this issue. Fluorine-18 has a half-life of 110 minutes, which is longer than the antibody ligands' half-life in the blood. However, [^{18}F]T3-Tribody A2 PET was able to tell the difference between transgenic mice (tg-ArcSwe) with Aβ deposits and wild-type mice 12 hours after infusion. This research shows that ^{18}F can be used to label bispecific antibodies, which lets them get into the brain. This method may be used for brain and spinal cord PET imaging if more changes are made. [50]

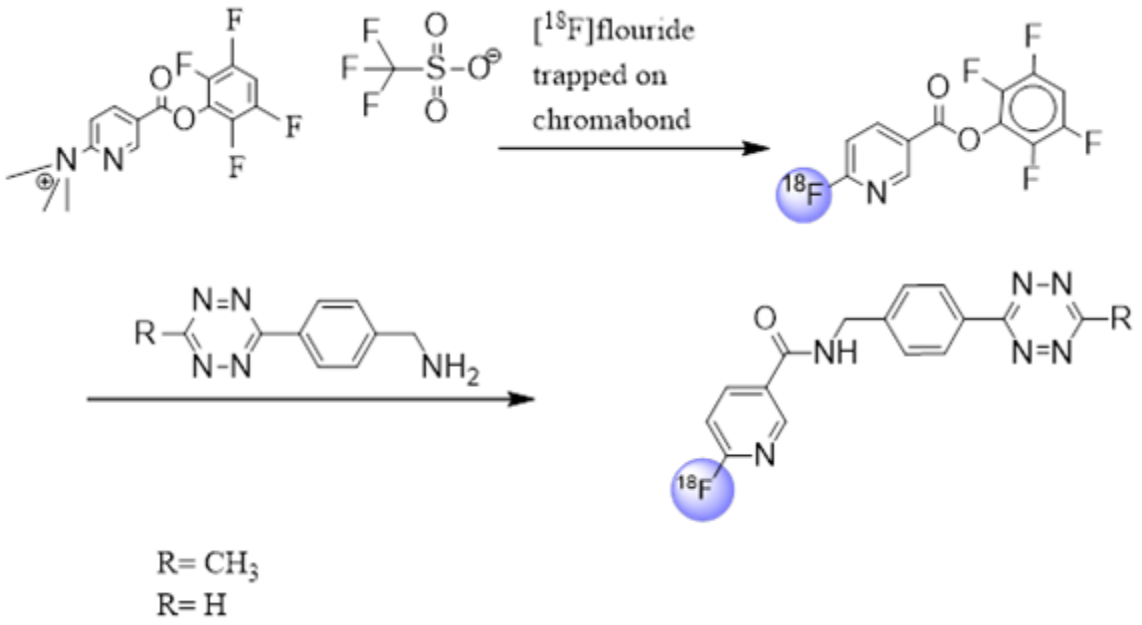

Figure 8 Synthesis of [^{18}F]Tetrazine

2.3.2.5 [^{18}F]FPy-TFP conjugation with PSMA ligands

Piron et al., (2022) studied [^{18}F]DCFPyL and [^{18}F]PSMA-1007, which are two PET tracers labelled with ^{18}F that specifically target prostate-specific membrane antigen (PSMA). These tracers have established themselves as important tracers in the field of prostate cancer imaging. [^{18}F]DCFPyL was initially provided to a group of nine patients with hormone-naïve or castration-resistant prostate cancer (PCa). This initial investigation in humans observed a swift removal of the tracer from the bloodstream through rapid elimination by the kidneys, and the subsequent accumulation of the tracer in the bladder. Giesel et al. synthesised [^{18}F]PSMA-1007, a compound derived from the theranostic ligand PSMA-617, with the purpose of assisting in the identification of patients who may be eligible for [^{177}Lu]PSMA-617 therapy. The compound possesses the identical Glu-urea-Lys binding pattern to engage with the enzyme's active binding site. Additionally, it includes a linker region based on naphthalene and glutamic acid groups to mimic the carboxylic acid groups found on the DOTA chelator. In the initial trial including humans, a more advanced 2-step automated synthesis module was utilised, resulting in yields of 5.1 ± 2.3% after a total synthesis duration of 80 minutes. The CONDOR trial assessed the use of [^{18}F]DCFPyl imaging in patients who experienced biochemical recurrence (BCR) with a median PSA level of

0.8 ng/mL (ranging from 0.17 to 98.45 ng/mL). The trial also tested the effectiveness of standard imaging, which yielded disappointing results. [51]

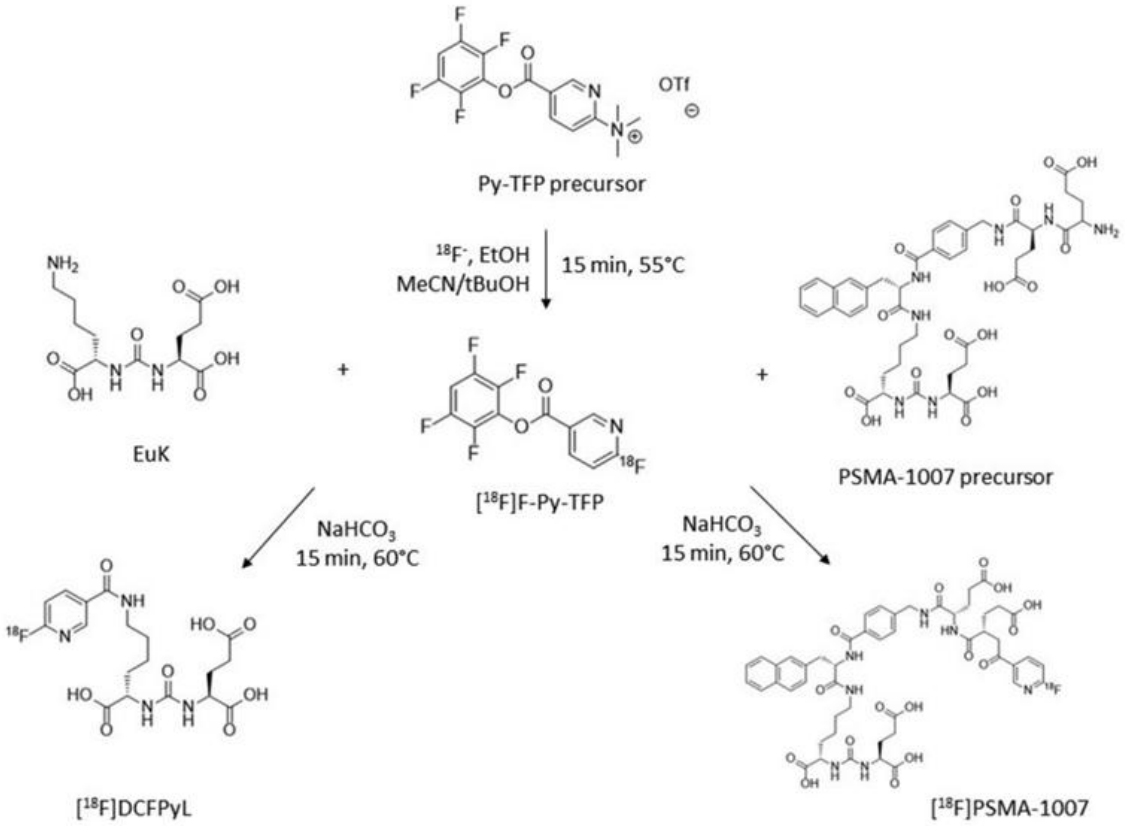

Figure 9 Radiosynthesis of [^{18}F]DCFPyL and [^{18}F]PSMA-1007 using the minimalist.

2.4 [^{18}F]FNA 4-NITROPHENYL CINJUGATION WITH ACooP AND CooP

The radioactive prosthetic group [^{18}F]FNA 4-nitrophenyl ester (Figure 10) was conjugated with the peptide sequence CooP (H-CGLSGLGVA-NH_2) in 2023[54]. The prosthetic group was picked because of its non-volatility and its characteristics that help it label with peptides at various temperatures, most notably room temperature[48]. The peptide CooP is a brain tumor-homing peptide that shows affinity with FABP3 and has been studied in different variants [56,57]. The peptide sequence contains two free functional groups in an amino and a sulfhydryl group.

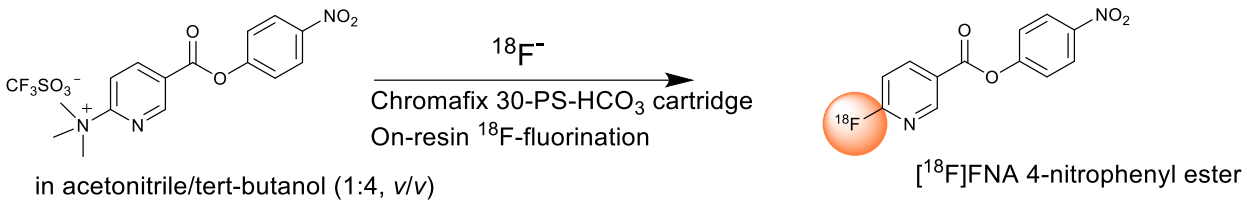

Figure 10. Radiosynthesis of the prosthetic group [^{18}F]FNA 4-nitrophenyl ester.

Dillemuth et al. conjugated, and the result yielded the expected *N-acylation* (seen in Figure 12) on the N-terminus of the cysteine in the sequence. The group then conjugated the prosthetic group with another variant of the previously conjugated peptide ACooP, which includes the addition of an alanine in the first position of the peptide sequence. The results yielded *S-acylation* (seen in Figure 11), which is absent in the literature for the radiosynthesis of biomolecules with [^{18}F]FNA esters.

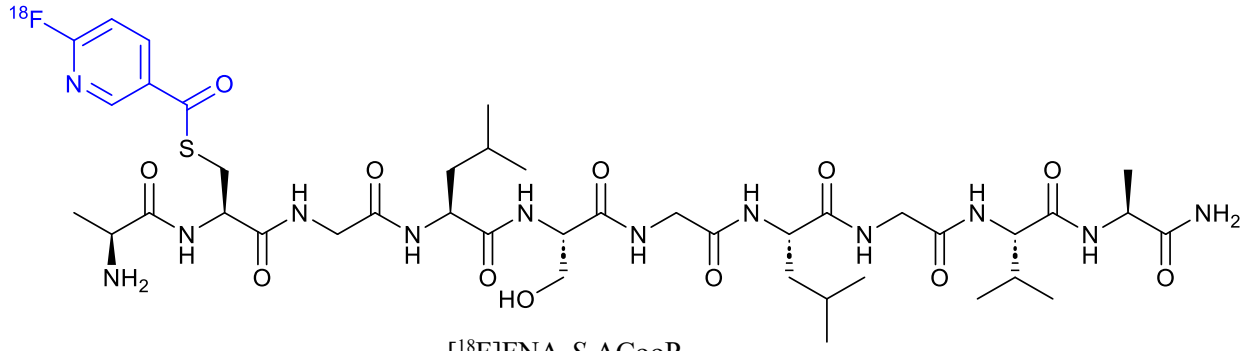

[^{18}F]FNA-*S*-ACooP

Figure 11. Product of the conjugation of [^{18}F]FNA and ACooP.

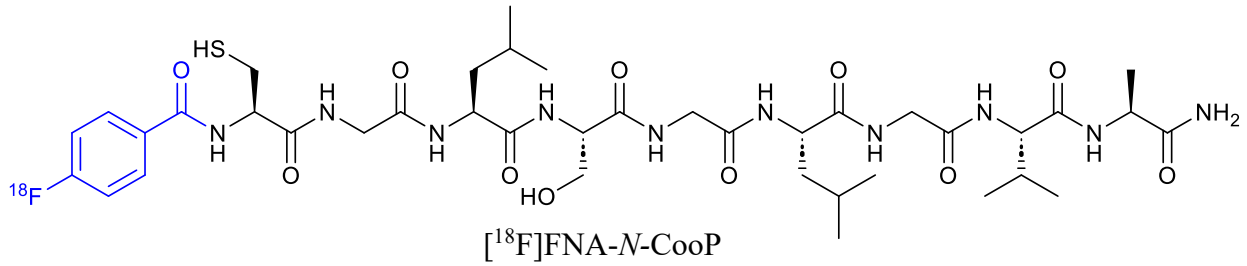

[^{18}F]FNA-*N*-CooP

Figure 12. Product of the conjugation of [^{18}F]FNA and CooP

3.0 HYPOTHESIS AND AIMS

The hypothesis of this work is that an intramolecular *S-to-N acyl transfer* has occurred in the case of the CooP because of the favourable ring size formed in the transition state, and *S-acylation* has remained in the case of ACooP because of the unfavourable ring size formed. To prove this hypothesis, four new peptides were conjugated with the prosthetic group. The variants of the peptide used for the experiment were H-**C**GLSGLGVA**K**-NH_2 (C@1-K), H-AG**C**LSGLGVA-NH_2 (C@3), H-AGL**C**SGLGVA-NH_2 (C@4), and H-AGLS**C**GLGVA-NH_2 (C@5).

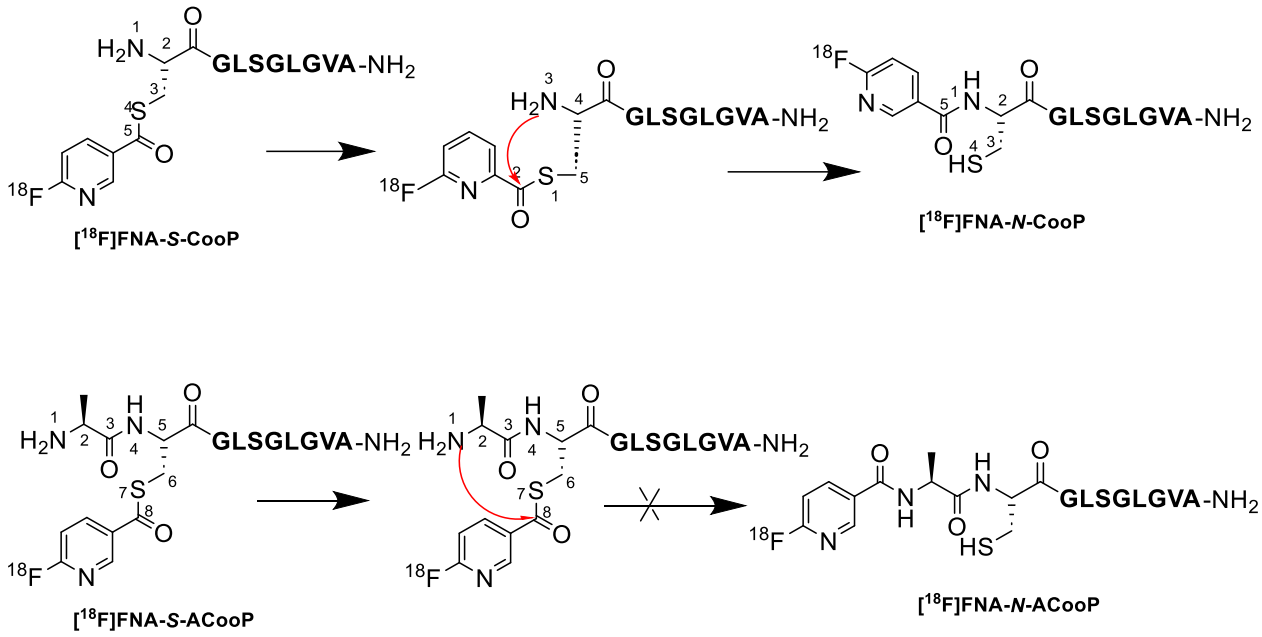

Figure 13. Hypothesis for the chemoselectivity mechanism.

The aims of this thesis are;

- To study the mechanisms of the chemoselectivity and/or regioselectivity of the peptides with four new peptide sequences H-**C**GLSGLGVA**K**-NH_2 (C@1-K), H-AG**C**LSGLGVA-NH_2 (C@3), H-AGL**C**SGLGVA-NH_2 (C@4), and H-AGLS**C**GLGVA-NH_2 (C@5) compared with the previously done two peptides ACooP and CooP.
- To radiosynthesize and characterise the conjugates of [^{18}F]FNA and H-AGLS**C**GLGVA-NH_2 (C@5) and H-**C**GLSGLGVA**K**-NH_2 (C@1-K).
- To confirm the structure of all conjugated peptides in this study.

- To confirm the hypothesis of *S- to N- acyl* transfer and regioselectivity.

4.0 MATERIALS AND METHODS

4.1 CHEMICALS AND EQUIPMENT

Chemicals used in these experiments are all analytical grade (e.g., for HPLC and NMR analysis). Primary precursor *N, N, N*-trimethyl-5-((4-nitrophenoxy) carbonyl) pyridin-2-aminium trifluoromethane sulfonate was purchased from R&S chemicals (Kannapolis, NC, USA), 1-ethyl-3-(3-dimethylaminopropyl)carbodiimide (EDC), 6-fluoronicotinic acid, 4-nitrophenol, 4-dimethylaminopyridine (DMAP) were all purchased from Sigma Aldrich. Peptides C@3, C@4, C@5, C@1-K and FNA-*N*-C@1-K were purchased from United Biosystems (Herndon, VA, USA). Sep-Pak Accell Plus QMA Plus Light cartridge (WAT023525), Sep-Pak C18 Plus Light cartridge (WAT023501), and Hydrophilic-Lipophilic-Balance (HLB) cartridge (Oasis, 30 mg) were purchased from Waters (Milford, MA, USA). Chromafix 30-PS-HCO_3 anion-exchange cartridge was procured from Macherey-Nagel GmbH& Co. KG, Duren, Germany. Analytical weight scale (100A-300M, Precisa), Heto Hetovac VR-1 and CT 60E Vacuum Concentrator, Vacuum Model Avc001dose calibrator (VDC-405, Comecer). FNA 4-nitrophenyl ester was made in large volume in-house.

4.2 ANALYTICAL TECHNIQUES

4.2.1 HPLC (High-performance liquid chromatography)

High-performance liquid chromatography (HPLC) is an effective chromatographic technique for analysing and purifying mixtures. HPLC comprises a solvent pump, sample injector, column, detection system, and computer data station. The solvent delivery system delivers the solvent at high pressure through the solid phase contained within a column. Numerous distinct solid phases exhibit varying qualities for analytical and semipreparative applications, characterised by diverse particle sizes, lengths, and diameters. The columns are constructed from stainless steel and incorporate small-sized (μm) solid phase particles for enhanced resolution and efficient separation. The sample injection into the column may be performed either automatically or manually. The compounds are separated by traversing the column, subsequently reaching the detector, where the type can be identified based on the characteristics of the analytes. The most commonly utilised detectors include ultraviolet/visible (UV/Vis), photodiode array, fluorescence, and conductivity detectors. The system may additionally contain a radiation detector. The duration required for the analyte to traverse the column and arrive at the detector is referred to as the retention time [58,59].

For this thesis, the reversed-phase liquid chromatography was used extensively. In this form of chromatography, there is a highly polar mobile phase and a nonpolar solid phase. The nonpolar solid phase could be, for example, octadecyl or octyl-functionalized silica gel[60]. An increasing percentage of acetonitrile in water can be used as the mobile phase mixture. The nonpolar compounds are eluted after the polar compounds in RP-HPLC. (or compounds are eluted in reverse polarity order). The HPLC used for all experiments except product purification and isolation of non-radiative conjugated compounds in this thesis is a Shimadzu HPLC system set up with a reversed-phase HPLC column (Jupiter 5 μm, 150 × 4.6 mm, 300 Å), an SDP-40 UV-detector (Shimadzu), a radioactivity detector (Ortec), and LabSolutions software (Shimadzu).

LaChrom Elite HPLC system (Hitachi, Ltd., Tokyo, Japan) setup with an L-2130 pump and an L-2400 UV detector, operated through EZchrome Elite software. This HPLC was used for the purification and isolation of non-radioactive conjugated compounds.

4.2.2 NUCLEAR MAGNETIC RESONANCE (NMR)

Nuclear magnetic resonance (NMR) is a significant technique for characterisation and analysis. It is predicated on the magnetic characteristics of nuclei with an odd mass number (e.g., ^{1}H, ^{19}F, ^{13}C, ^{31}P) that exhibit spin angular momentum. When compounds containing these atoms are subjected to an external magnetic field, their spins may align with or oppose the field. The resonance situation is influenced by electromagnetic radiation, contingent upon the applied magnetic field and the particular nuclei involved. The compound's structure influences the resonance frequency of a certain nucleus and the chemical shift (δ) relative to a magnetically active reference compound. Chemical shifts are prompted by adjacent electronegative atoms and unsaturated groups [61].

For this thesis, the NMR spectra were obtained by using the frequencies 500 MHz and 600 MHz Bruker Avance III spectrometer (Bruker, Billerica, MA, USA), using *d*6-DMSO as deuterated solvent. The operational frequencies were 600 MHz, and 125.75 MHz for ^{1}H and ^{13}C, respectively. 1D and 2D NMR methods are both applied for confirmation of the structures (characterisation). Signal classification includes categories such as singlet (s), doublet (d), triplet (t), quartet (q), multiplet (m), and wide singlet (br s). Coupling constants, marked as J values, are measured in Hertz (Hz). The two-dimensional NMR experiments include Total Correlation Spectroscopy (TOCSY), Heteronuclear Single Quantum Coherence (HSQC), and Heteronuclear Multiple Bond

Correlation (HMBC).The obtained NMR spectra of the compounds were analysed utilising Bruker Topspin software (version 4.0).

4.2.3 LIQUID CHROMATOGRAPHY- MASS SPECTROMETRY

Two techniques are used in liquid chromatography-mass spectrometry to obtain analytical data about a sample. First, liquid chromatography (LC), such as HPLC, is used to separate the mixture's various components. The molecules are ionised following the separation. Electrospray ionisation (ESI), atmospheric pressure chemical ionisation (APCI), matrix-assisted laser desorption/ionization (MALDI), and atmospheric pressure photoionisation (APPI) are a few of the ionisation procedures. [62] For this thesis, the LC-ESI-MS/MS analysis was done on a nanoflow HPLC system (Easy-nLC1000, Thermo Fisher Scientific) coupled to the Q Exactive HF mass spectrometer (Thermo Fisher Scientific) equipped with a nano-electrospray ion source.

4.3 SYNTHESIS

4.3.1 CONJUGATION AND PURIFICATION OF FLUORONICOTINIC ACID 4-NITROPHENYL ESTER (FNA) WITH PEPTIDES (C@1-K, C@3, C@4, C@5)

The following was added to a 1.5 mL tube: 40 µL of borate buffer (300 mM, pH 8.6), 150 µL of peptide (C@1-K (5.54 µmol, 5 mg), C@3 (5.91 µmol, 5 mg), C@4 (5.91 µmol, 5 mg), or C@5 (5.91 µmol, 5 mg)) solution in water (Trace SELECT Honeywell), 40 µL of 5 mM FNA (0.02 mmol, 5 mg) in acetonitrile, and 200 µL of acetonitrile. The mixture was vortexed and then left to react at room temperature for about 8–10 minutes. A semi-preparative HPLC system was used to purify the reaction mixture. The system included a C18 column manufactured by Phenomenex in Torrance, CA, USA, with dimensions of 250 × 10 mm, 4 µm, and 90 A. The flow rate of the column was set at 5 mL/min. Solutions A and B were prepared using 0.1% trifluoroacetic acid (TFA) in water and 0.1% TFA in acetonitrile, respectively. The HPLC elution gradient in Table 2. Since an alternate gradient was required for C@3, it can be achieved; see the HPLC gradient that was used in Table 3. The primary peak of the targeted product was observed at a retention time of 6.20 minutes. Each step of the process was repeated three times to guarantee accuracy. Following that, the product's fractions were mixed and dried in a vacuum drier (Heto Hetovac VR-1 and CT 60E Vacuum Concentrator, Vacuum Model Avc001). Following drying, a solid white product appeared, and this product was subjected to additional NMR analysis. LC-MS analysis is performed to classify the products and any by-products in the reaction mixture.

Table 3. HPLC gradient for C@1-K, C@4, C@5

Time after injection	ACN (0.1% TFA)	WATER (0.1% TFA)	FLOW RATE
0 min	25%	75%	5ml/min
10 min	50%	50%	5ml/min
10.5 min	20%	80%	5ml/min
20 min	20%	80%	5ml/min

Table 4. HPLC gradient for C@3

Time after injection	ACN (0.1% TFA)	WATER (0.1% TFA)	FLOW RATE
0 min	25%	75%	5ml/min
10 min	39%	61%	5ml/min
10.5 min	80%	20%	5ml/min
20 min	80%	20%	5ml/min

4.3.2 LC-MS ANALYSIS

A nanoflow HPLC system (Easy-nLC1000, Thermo Fisher Scientific) connected to a Q Exactive HF mass spectrometer (Thermo Fisher Scientific) with a nano-electrospray ion source was used for the LC-ESI-MS/MS examination. The samples were separated inline on an analytical column (75 µm ID × 15 cm) after first being loaded onto a trapping column (100 µm ID × 2 cm). ReproSil-Pur 3 µm 120 Å C18-AQ packing material (Dr. Maisch HPLC GmbH, Ammerbuch-Entringen, Germany) was used to pack both columns internally. Water with 0.1% formic acid (solvent A) and acetonitrile/water (80:20 (v/v)) with 0.1% formic acid (solvent B) made up the mobile phase. The following gradient was used to isolate the peptides: 10% to 50% solvent B in 10 minutes, 50% to 100% solvent B in 5 minutes, and then wash at 100% solvent B for 5 minutes. Software called Thermo Xcalibur 4.1 (Thermo Fisher Scientific) was used to record the MS data. Repeated cycles of an MS1 scan covering m/z 300–2000 were used to collect data. This was followed by Higher-energy Collisional Dissociation (HCD) fragment ion scans (MS2 scans) for up to 10 of the most intense precursor ions from the MS1 scan. In HCD fragmentation, stepped collision energy (Normalised Collision Energy (NCE) 15%, NCE 20%, and NCE 25%) was used. Mass

spectrometry analyses were performed at the Turku Proteomics Facility supported by Biocenter Finland.

4.3.4 RADIOSYNTHESIS

4.3.4.1 Production of fluorine-18 and radiosynthesis device

Numerous techniques, utilising reactors or particle accelerators, have been reported in the literature for producing fluorine-18 [65]. The most common method for producing it is the $^{18}O(p,n)^{18}F$ nuclear reaction in a cyclotron, which, depending on the target material used, produces either an electrophilic [^{18}F]fluorine gas or a nucleophilic [^{18}F]fluoride ion[64]. A proton collides with an oxygen-18 nucleus and becomes entrenched within it, while a neutron is released, according to the $^{18}O(p,n)^{18}F$ reaction. The unstable fluorine-18 nucleus is thus created from the oxygen-18 nucleus, and to stabilise it, it goes through positron decay (96.9%) and electron capture (EC, 3.1%). This is the method used in the Turku PET Center to produce Fluorine-18 Radiosynthesis experiments were all carried out at the radiosynthesis lab in Aurum at the University of Turku. The radiosynthesis device used for these experiments can be seen in the Figure below.

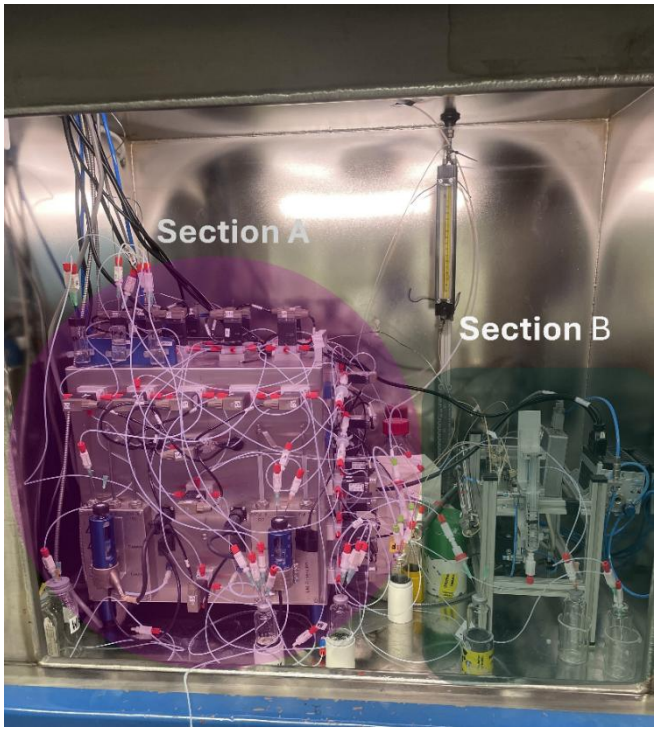

Figure 14. Radiosynthesis device by DM Automation (Nykvarn, Sweden) in Section A, HPLC integrated into the device, all inside a lead shield in Section B.

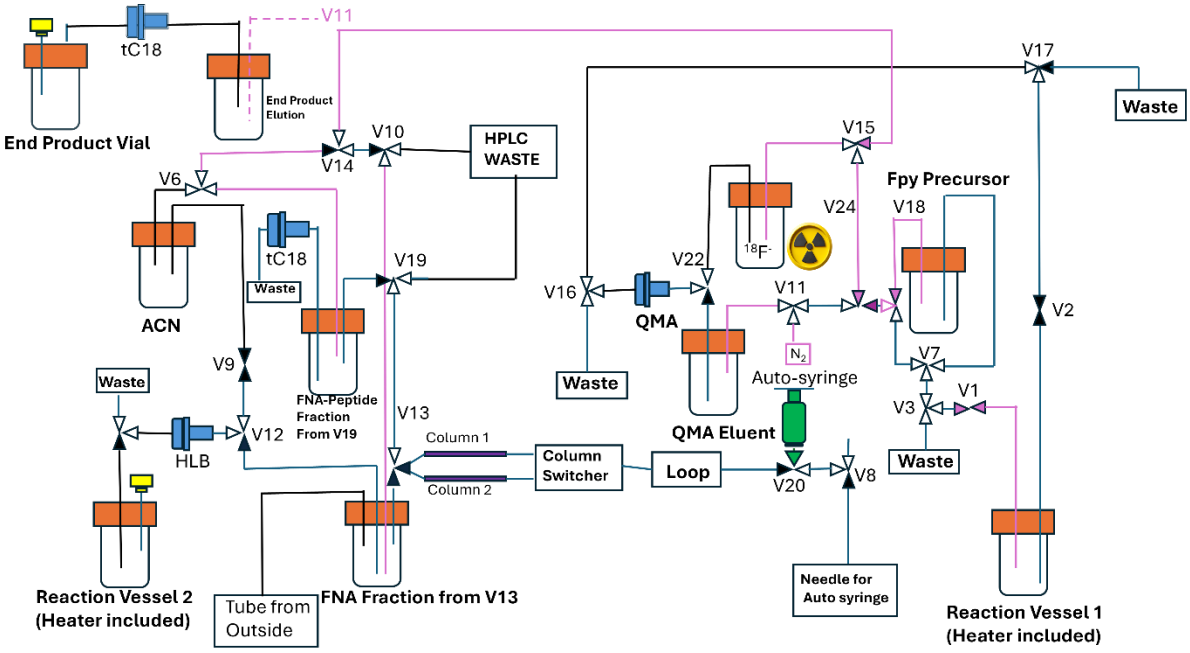

Figure 15. Schematic design for radiosynthesis design and HPLC system.

4.3.4.2 Radiosynthesis of C@5 and C@1-K

4.3.4.2.1 Radiosynthesis of [^{18}F]FNA

The synthesis was based on a new technique that came from the earlier synthesis of [^{18}F]FNA-*S*-ACooP by Dillemuth et al. (2024). Pressurised nitrogen gas moves liquids through the tiny tubes (capillaries) of the synthesis equipment. Oxygen-18 water mixed with [^{18}F]fluoride passed via a Sep-Pak Accell Plus QMA Plus Light cartridge, trapping the fluoride. The [^{18}F]fluoride was taken out of the cartridge and put into a container using Kryptofix® 222 and potassium carbonate mixed with acetonitrile and water. Heating the reaction vessel to 120°C for 15 minutes while continuously flowing N_2 gas eliminated the remaining water from the solution. After that, the vessel temperature was reduced to 37°C. The primary precursor N, N, N-trimethyl-5-((4-nitrophenoxy) carbonyl) pyridin-2-aminium trifluoromethane sulfonate (8 mg, 0.02 mmol) was submerged in 1,4-diazabicyclo[2.2.2] octane (DABCO, 14 mg, 0.13 mmol) in acetonitrile: tert-butanol (1:4, v/v, 1.2 mL), put into the reaction vessel (RV) and permitted to react for 10 minutes. Trace-select water was introduced into the RV, and the diluted combination was subsequently drawn into an auto-syringe. The mixture in the syringe was transferred to an HPLC loop by exchanging valves with Milli-Q water. A reverse phase 90 Å HPLC column (Jupiter Proteo 4 µm 250 × 10 mm) integrated the loop content into the mixture.

The mobile phase was made up of milli-Q water and acetonitrile (ACN), both of which had 0.1% TFA in them. We used a Hitachi L-6200 pump to move the mobile phase. The programme is shown in Table 4. A radio detector and a valve directed the flow of the column into a waste bottle. At 15 minutes, the [^{18}F]FNA 4-nitrophenyl ester was observed. After observing the product, we changed the controlled valves and transferred it to an already prepared container.

This chemical reaction is seen in Figure 10.

Table 4. HPLC program for radiosynthesis of [^{18}F]FNA

Time after injection	ACN (0.1% TFA)	WATER (0.1% TFA)	FLOW RATE
0 min	45%	55%	1ml/min
1 min	45%	55%	4ml/min
13 min	70%	30%	4ml/min
25 min	70%	30%	4ml/min

4.3.3.2.2 Radiosynthesis of [^{18}F]FNA and C@1-K, C@5

The purified product from the HPLC fraction of [18F]FNA 4-nitrophenyl ester was extracted using an HLB cartridge (Oasis, 30 mg). Subsequently, the cartridge was flushed with 5 mL of water to eliminate any contaminants acquired from the hot cell tube. 0.4 ml of acetonitrile was utilised to remove the [^{18}F]FNA 4-nitrophenyl ester from the cartridge into a reaction vessel. The C@5 peptide (5 mg, 5.91 µmol) was combined with 450 µl of borate buffer (pH 8.6, 300 mM) and 150 µl of trace-select water in the reaction vessel to synthesise [18F]FNA-S-C@5. The ACN concentration was reduced, and the pH was restored to normal by adding 30 mM HCl to water and stirring the mixture by hand with a syringe after the liquid had been reacting for 10 minutes. The solution was placed in a syringe, introduced into an HPLC loop, and passed through a reversed-phase HPLC column identical to the previously utilised one. The mobile phase components used to purify [18F]FNA 4-nitrophenyl ester remained unchanged. The gradient program is presented in Table 5. The separation of [^{18}F]FNA-S-C@5 occurred around 25 minutes later, after which it was placed in a container. An identical procedure was done for C@1-K (5 mg, 5.54 µmol) in 350 µl of borate buffer (pH 8.6, 300 mM). The synthesis of [^{18}F]FNA-*N*-C@1-K was achieved via the aminolysis reaction between the ester and the amino group at the peptide's N-terminus. At 26 minutes, [^{18}F]FNA-*N*-C@1-K was observed to elute. An ascorbic acid solution was employed to

dilute [^{18}F]FNA-*N*-C@1-K, which was subsequently passed through a tC18 cartridge (Sep-Pak Plus Light) to capture the [^{18}F]FNA-*N*-C@1-K. A 1:1 mix of ethanol and 30 mM ascorbic acid in trace-select water was utilised to isolate the tC18 cartridge into the product vial.

Table 5. HPLC program for radiosynthesis of [^{18}F]FNA-*S*-C@5 and [^{18}F]FNA-*N*-C@1-K

Time after injection	ACN (0.1% TFA)	WATER (0.1% TFA)	FLOW RATE
0 min	0%	100%	1ml/min
1 min	0%	100%	4ml/min
5 min	0%	100%	4ml/min
20+ min	55%	45%	4ml/min

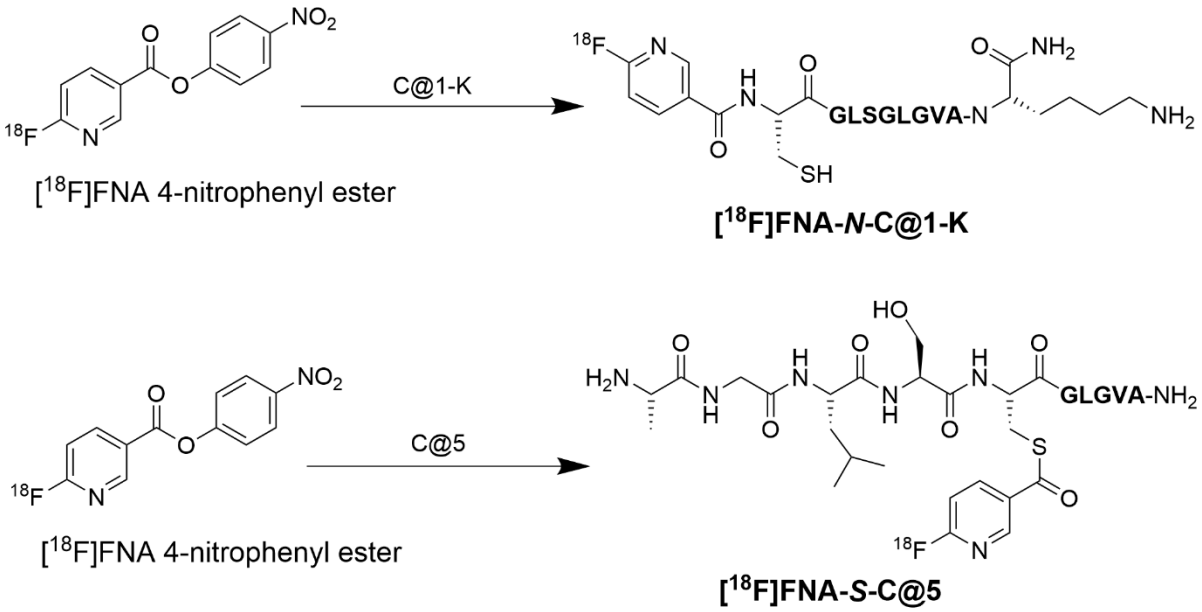

Figure 16. Radiosynthesis reactions

4.3.3.2.3 QUALITY CONTROL FOR [^{18}F]FNA AND C@1-K, C@5

Quality control included evaluating the confirmed presence of [^{18}F]FNA-*N*-C@1-K from the final product with that of commercial FNA-*N*-C@1-K through HPLC analysis. The retention durations (RT) of FNA-*N*-C@1-K and [^{18}F]FNA-*N*-C@1-K were assessed using an HPLC system fitted with a reverse-phase HPLC column. The column was followed up by radio-HPLC for the detection of FNA-*N*-C@1-K and [^{18}F]FNA-*N*-C@1-K, respectively. Table 6 outlines the HPLC protocol utilised. The product identity was established by confirming that FNA-*N*-C@1-K displayed a

consistent retention time, as indicated by UV absorbance, and that [^{18}F]FNA-*N*-C@1-K was validated using a radioactivity detector. The assessment of radiochemical purity involved analysing the chromatograms from the radioactivity detector for any additional peaks. A similar experiment was carried out for [^{18}F]FNA-*S*-C@5.

Table 6. HPLC program for quality control

Time after injection	ACN (0.1% TFA)	WATER (0.1% TFA)	FLOW RATE
0 min	23%	77%	1ml/min
12 min	42%	58%	1ml/min
13 min	70%	30%	1ml/min
14 min	23%	77%	1ml/min

4.3.3.2.4 Analysis of statistics and other calculations

The radiochemical purity of the formulated product was assessed using radio-HPLC. The decay-corrected radiochemical yield (RCY) is calculated by comparing the product's activity at the end of the synthesis to its activity at the start of the synthesis. All activities were adjusted for decay to align with the beginning of the synthesis. All reported RCYs have been adjusted for decay. The RCP and RCY are represented as percentages.
RCY was determined using Equation 1, where A_{EOS} represents the activity of the product after synthesis, adjusted for decay. A_S refers to the activities of the starting material.

The end of synthesis was adjusted for decay to align with the initial synthesis time, as described in Equation 2. A represents the activity decay corrected to time t, while A_0 denotes the activity at t = 0, and $T_{1/2}$ denotes the half-life of the radionuclide.

Equation 1 $RCY\% = A_{EOS} \div A_S$

Equation 2 $A = 2^{-t/T_{1/2}} * A_O$

The statistical analysis was done using Microsoft Excel. The mean and standard deviation are calculated for data with three or more sets; for data with two or fewer sets, only the mean is calculated. All data from HPLC were expressed using Microsoft Excel upon receiving the text file from Lab Solutions and EZ Chrome software.

5.0 RESULTS AND DISCUSSIONS

5.1 LC-MS/MS RESULTS

In the LC-MS/MS study of C@1-K and C@3, some side products with extra modifications were identified. These were also noticed during HPLC purification. The side products were isolated during purification, but the yield was too low for analysis with NMR. This opens up a discussion for further study, as it was also reported by Dillemuth (2024) that 1% of the product was *N-acylated* and 99% *S-acylated.*

FNA-*S*-C@3

The total ion chromatogram and the MS1 spectra for the main peaks are shown in Figure 17. The first peak matched to the peptide AGCLSGLGVA with C-terminus amidation, with a retention time of 12.05 mins. The aim was to confirm the modification at C3. The most confident spectra match to the modification +123.012 at C3 are shown in 13.69 minutes in Figure 17.

The molecular formula is $C_{41}H_{66}N_{12}O_{12}SF$ with an expected monoisotopic mass of 969.462. m/z = 969.462

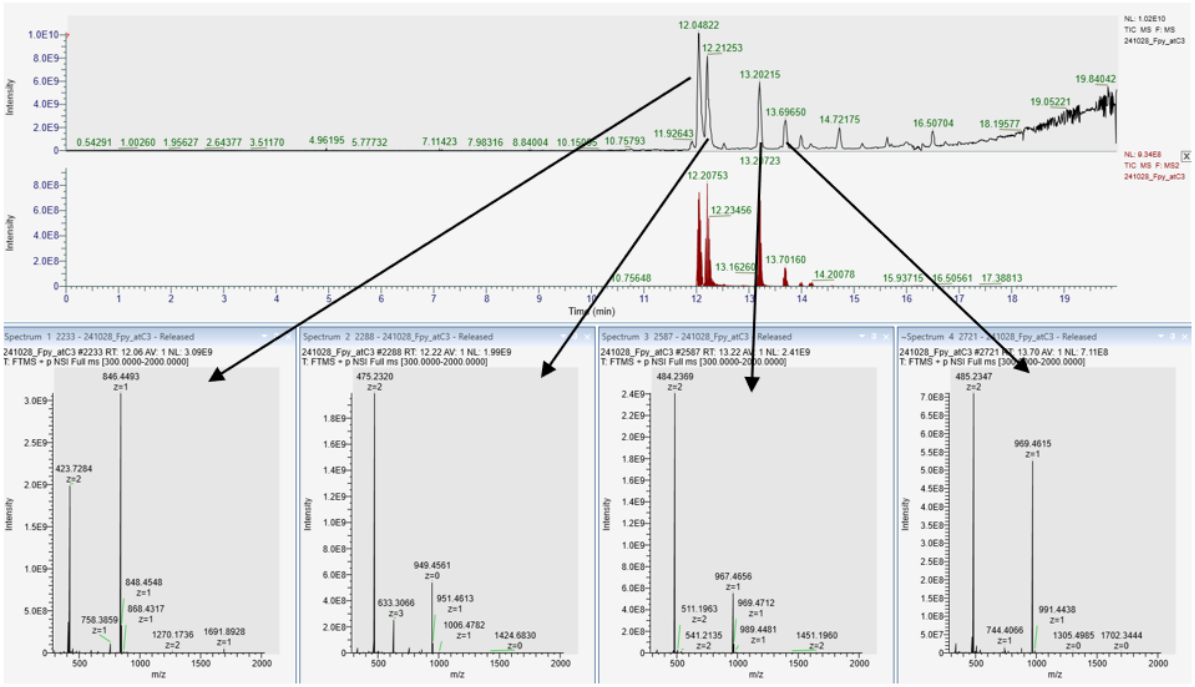

Figure 17. The total ion chromatogram and the MS1 spectra for the main peaks of the sample FNA-*S*-C@3

FNA-*S*-C@4

The theoretical singly charged and doubly charged monoisotopic ions for the peptide AGLCSGLGVA are m/z 846.450 and m/z 423.729, respectively. The theoretical singly charged and doubly charged monoisotopic ions for the amidated peptide with the Fpy modification (+123.012 Da) are m/z 969.462 and m/z 485.235, respectively. The first peak matched to the peptide AGLCSGLGVA with C-terminus amidation, with a retention time of 10.53 mins. The expected modification peak was eluted at 12.19 mins. The molecular formula is $C_{41}H_{66}N_{12}O_{12}SF$ with an expected monoisotopic mass of 969.462. m/z = 969.462

The total ion chromatogram and the MS1 spectra for the main peaks are shown in Figure 18.

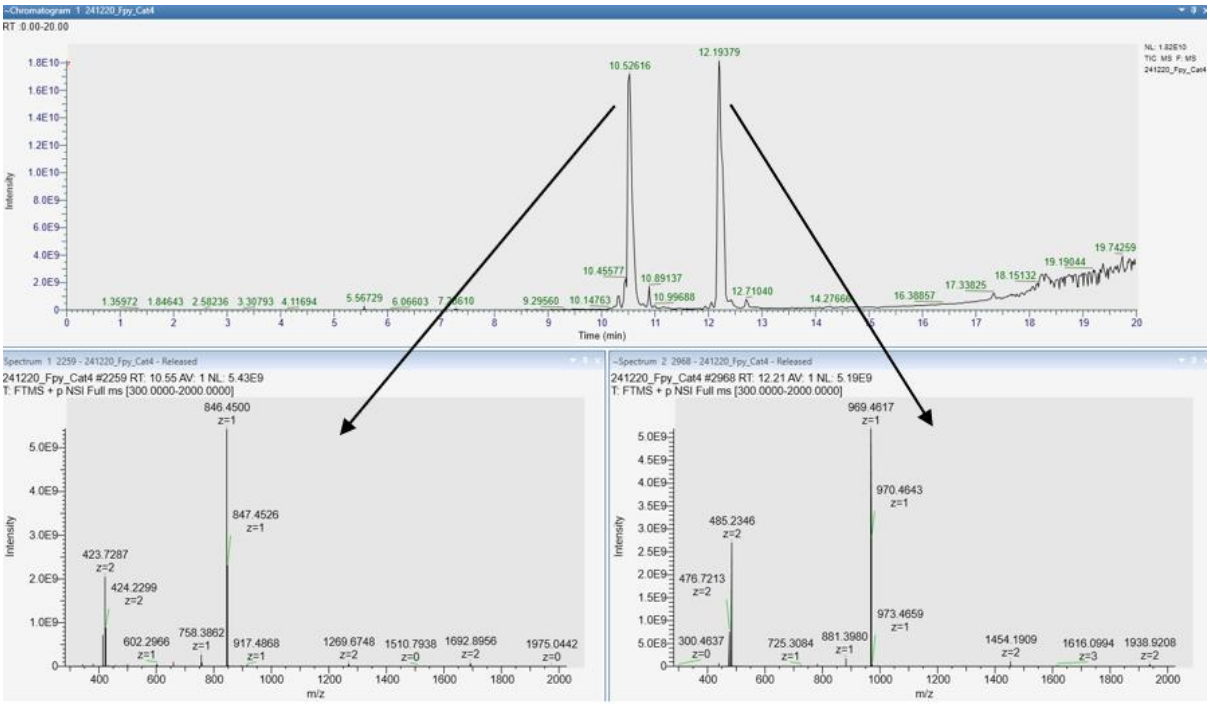

Figure 18. The total ion chromatogram and the MS1 spectra for the main peaks of the sample FNA-*S*-C@4

FNA-*S*-C@5

The theoretical singly charged and doubly charged monoisotopic ions for the amidated peptide are m/z 846.450 and m/z 423.729, respectively. The theoretical singly charged and doubly charged monoisotopic ions for the amidated peptide with the Fpy modification (+123.012 Da) are m/z 969.462 and m/z 485.235, respectively.The first peak matched to the peptide AGLSCGLGVA with

C-terminus amidation, with a retention time of 10.42 mins. The expected modification peak was eluted at 12.11 mins. The molecular formula is $C_{41}H_{66}N_{12}O_{12}SF$ with an expected monoisotopic mass of 969.462. m/z = 969.462

The total ion chromatogram and the MS1 spectra for the main peaks are shown in Figure 19. The main peaks in the chromatogram match well with the expected theoretical ions.

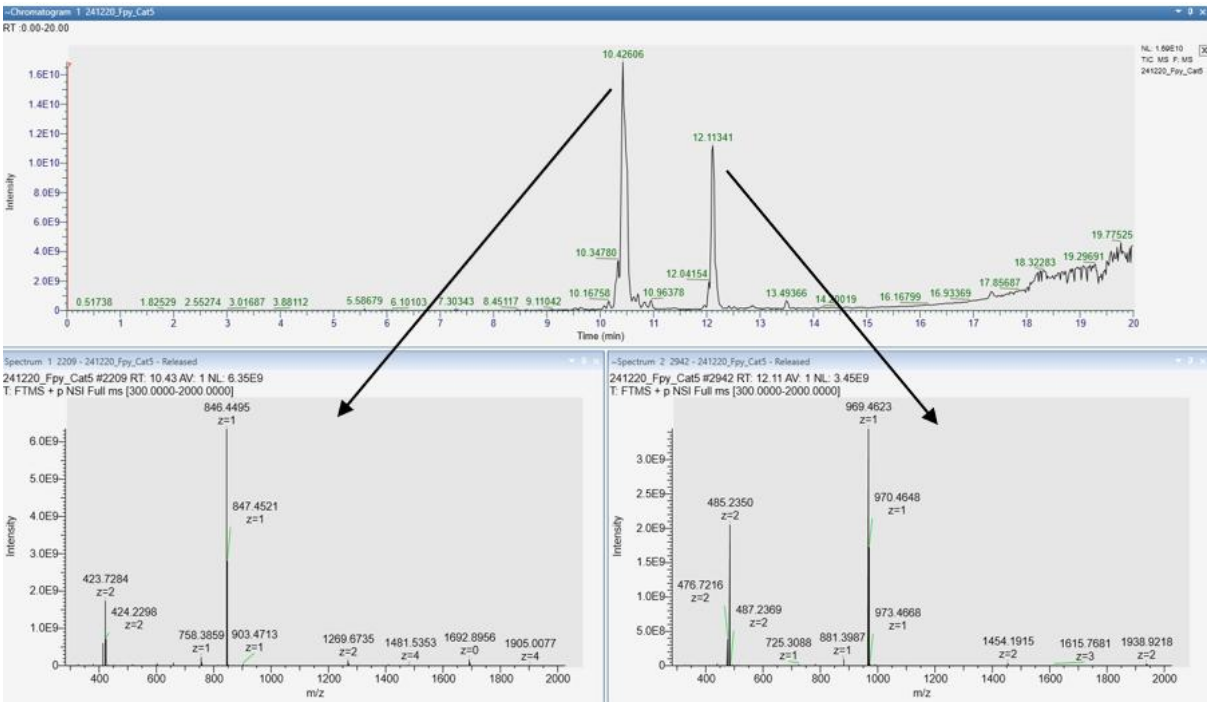

Figure 19. The total ion chromatogram and the MS1 spectra for the main peaks of the sample FNA-*S*-C@5

FNA-*N*-C@1-K

The theoretical singly charged and doubly charged monoisotopic ions for the amidated peptide are m/z 903.508 and m/z 452.258, respectively. The theoretical singly charged and doubly charged monoisotopic ions for the amidated peptide with the Fpy modification (+123.012 Da) are m/z 1026.520 and m/z 513.764, respectively.

The first peak matched to the peptide CGLSGLGVAK, with a retention time of 9.06 mins. The expected modification peak was eluted at 12.24 mins. The molecular formula is $C_{41}H_{66}N_{12}O_{12}SF$ with an expected monoisotopic mass of 1026.196. m/z = 1026.013

The total ion chromatogram and the MS1 spectra for the main peaks are shown in Figure 20. The sample is moderately complex, showing several peaks in the total ion chromatogram. Both expected forms (amidated and amidated with the Fpy modification) were identified.

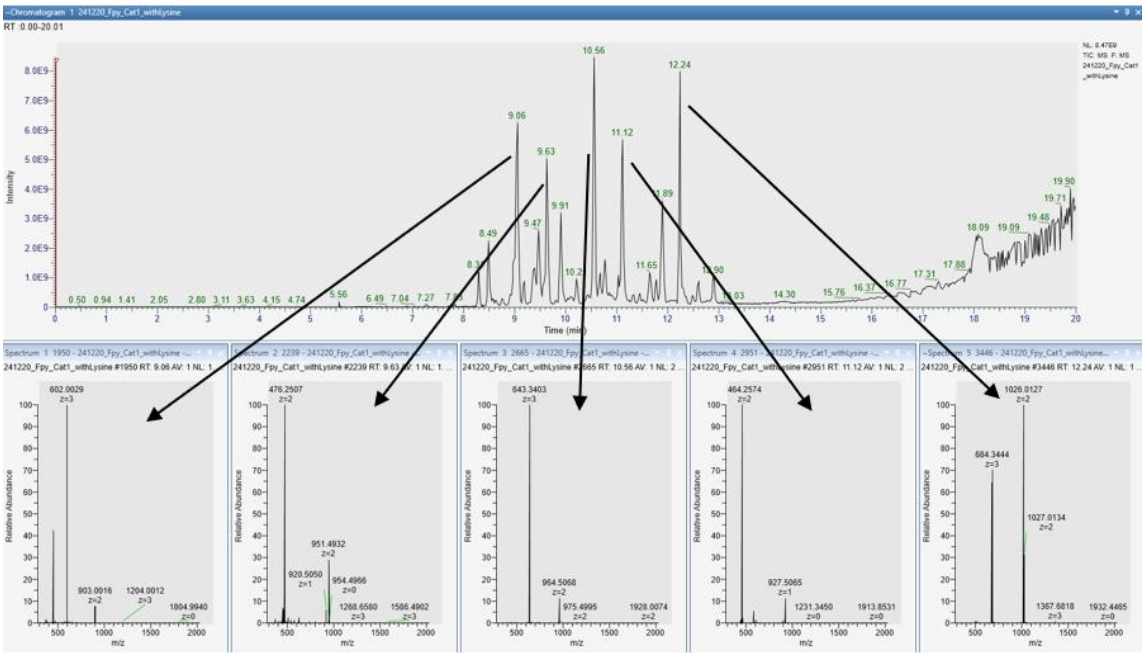

Figure 20. The total ion chromatogram and the MS1 spectra for the main peaks of the sample FNA-*N*-C@1-K

5.2 NMR RESULTS

The high chemoselectivity was proven by studying the conjugation of the prosthetic group and variants of the peptide used by Dillemuth et al. (2024). In this study, the four peptides underwent all analyses, ranging from LC-MS/MS, radiosynthesis, and NMR for structure and characterisation. The NMR results after analysing the four peptides confirmed the following: C@3, C@4, and C@5 were *S-acylated,* while C@1-K was *N-acylated.* The position of the cysteine in the peptide sequence and the intermediate ring formed in the transition state serve as the most important factors in the conjugation of these radiopharmaceuticals. Even further proving the proposed regioselectivity, a lysine was included in one of the peptides. Lysine has a primary amino group in the side chain, which could react with the activated label as well. However, the conjugation still preferred cysteine. This confirmed the regioselectivity, which means that an adjacent sulfhydryl group can promote *N*-acylation. In a case where an adjacent sulfhydryl is absent, the *N*-acylation is slow. It is also worth noting that the analysis reveals that FNA-*N*-C@1-K, both in-house and

commercial, are not entirely pure products. However, the product was observed to be *N*-acylated in cysteine; the impurity is not known and would be further investigated.

FNA-*S*-C@3

δ^1H (600 MHz; DMSO-*d*6) 0.80 (3 H, br, Me (Val)),0.82 (3 H, d, Me (Leu)), 0.83 (3 H, d, Me (Leu)), 0.84 (3 H, br, Me (Val)), 0.87 (6 H, d, Me (Leu)), 1.20 (3 H, d, Me (Ala2)),1.23(2 H, br, CH_2(Leu 1β)), 1.30 (3 H, d, Me (Ala1)), 1.48(2 H, m, CH_2(Leu 2β)) , 1.58(2 H, m, CH(Leuγ)) , 1.97(1 H, m, CH(Valβ)), 3.31(1 H, d, CH_2 (Cysβ), 3.48(1 H, d, CH_2 (Cysβ), 3.55(1 H, dd, CH_2 (Serβ), 3.6(1 H, m, CH_2 (Serβ), 3.74 (2 H, dd, CH(Gly 1α), 3.75(2 H, dd, CH (Gly 2α), 3.76(1 H, dd, CH (Ala1α)), 3.81 (2 H, br, CH (Gly 3α), 4.15 (1 H, d, CH (Valα), 4.19(1 H, m, CH (Ala2α)), 4.25(1 H, m, CH (Serα)), 4.29(1 H, m, CH (Leu1α)), 4.38(1 H, m, CH (Leu 2α)), 4.64(1 H, m, CH (Cysα)), 5.05 (1 H, br, (SerOH)), 6.96 (1 H, s, $CONH_2$ (Ala2), 7.20 (1 H, s, $CONH_2$ (Ala2) ,**7.40** (1 H, dd, **5-H Fpy),** 7.74 (1 H, d, NH (Val)),7.78 (1 H, d, NH (Gly 3)),7.97 (1 H, d, NH (Leu 1),7.99 (2 H, d, NH (Ala 2), 8.00 (2 H, m, NH(Ala1)) , 8.13 (1 H, t, NH (Gly1), 8.17 (1 H, m, NH (Leu 2) 8.24 (1 H, d, NH (Gly 2), 8.35 (1 H, d, NH (Ser), 8.41(1 H, d, NH (Cys) , **8.45**(1 H, dt, **4-H (Fpy))**, **8.78** (1 H, d, **2-H (Fpy))**. δ^{13}C(125 MHz; DMSO-*d*6)17.69 Me(Val), 18.00 Me(Ala2), 18.16 Me(Ala1), 19.13 Me(Val), 21.56 Me(Leu), 23.09 Me(Leu), 24.02 Me(Leu), 24.10 Me(Leuγ), 28.96 Cβ(Leu1) , 30.47 Cβ(Val), 30.80 Cβ(Cys), 30.81 Cβ(Cys), 40.63 Cβ(Leu2), 41.78 Cα(Gly), 42.10 Cα(Gly), 47.84 Cα(Ala1) , 48.60 Cα(Gly), 49.39 Cα(Ala2), 51.03 Cα(Leu1), 51.20 Cα(Leu2), 51.62 Cα(Cys), 55.15 Cα(Ser), 57.50 Cα(Val), 61.59 Cβ(Ser), **110.46 (d, 5-C(Fpy)) , 131.72 (d, 3-C(Fpy)), 141.24 (d, 4-C(Fpy)), 146.99 (d, 2-C(Fpy)), 164.78 (d, 6-C(Fpy)),** 168.23 (CO(Gly)), 168.29 (CO(Gly)), 169.83 (CO(Gly)),169.91 (CO(Cys)),169.95 (CO(Ala2)),169.98 (CO(Ser)), 170.09(CO(Ala1)), 171.14 (CO(Val)), 171.34(CO(Leu1)), 171.43 (CO(Leu2)), **189.01 (CO(Fpy).**

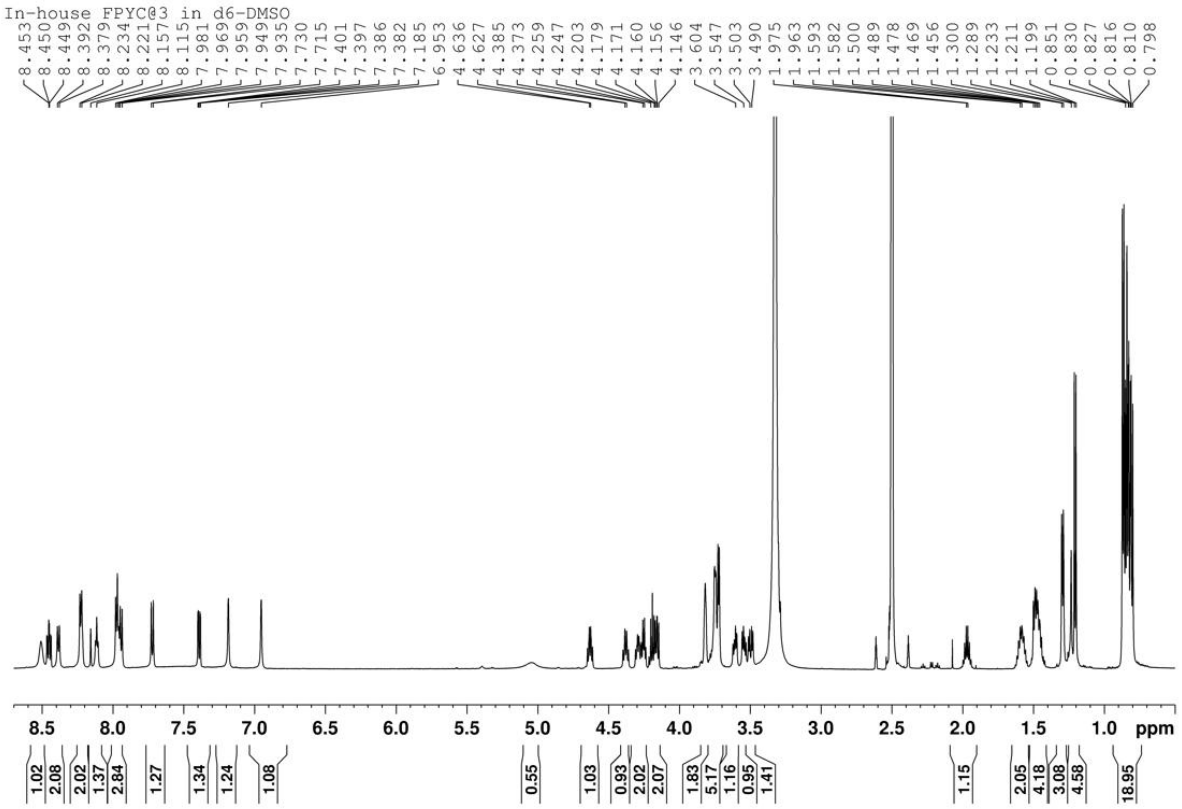

Figure 21. ^{1}H NMR spectrum of in-house made [^{19}F]FNA-*S*-C@3

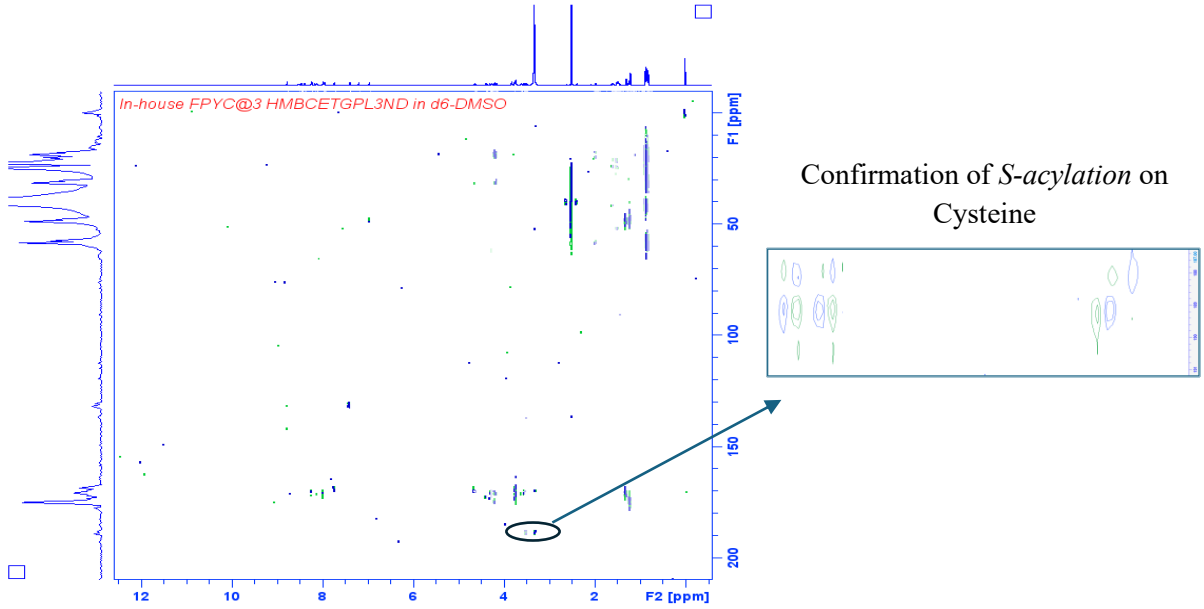

Figure 22. HMBC spectrum of in-house made [^{19}F]FNA-*S*-C@3

FNA-*S*-C@4

δ^1H (600 MHz; DMSO-*d*6) 0.80 (3 H, d, Me (Val)), 0.81 (3 H, d, Me (Val)), 0.82 (3 H, d, Me (Leu)), 0.84 (3 H, d, Me (Leu)), 0.86 (6 H, d, Me (Leu)), 1.21 (3 H, d, Me (Ala2)), 1.34 (3 H, d, Me (Ala1)), 1.45 (4 H, m, CH_2(Leu 1,2β)), 1.58 (2 H, m, CH(Leuγ)), 1.97 (1 H, m, CH(Valβ)) ,3.32 (1 H, br, CH_2 (Cysβ)), 3.52 (1 H, m, CH_2 (Cysβ)), 3.55 (1 H, m, CH_2 (Serβ) ,3.62 (1 H, m, CH_2 (Serβ), 3.74-3.83 (6 H, d, CH(Glyα), 3.87 (1 H, br, CH(Ala1α)), 4.15 (1 H, d, CH (Valα), 4.20 (1 H, d, CH (Ala2α)), 4.25 (1 H, m, CH(Serα))4.27 (1 H, m, CH (Leu1α)), 4.30 (1 H, m, CH (Leu2α)), 4.60 (1 H, m, CH (Cysα)), 5.05 (1 H, t, (SerOH)), 6.96 (1 H, s, $CONH_2$ (Ala2), 7.20 (1 H, s, $CONH_2$ (Ala2), **7.40 (1 H, dd, 5-H(FPy)),** 7.74 (1 H, d, NH (Val), 7.80 (2H, m, NH (Ala 1), 7.97 (1 H, d, NH(Ser)), 8.00 (1 H, m, NH (Leu 1), 8.17 (1 H, m, NH (Gly 1),8.19 (1 H, dd, NH (Gly2) ,8.24 (1 H, dd, NH (Gly3), 8.36 (1 H, d, NH (Leu 2), **8.45**(1 H, dt, **4-H(Fpy)),** 8.56 (2 H, br, NH (Ala 2), NH (Cys)),**8.78** (1 H, d, **2-H (Fpy))**. δ^{13}C(125 MHz; DMSO*d*6)17.06 Me(Ala1), 17.74 Me(Val) , 17.94 Me(Ala2), 19.02 Me(Leu), 21.44 Me(Val), 22.85 Me(Leu), 23.95 Me(Leu), 23.97 Me(Leuγ), 30.46 Cβ(Val), 30.81 Cβ(Cys), 40.72 Cβ(Leu 1,2) , 41.51 Cα(Gly1), 41.95 Cα(Gly2,3), 47.79 Cα(Ala2) , 48.08 Cα(Ala1), 50.91 Cα(Leu 2) , 51.36 Cα(Cys), 51.75 Cα(Leu2),55.14 Cα(Ser),57.42 Cα(Val),61.59 Cβ(Ser) , **110.25 (d, 5-C(Fpy)) , 130.9 (d, 3-C(Fpy)) , 140.94 (d, 4-C(Fpy)), 147.05 (d, 2-C(Fpy))** , **164.71 (d, 6-C(Fpy)) ,** 167.94(CO(Gly1)), 167.93(CO(Gly2)), 168.54(CO(Gly3)),169.30 (CO(Cys)), 169.62 (CO(Ala1)) ,170.18 (CO(Ser)), 170.30 (CO(Val)),171.73 (CO(Leu2)), 172.27(CO(Leu1)),174.01(CO(Ala2)),**188.16(CO(Fpy).**

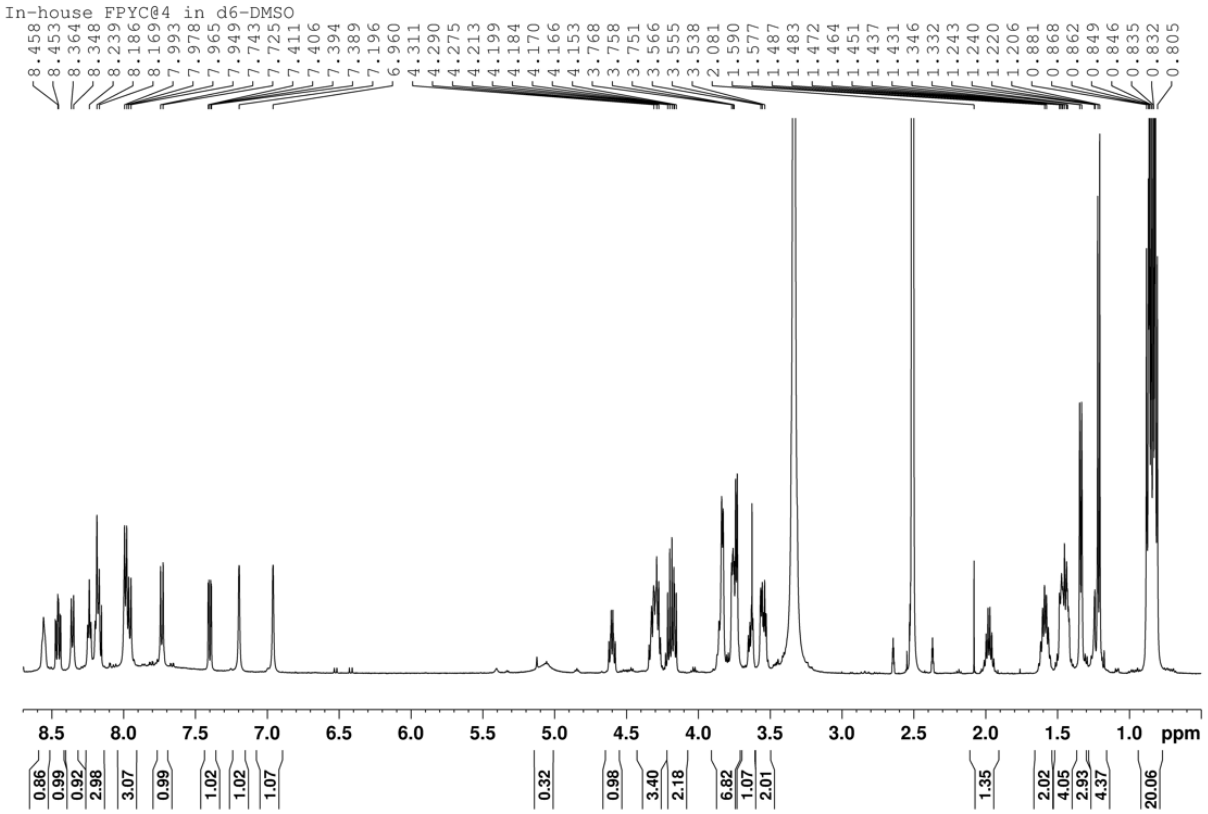

Figure 23. ^{1}H NMR spectrum of in-house made [^{19}F]FNA-*S*-C@4

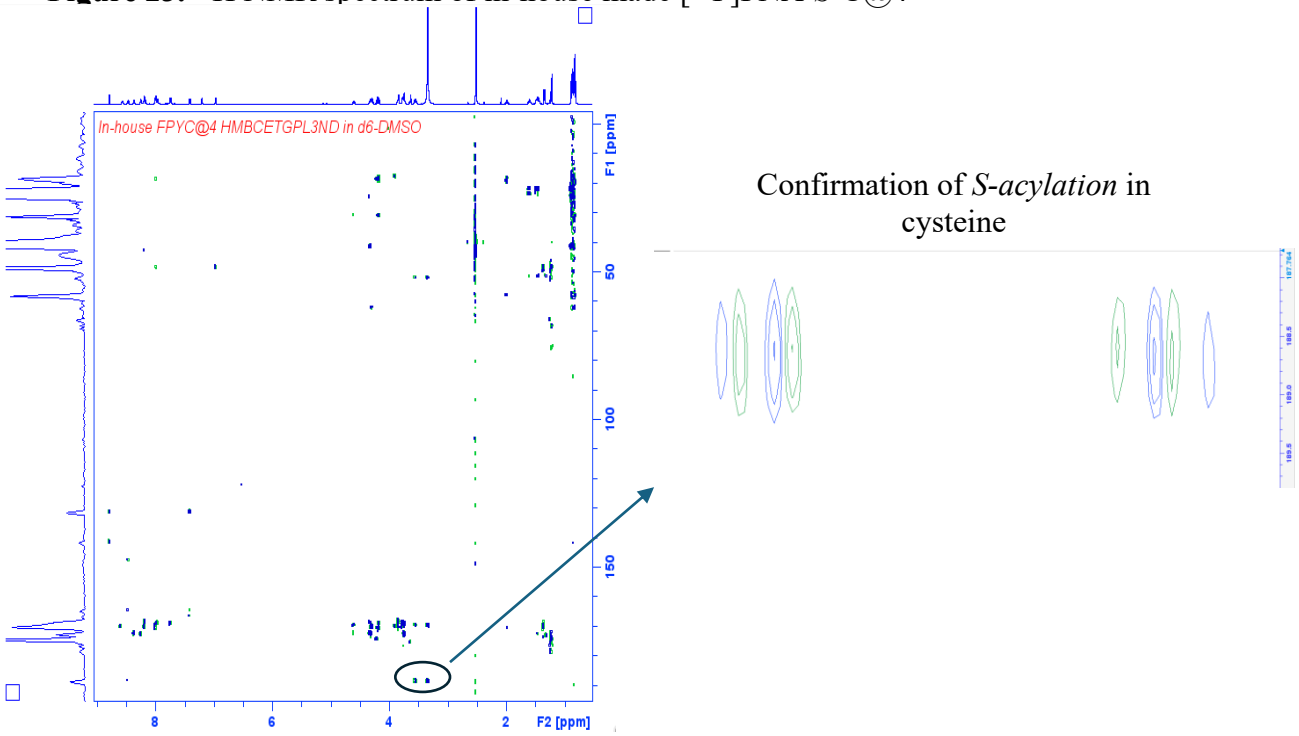

Figure 24. HMBC spectrum of in-house made [^{19}F]FNA-*S*-C@4

FNA-*S*-C@5

δ^1H (600 MHz; DMSO-*d*6) 0.80 (3 H, d, Me (Val)), 0.82 (3 H, d, Me (Leu)), 0.83 (3 H, d, Me (Leu)), 0.84 (3 H, br, Me (Val)), 0.86 (6 H, d, Me (Leu)), 1.23 (3 H, dd, Me (Ala2)), 1.35 (3 H, br, Me (Ala1)), 1.45 (4 H, m, CH_2(Leu 1,2β)), 1.58 (2 H, m, CH(Leuγ)), 1.97 (1 H, m, CH(Valβ)) ,3.31 (1 H, br, CH_2 (Cysβ), 3.56 (1 H, d, CH_2 (Cysβ), 3.59 (1 H, m, CH_2 (Serβ),3.64(1 H, br, CH (Ala1α)),3.66 (1 H, m, CH_2 (Serβ), 3.73-3.81 (6 H, d, CH(Glyα), 4.15 (1 H, m, CH (Valα), 4.18 (1 H, m, CH (Ala2α)), 4.28 (1 H, m, CH(Serα)),4.30 (1 H, m, CH (Leu2α)),4.38 (1 H, q, CH (Leu1α)), 4.56 (1 H, q, CH (Cysα)), 5.05 (1 H, br, (SerOH)), 6.96 (1 H, s, $CONH_2$ (Ala2), 7.20 (1 H, s, $CONH_2$ (Ala2), **7.39 (1 H, dd, 5-H(FPy)),** 7.74 (1 H, d, NH (Ala 2), 8.00 (2 H, d, NH (Val), NH(Leu1)), 8.05(1H, d, NH (Ala1)) ,8.06 (1 H, d, NH (Leu2), 8.11(1 H, d, NH(Ser)), 8.23 (1 H, m, NH (Cys); 1 H, m, NH (Gly2)), 8.26 (1 H, t, NH (Gly1) , 8.37 (1 H, br, NH(Gly3)),**8.43**(1 H, dt, **4-H(Fpy)),8.75** (1 H, d, **2-H (Fpy)**). δ^{13}C(125 MHz; DMSO-*d*6)17.07 Me(Ala1), 17.66 Me(Val) ,18.94 Me(Val), 21.35 Me(Leu), 22.79 Me(Leu), 22.83 Me(Leu), 23.77 Me(Leuγ), 28.53 Me(Ala2), 30.36 Cβ(Val), 30.65 Cβ(Cys), 40.72 Cβ (Leu 1,2), 41.59 Cα(Gly), 41.82 Cα(Gly), 47.75 Cα(Ala2) , 50.57 Cα(Leu2), 50.80 Cα(Leu2), 51.36 Cα(Cys), 54.80 Cα(Ser),57.34 Cα(Val),60.99 Cβ(Ser) , **110.24 (d, 5-C(Fpy)), (d, 6-C(Fpy)) ,131.89 (d, 3-C(Fpy)) , 140.87 (d, 4-C(Fpy)), 146.58 (d, 2C(Fpy))**, 169.16(CO(Gly)), 169.58(CO(Gly)), 168.93 (CO(Gly)),168.84 (CO(Cys)), 169.57(CO(Ser)), 171.33 (CO(Leu1)), 171.54 (CO(Leu2)), 169.73 (CO(Ala2)), 173.12(CO(Ala1)), **188.97 (CO(Fpy).**

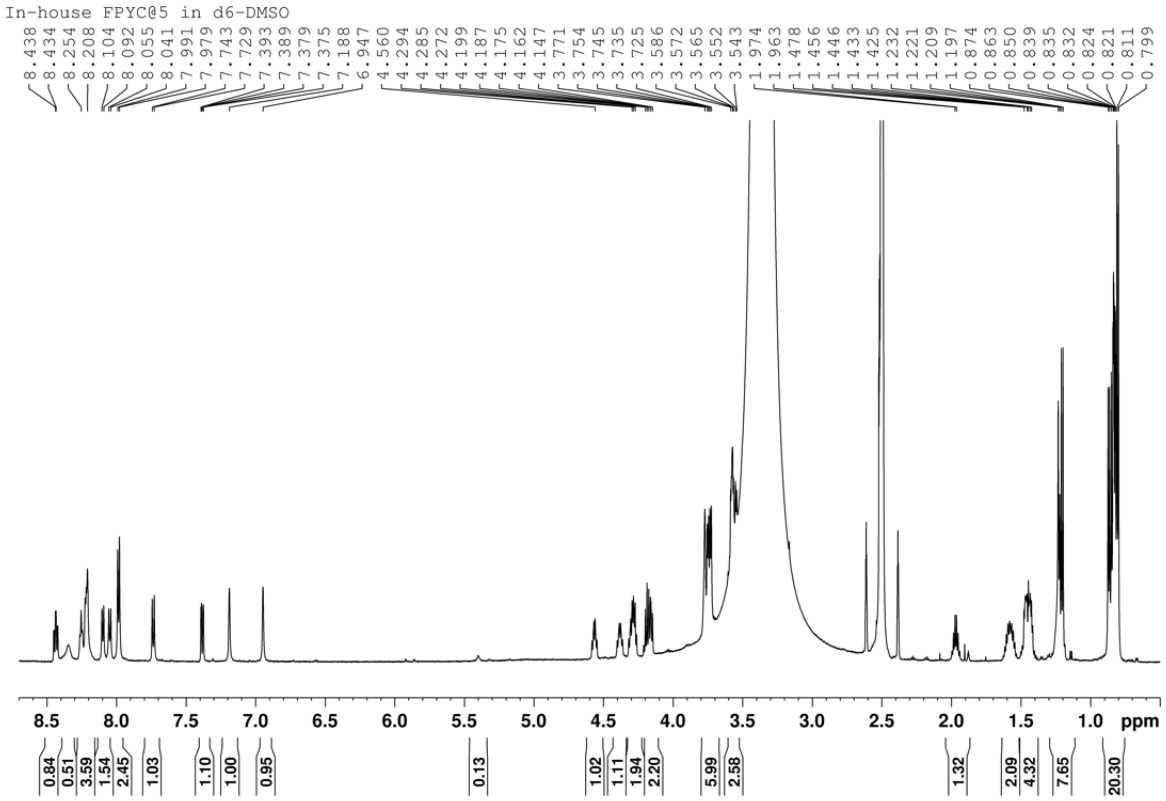

Figure 25. ^{1}H NMR spectrum of in-house made [^{19}F]FNA-*S*-C@5

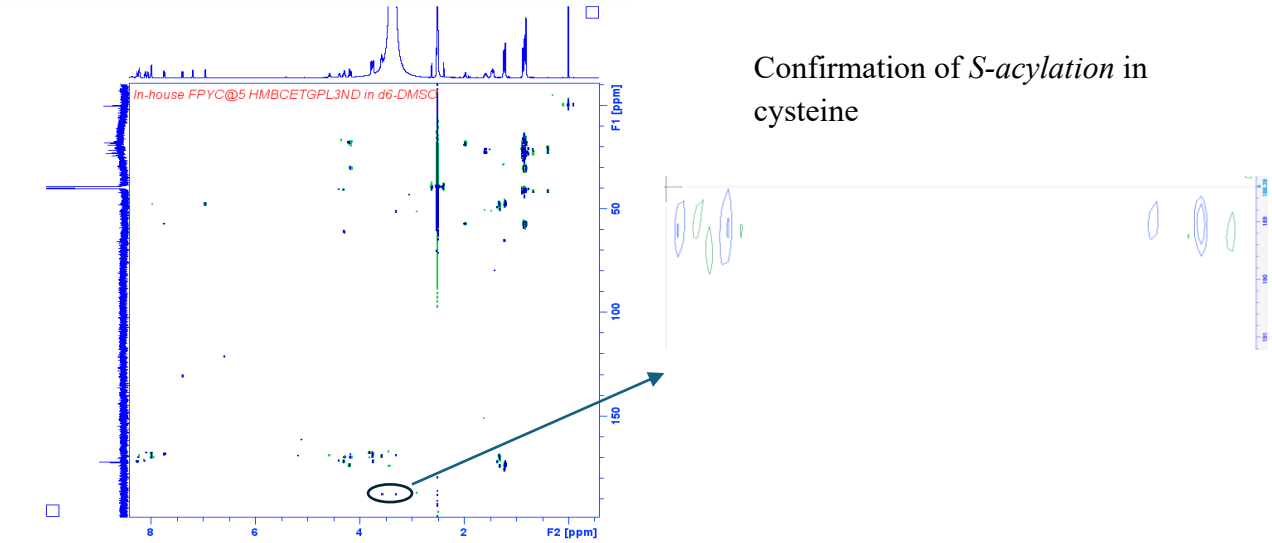

Confirmation of *S-acylation* in cysteine

Figure 26. HMBC spectrum of in-house made [^{19}F]FNA-*S*-C@5

FNA-*N*-C@1-K

δ^1H (600 MHz; DMSO-*d*6) 0.81 (3 H, d, Me (Val)), 0.82 (3 H, d, Me (Leu)), 0.83 (3 H, br, Me (Leu)), 0.84 (3 H, m, Me (Val)), 0.87 (6 H, d, Me (Leu)), 1.21 (3 H, d, Me (Ala)), 1.24 (2 H, d, CH_2(Lys)) 1.28 (2 H, m, CH_2(Lys)), 1.46 (4 H, m, CH_2(Leu 1,2β)), 1.50 (2 H, d, CH_2(Lys)) 1.58 (2 H, m, CH(Leuγ)), 1.65 (2 H, br, CH_2(Lys)) 1.97 (1 H, m, CH(Valβ)) ,2.83 (1 H, m, CH_2 (Cysβ), 2.95 (1 H, m, CH_2 (Cysβ), 3.51 (1 H, m, CH_2 (Serβ) ,3.59 (1 H, m, CH_2 (Serβ), 3.73-3.78 (6 H, m, CH(Glyα)),4.14 (1 H, d, CH (Valα), 4.18 (1 H, d, CH (Alaα)), 4.22 (1 H, m, CH (Lysα)), 4.25 (1 H, m, CH(Serα)),4.27 (1 H, m, CH (Leu2α)),4.40 (1 H, br, CH (Leu1α)), 4.56 (1 H, m, CH (Cysα)),5.05 (1 H, br, (SerOH)), 7.07 (1 H, s, $CONH_2$ (Ala), 7.22 (1 H, s, $CONH_2$ (Ala), **7.33 (1 H, dd, 5-H(FPy)),** 7.68 (1 H, d, NH (Ala)), 7.70 (1 H, m, NH (Val), 7.78 (2 H, d, NH (Lys)), 7.90(1 H, m, NH (Leu1)) ,8.05(1 H, m, NH(Ser)), 8.14 (1 H, d, NH (Leu2)), 8.20 (1 H, dd, NH (Gly2)), 8.26 (1 H, m, NH (Gly1), 8.37 (1 H, m, NH(Gly3)), **8.45**(1 H, dt, **4-H(Fpy))** **8.76** (1 H, dd, **2-H (Fpy)),** 8.90 (1 H, d, NH (Cys)). δ^{13}C (125 MHz; DMSO-*d*6)17.69 Me (Ala), 17.83 Me (Val), 18.99 Me (Val), 21.36 Me (Leu), 21.94 Cβ (Lys), 22.95 Me (Leu), 23.83 Me (Leuγ), 26.83 Cβ(Lys), 28.56 Cβ(Lys),30.34 Cβ(Val), 31.41 Cβ(Lys), 38.57 Cβ(Cys), 40.61 Cβ (Leu 1,2), 47.29 Cα(Ser), 49.79 Cβ(Cys), 41.78 Cα(Gly), 42.10 Cα(Gly), 48.60 Cα(Gly), 50.64 Cα(Leu1),51.02 Cα(Leu2), 51.77 Cα(Val), 55.07 Cα(Lys), 56.21 Cα(Cys), 57.43 Cα(Ala), 61.49 Cβ(Ser), **109.22 (d, 5-C(Fpy)) ,127.48 (d, 3-C(Fpy)), 141.18 (d, 4-C(Fpy)), 141.64 (d, 6-C(Fpy)), 147.70 (d, 2-C(Fpy)), 164.60 (CO(Fpy),** 168.18 (CO(Gly)), 168.19 (CO(Gly)), 169.90 (CO(Gly)),169.95 (CO(Lys)**),** 170.34 (CO(Ala)), 171.53 (CO(Ser)),171.88(CO(Leu1)), 172.04(CO(Leu2)), 172.02(CO(Cys)), 173.04 (CO(Val)).

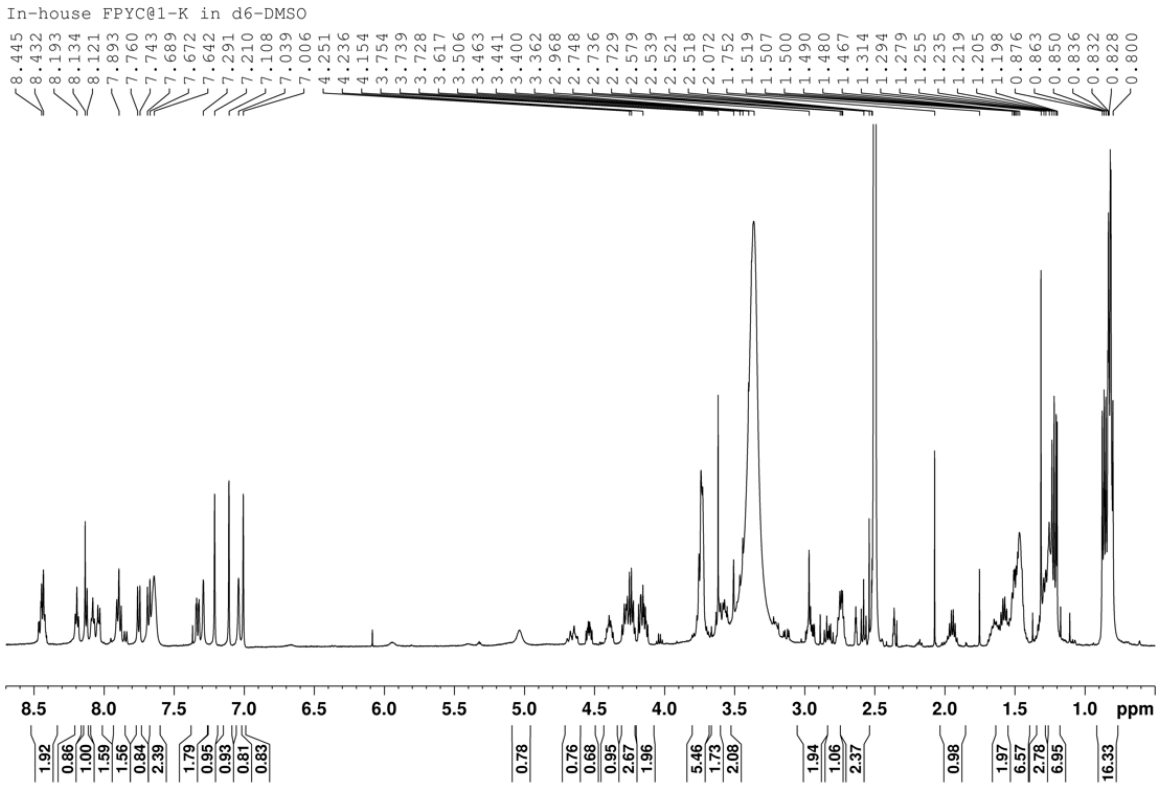

Figure 27. ^{1}H NMR spectrum of in-house made [^{19}F]FNA-*S*-C@1-K

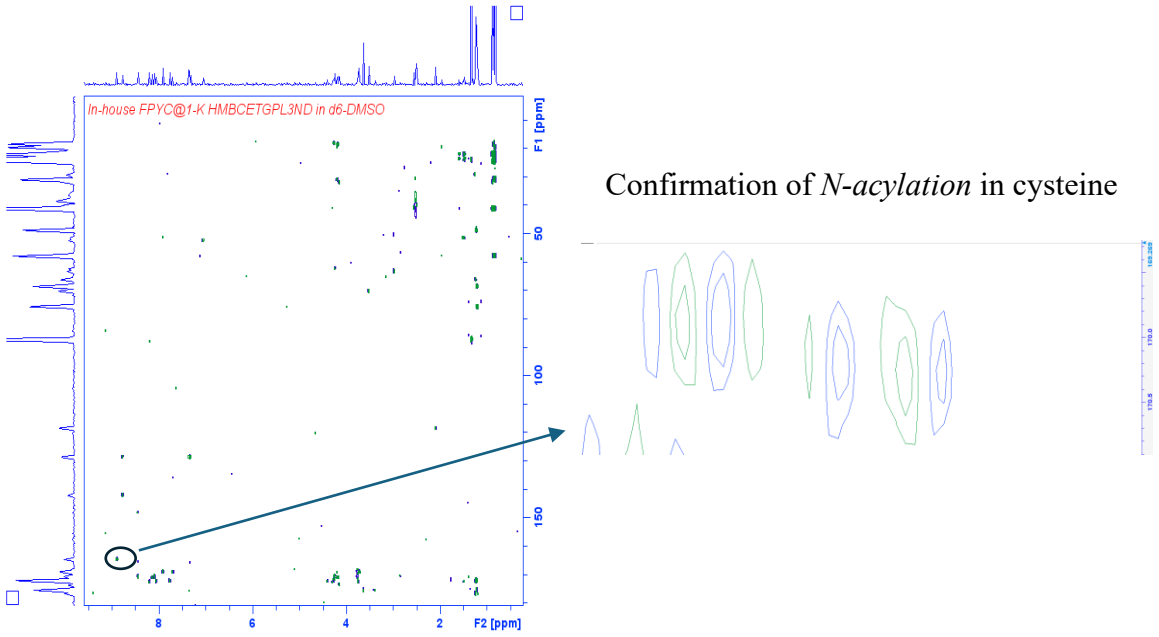

Figure 28. HMBC spectrum of in-house made [^{19}F]FNA-*N*-C@1-K

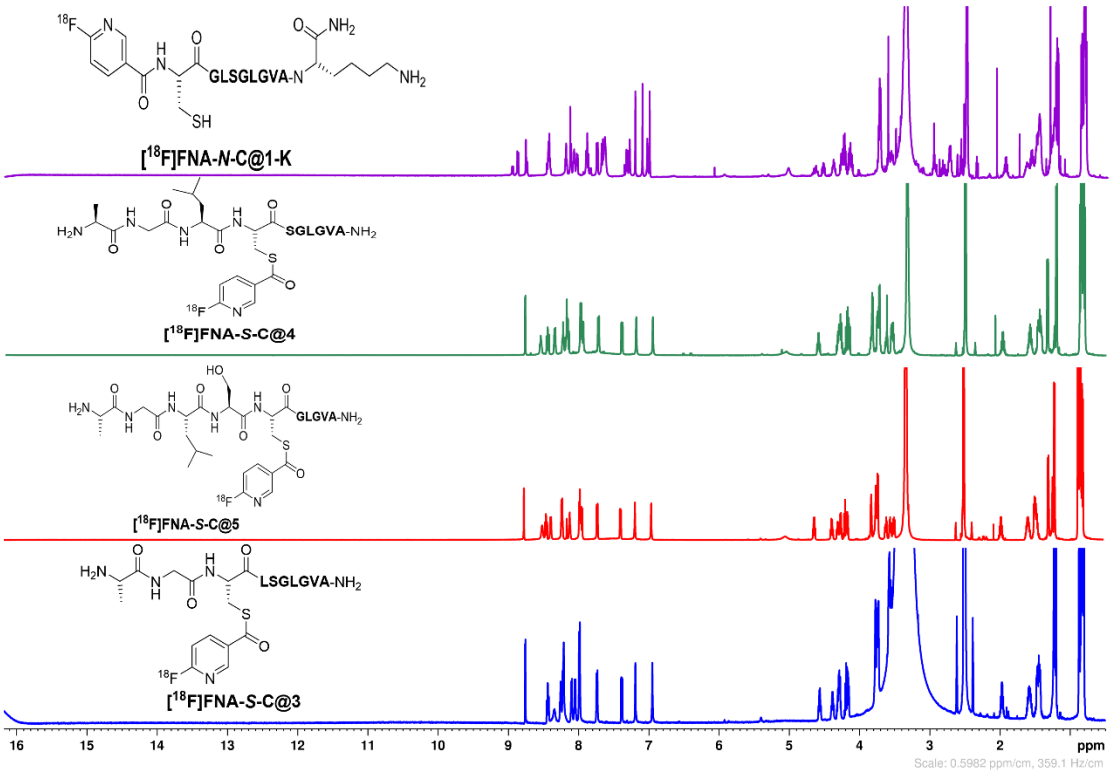

Figure 29. Stacked ^{1}H NMR results of all peptides conjugated with FNA

5.1 RADIOSYNTHESIS

In literature, the acylation of sulfhydryl *(S-acylation)* with activated esters of [^{18}F]FNA had not been noted in the conjugation of peptides, proteins, and antibodies with various prosthetic groups in radiopharmaceutical chemistry until the published results by Dillemuth et al in 2024. This served as the basis for this study, which entails understanding the underlying mechanism that has occurred. The proposed hypothesis involves the cysteine's intramolecular reaction or acyl migration that possesses both a sulfhydryl and an amino reaction site. The qualitative and quantitative analysis of the radiosynthesis of this thesis was done in two parts, C@5 and C@1-K, in a total of 5 syntheses. The first three syntheses involved the conjugation of [^{18}F]FNA-*S*-C@5, and the activity at the beginning of the synthesis was recorded as 7.5 ± 1.2 GBq (n=3). The activity of the product was calculated to be 266.3 ± 131.1 MBq, and the total synthesis time was recorded as 210.7 ± 25.7 minutes. The radioactivity recorded at the beginning of the synthesis and the activity of the final

product were decay corrected to the same time frame, and the RCY was recorded as 14.4 ± 7.4% (n=3). The molar activity was not measured yet in this study, which will be done in the near future.

The QC of the product was done using the HPLC with the solution of the product containing less than 1 MBq of radioactivity. The chromatogram is seen in Figure 18; the radiochemical purity is >98% (98.5 % ± 1.3, n=3), which was observed in all three syntheses conducted. The cold reference for the [^{18}F]FNA-*S*-C@5 was not analysed, as the MS confirmed that only one product was formed, and the NMR confirmed the acylation of the final product.

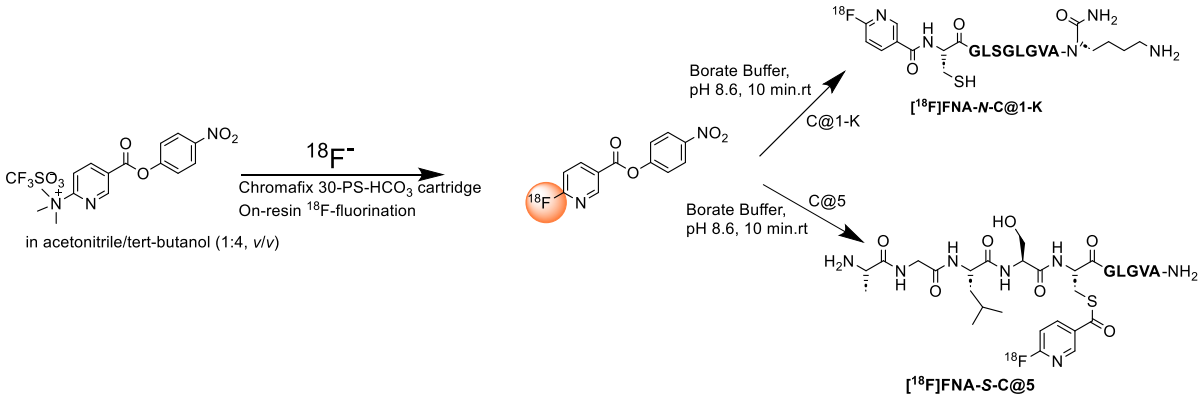

Figure 30. Radiosynthesis of [^{18}F]FNA-*S*-C@5 and [^{18}F]FNA-*N*-C@1-K

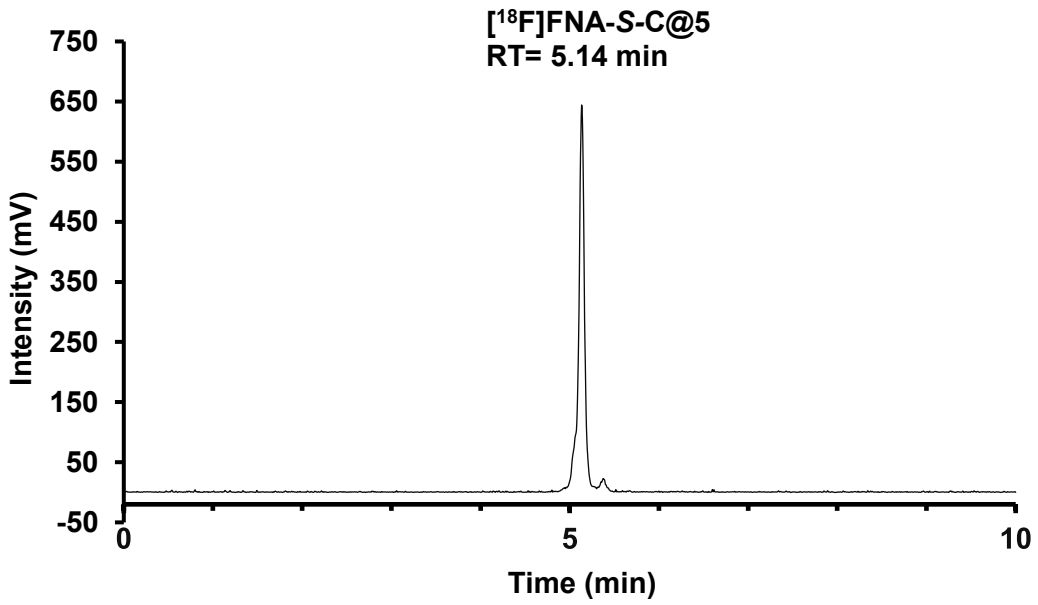

Figure 31. QC of [^{18}F]FNA-*S*-C@5

Two radiosyntheses were carried out for [^{18}F]FNA-*N*-C@1-K, and radioactivity at the start of the synthesis was 9.13 GBq (mean of two). The mean of the two products was recorded as 207 MBq. The total synthesis time recorded was 174.5 minutes. The radioactivity recorded at the beginning of the synthesis and the activity of the final product were decay corrected to the same time frame, and the RCY was recorded as 6.4% (n=2).

The QC of the product was done using the HPLC with the solution of the product containing less than 1 MBq of radioactivity. The chromatogram is seen in Figure 19; the radiochemical purity is > 98%, which was observed in the two syntheses conducted. The cold reference (Commercial standard) was also first spiked with the radioactive in-house compound made, and they were eluted around the same time, with a difference of more than 0.03 minutes, which confirmed the similarity of the main products of the cold reference (non-radioactive product) and the main radioactive product.

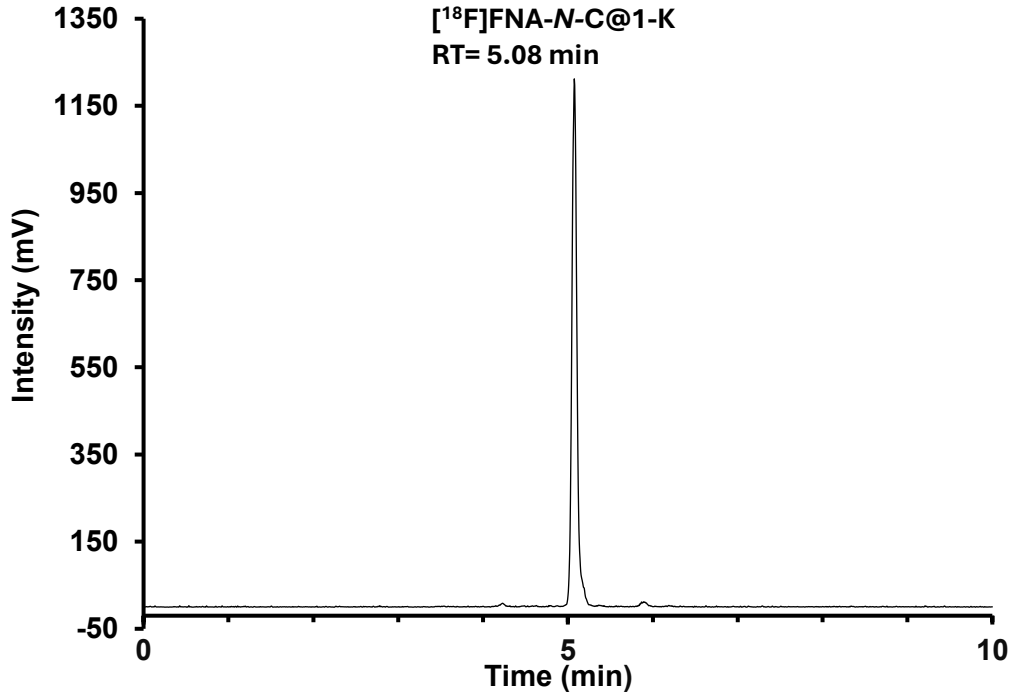

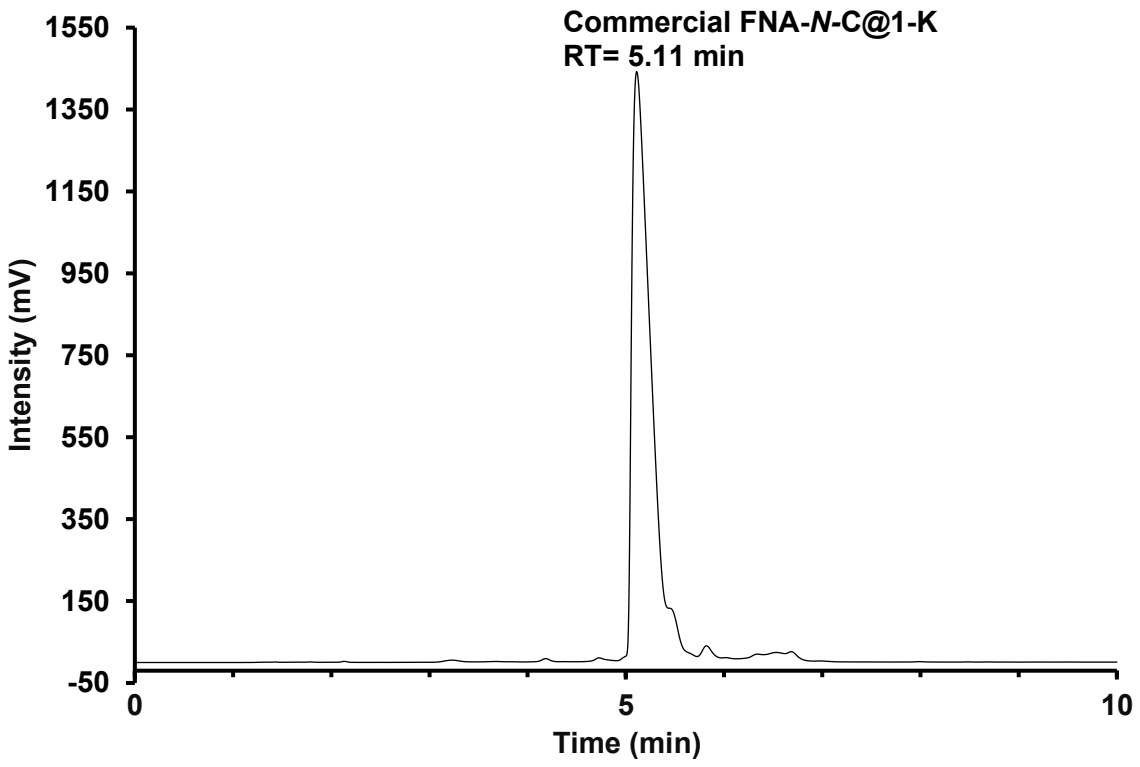

Figure 32. QC of [^{18}F]FNA-*N*-C@1-K alongside the commercial reference compound FNA-*N*-C@1-K

The study was a success overall and now serves as a pilot study to understand the high chemoselectivity of peptides in conjugation with fluorine-18 prosthetic groups. The structure of all the peptides were confirmed by analysing the proton, HSQC, TOCSY, and HMBC of the conjugated products (FNA-*S*-C@3, FNA-*S*-C@4, FNA-*S*-C@5, FNA-*N*-C@1-K). In a case where a study would need the amino-reactive site available for binding with a tumor or for research purposes, the introduction of cysteine can be proposed as a solution, as the study confirms.

6.0 CONCLUSION

In summary, a previous study on the understanding of the mechanism of high chemoselectivity in the radiosynthesis of fluorine-18 chemistry of activated esters of 6-[^{18}F]fluoronicotinic acid as prosthetic groups is non-existent; this might be because of the expected *N*-acylation that has been reported in previous studies. The paper by Dillemuth et al. (2024) changed the trajectory of previous studies and created the avenue to understand the high chemoselectivity mechanism that can occur in fluorine-18 radiolabelling of peptides with free amino and sulfhydryl groups.

The NMR analysis of the four peptides indicated that C@3, C@4, and C@5 were *S*-acylated, whereas C@1-K was *N*-acylated at the cysteine residue. The regioselectivity was demonstrated by the use of peptide C@1-K bearing two free amino groups, and the *N*-acylation took place at the amino group of cysteine instead of lysine. This indicates that the adjacent sulfhydryl group has a function to promote the *N*-acylation. The chemo- and region-selectivity have been further confirmed by LC-MS analyses. In addition to the expected acylation products, some unidentified side products have been observed in the non-radioactive conjugation. For example, in the LC-MS/MS analysis of two peptides, specifically C@1-K and C@3, at several other locations, we found some side products with additional alterations. These were also noted during the purification process of high-performance liquid chromatography. The side products were observed during purification; however, the fractions were too small for NMR analysis. It is also noted that the NMR analysis indicates that FNA-*N*-C@1-K, irrespective of whether in-house or commercial, is not pure. We discovered that the majority the product was *N*-acylated in cysteine, while the impurity is unidentified and requires additional analysis. The chemo- and regio-selective acylation in the non-radioactive conjugation experiments have been verified with radiosynthesis in the cases of C@5 and C@1-K. In each case, the selectivity in radiosynthesis was exclusive, which may be derived from the fact that peptides are in massive excess amounts in relation to the radioactive prosthetic group. In the non-radioactive experiments, the prosthetic group was used in 1.5-fold excess to peptides to enhance the conjugation efficiency of peptides, and this may explain the appearance of multiple side product formation.

The macrocyclic ring formed in the transition state of the conjugation proved to be the most important factor that aids the acyl migration, with a favourable ring completing the acyl migration and an unfavourable ring halting the migration, making the conjugation yield an *S*-acylated product.

In addition, the presence of an adjacent sulfhydryl group seems to have a promoting effect on *N*-acylation of the amino group.

This study can serve as a starting point for future studies in the selective conjugation of biomolecules with free amino and sulfhydryl groups, not only for PET radiopharmaceuticals but also for other applications.

8.0 REFERENCES

1. Trost B. M. (1983). Selectivity: A Key to Synthetic Efficiency. *Science (New York, N.Y.)*, *219*(4582), 245–250. https://doi.org/10.1126/science.219.4582.245
2. Sletten, E. M., & Bertozzi, C. R. (2009). Bioorthogonal chemistry: fishing for selectivity in a sea of functionality. *Angewandte Chemie (International ed. in English)*, *48*(38), 6974–6998. https://doi.org/10.1002/anie.200900942
3. Patterson, D. M., Nazarova, L. A., & Prescher, J. A. (2014). Finding the right (bioorthogonal) chemistry. *ACS Chemical Biology*, *9*(3), 592–605. https://doi.org/10.1021/cb400828a
4. Goswami, A., & Van Lanen, S. G. (2015). Enzymatic strategies and biocatalysts for amide bond formation: tricks of the trade outside of the ribosome. *Molecular bioSystems*, *11*(2), 338–353. https://doi.org/10.1039/c4mb00627e
5. de Figueiredo, R. M., Suppo, J. S., & Campagne, J. M. (2016). Nonclassical Routes for Amide Bond Formation. *Chemical reviews*, *116*(19), 12029–12122. https://doi.org/10.1021/acs.chemrev.6b00237
6. Yoshiya, T., Ito, N., Kimura, T., & Kiso, Y. (2008). Isopeptide method: development of S-acyl isopeptide method for the synthesis of difficult sequence-containing peptides. *Journal of peptide science: an official publication of the European Peptide Society*, *14*(11), 1203–1208. https://doi.org/10.1002/psc.1053
7. Katritzky, A. R., Tala, S. R., Abo-Dya, N. E., Ibrahim, T. S., El-Feky, S. A., Gyanda, K., & Pandya, K. M. (2011). Chemical ligation of S-scylated cysteine peptides to form native peptides via 5-, 11-, and 14-membered cyclic transition states. *The Journal of organic chemistry*, *76*(1), 85–96. https://doi.org/10.1021/jo1015757
8. Katritzky, A. R., Abo-Dya, N. E., Tala, S. R., & Abdel-Samii, Z. K. (2010). The chemical ligation of selectively S-acylated cysteine peptides to form native peptides via 5-, 11- and 14-membered cyclic transition states. *Organic & biomolecular chemistry*, *8*(10), 2316–2319. https://doi.org/10.1039/c003234d
9. Hackenberger, C. P., & Schwarzer, D. (2008). Chemoselective ligation and modification strategies for peptides and proteins. *Angewandte Chemie (International ed. in English)*, *47*(52), 10030–10074. https://doi.org/10.1002/anie.200801313

10. Panda, S. S., El-Nachef, C., Bajaj, K., Al-Youbi, A. O., Oliferenko, A., & Katritzky, A. R. (2012). Study of chemical ligation via 17-, 18- and 19-membered cyclic transition states. *Chemical biology & drug design*, *80*(6), 821–827. https://doi.org/10.1111/cbdd.12053
11. Bol'shakov, O., Kovacs, J., Chahar, M., Ha, K., Khelashvili, L., & Katritzky, A. R. (2012). S- to N-Acyl transfer in S-acylcysteine isopeptides via 9-, 10-, 12-, and 13-membered cyclic transition states. *Journal of peptide science: an official publication of the European Peptide Society*, *18*(11), 704–709. https://doi.org/10.1002/psc.2438
12. Ha, K., Chahar, M., Monbaliu, J. C., Todadze, E., Hansen, F. K., Oliferenko, A. A., Ocampo, C. E., Leino, D., Lillicotch, A., Stevens, C. V., & Katritzky, A. R. (2012). Long-range intramolecular S → N acyl migration: a study of the formation of native peptide analogues via 13-, 15-, and 16-membered cyclic transition states. *The Journal of organic chemistry*, *77*(6), 2637–2648. https://doi.org/10.1021/jo2023125
13. Vaquero, J. J., & Kinahan, P. (2015). Positron Emission Tomography: Current Challenges and Opportunities for Technological Advances in Clinical and Preclinical Imaging Systems. *Annual review of biomedical engineering*, *17*, 385–414. https://doi.org/10.1146/annurev-bioeng-071114-040723
14. Turkington T. G. (2001). Introduction to PET instrumentation. *Journal of nuclear medicine technology*, *29*(1), 4–11.
15. Shukla, A. K., & Kumar, U. (2006). Positron emission tomography: An overview. *Journal of medical physics*, *31*(1), 13–21. https://doi.org/10.4103/0971-6203.25665
16. Rahmim, A., & Zaidi, H. (2008). PET versus SPECT: strengths, limitations and challenges. *Nuclear medicine communications*, *29*(3), 193–207. https://doi.org/10.1097/MNM.0b013e3282f3a515
17. Bergström, M., Grahnén, A., & Långström, B. (2003). Positron emission tomography microdosing: a new concept with application in tracer and early clinical drug development. *European journal of clinical pharmacology*, *59*(5-6), 357–366. https://doi.org/10.1007/s00228-003-0643-x
18. Aboagye, E. O., & Price, P. M. (2003). Use of positron emission tomography in anticancer drug development. *Investigational new drugs*, *21*(2), 169–181. https://doi.org/10.1023/a:1023521412787

19. Sergeev, M. E., Lazari, M., Morgia, F., Collins, J., Javed, M. R., Sergeeva, O., Jones, J., Phelps, M. E., Lee, J. T., Keng, P. Y., & van Dam, R. M. (2018). Performing radiosynthesis in microvolumes to maximize molar activity of tracers for positron emission tomography. *Communications chemistry*, *1*(1), 10. https://doi.org/10.1038/s42004-018-0009-z
20. Bolus, N. E., George, R., Washington, J., & Newcomer, B. R. (2009). PET/MRI: the blended-modality choice of the future?. *Journal of nuclear medicine technology*, *37*(2), 63–73. https://doi.org/10.2967/jnmt.108.060848
21. Lewellen T. K. (2008). Recent developments in PET detector technology. *Physics in medicine and biology*, *53*(17), R287–R317. https://doi.org/10.1088/0031-9155/53/17/R01
22. Conti, M., & Eriksson, L. (2016). Physics of pure and non-pure positron emitters for PET: a review and a discussion. *EJNMMI physics*, *3*(1), 8. https://doi.org/10.1186/s40658-016-0144-5
23. Nayak, T. K., & Brechbiel, M. W. (2009). Radioimmunoimaging with longer-lived positron-emitting radionuclides: potentials and challenges. *Bioconjugate chemistry*, *20*(5), 825–841. https://doi.org/10.1021/bc800299f
24. Jacobson, O., Kiesewetter, D. O., & Chen, X. (2015). Fluorine-18 radiochemistry, labeling strategies and synthetic routes. *Bioconjugate chemistry*, *26*(1), 1–18. https://doi.org/10.1021/bc500475e
25. Deng, X., Rong, J., Wang, L., Vasdev, N., Zhang, L., Josephson, L., & Liang, S. H. (2019). Chemistry for Positron Emission Tomography: Recent Advances in ^{11}C-, ^{18}F-, ^{13}N-, and ^{15}O-Labeling Reactions. *Angewandte Chemie (International ed. in English)*, *58*(9), 2580–2605. https://doi.org/10.1002/anie.201805501
26. Gómez-Vallejo, V., Rejc, L., López-Gallego, F., Llop, J. (2019). The Radiopharmaceutical Chemistry of Nitrogen-13 and Oxygen-15. In Lewis, J. S., Windhorst, A. D., Zeglis, B. M., (Eds), *Radiopharmaceutical Chemistry*; Springer International Publishing (pp 237–254). https://doi.org/10.1007/978-3-319-98947-1_13.
27. Chomet, M., van Dongen, G. A. M. S., & Vugts, D. J. (2021). State of the Art in Radiolabeling of Antibodies with Common and Uncommon Radiometals for Preclinical and Clinical Immuno-PET. *Bioconjugate chemistry*, *32*(7), 1315–1330. https://doi.org/10.1021/acs.bioconjchem.1c00136

28. Fu, R., Carroll, L., Yahioglu, G., Aboagye, E. O., & Miller, P. W. (2018). Antibody Fragment and Affibody ImmunoPET Imaging Agents: Radiolabelling Strategies and Applications. *ChemMedChem*, *13*(23),2466–2478. https://doi.org/10.1002/cmdc.201800624
29. Price, E. W., & Orvig, C. (2014). Matching chelators to radiometals for radiopharmaceuticals. *Chemical Society reviews*, *43*(1), 260–290. https://doi.org/10.1039/c3cs60304k
30. Ross, T. L., Wester, H. J. ^{18}F: Labeling Chemistry and Labeled Compounds (2011). In Vértes, A., Nagy, S., Klencsár, Z., Lovas, R. G., Rösch, F., (Eds), *Handbook of Nuclear Chemistry*, *Springer* US: Boston, MA (pp 2021–2071). https://doi.org/10.1007/978-1-4419-0720-2_42.
31. Miller, P. W., Kato, K., Långström, B. Carbon-11, Nitrogen-13, and Oxygen-15 Chemistry (2014). In *The Chemistry of Molecular Imaging*, John Wiley & Sons, Ltd, (pp 79–103). https://doi.org/10.1002/9781118854754.ch4.
32. Blasi, F., Oliveira, B. L., Rietz, T. A., Rotile, N. J., Day, H., Looby, R. J., Ay, I., & Caravan, P. (2014). Effect of Chelate Type and Radioisotope on the Imaging Efficacy of 4 Fibrin-Specific PET Probes. *Journal of nuclear medicine : official publication, Society of Nuclear Medicine*, *55*(7), 1157–1163. https://doi.org/10.2967/jnumed.113.136275
33. Lin, M., Welch, M. J., Lapi, *S. E. Effects of Chelator Modifications on ^{68}Ga-Labeled [Tyr3]Octreotide Conjugates*. Mol Imaging Biol 2013, 15 (5), 606–613. https://doi.org/10.1007/s11307-013-0627-x
34. Sanchez-Crespo A. (2013). Comparison of Gallium-68 and Fluorine-18 imaging characteristics in positron emission tomography. *Applied radiation and isotopes: including data, instrumentation and methods for use in agriculture, industry and medicine*, *76*, 55–62. https://doi.org/10.1016/j.apradiso.2012.06.034
35. Coenen, H. H., Gee, A. D., Adam, M., Antoni, G., Cutler, C. S., Fujibayashi, Y., Jeong, J. M., Mach, R. H., Mindt, T. L., Pike, V. W., & Windhorst, A. D. (2017). Consensus nomenclature rules for radiopharmaceutical chemistry - Setting the record straight. *Nuclear medicine and biology*, *55*, v–xi. https://doi.org/10.1016/j.nucmedbio.2017.09.004

36. Sergeev, M. E., Lazari, M., Morgia, F., Collins, J., Javed, M. R., Sergeeva, O., Jones, J., Phelps, M. E., Lee, J. T., Keng, P. Y., & van Dam, R. M. (2018). Performing radiosynthesis in microvolumes to maximize molar activity of tracers for positron emission tomography. *Communications chemistry*, *1*(1), 10. https://doi.org/10.1038/s42004-018-0009-z
37. Lapi, S. E., & Welch, M. J. (2012). A historical perspective on the specific activity of radiopharmaceuticals: what have we learned in the 35 years of the ISRC?. *Nuclear medicine and biology*, *39*(5), 601–608. https://doi.org/10.1016/j.nucmedbio.2011.11.005
38. Gómez-Vallejo, V., Gaja, V.; Koziorowski, J., Llop, J (2012*). Specific Activity of 11C-Labelled Radiotracers: A Big Challenge for PET Chemists*. https://doi.org/10.5772/31491
39. Collet, C., Maskali, F., Clément, A., Chrétien, F., Poussier, S., Karcher, G., Marie, P. Y., Chapleur, Y., & Lamandé-Langle, S. (2016). Development of 6-[(18) F]fluoro-carbohydrate-based prosthetic groups and their conjugation to peptides via click chemistry. *Journal of labelled compounds & radiopharmaceuticals*, *59*(2), 54–62. https://doi.org/10.1002/jlcr.3362
40. Fani, M., & Maecke, H. R. (2012). Radiopharmaceutical development of radiolabelled peptides. *European journal of nuclear medicine and molecular imaging*, *39 Suppl 1*, S11–S30. https://doi.org/10.1007/s00259-011-2001-z
41. Okarvi S. M. (2004). Peptide-based radiopharmaceuticals: future tools for diagnostic imaging of cancers and other diseases. *Medicinal research reviews*, *24*(3), 357–397. https://doi.org/10.1002/med.20002
42. Jacobson, O., Kiesewetter, D. O., & Chen, X. (2015). Fluorine-18 radiochemistry, labeling strategies and synthetic routes. *Bioconjugate chemistry*, *26*(1), 1–18. https://doi.org/10.1021/bc500475e
43. Jacobson, O., & Chen, X. (2010). PET designated flouride-18 production and chemistry. *Current topics in medicinal chemistry*, *10*(11), 1048–1059. https://doi.org/10.2174/156802610791384298
44. Zhang, M., Li, S., Zhang, H., & Xu, H. (2020). Research progress of ^{18}F labeled small molecule positron emission tomography (PET) imaging agents. *European journal of medicinal chemistry*, *205*, 112629. https://doi.org/10.1016/j.ejmech.2020.112629

45. Bars, D. (2006). *Fluorine-18 and Medical Imaging: Radiopharmaceuticals for Positron Emission Tomography. Journal of Fluorine Chemistry*. https://doi.org/10.1016/j.jfluchem.2006.09.015
46. Schirrmacher, R., Wängler, B., Bailey, J., Bernard-Gauthier, V., Schirrmacher, E., & Wängler, C. (2017). Small Prosthetic Groups in ^{18}F-Radiochemistry: Useful Auxiliaries for the Design of ^{18}F-PET Tracers. *Seminars in nuclear medicine*, *47*(5), 474–492. https://doi.org/10.1053/j.semnuclmed.2017.07.001
47. Jeppesen, T. E., Kristensen, J. B., Behrens, C., Madsen, J., & Kjaer, A. (2021). Fluorine-18 labeled aldehydes as prosthetic groups for oxime coupling with a FVIIa protein. *Journal of labelled compounds & radiopharmaceuticals*, *64*(5), 198–208. https://doi.org/10.1002/jlcr.3900
48. Basuli, F., Zhang, X., Woodroofe, C. C., Jagoda, E. M., Choyke, P. L., & Swenson, R. E. (2017). Fast indirect fluorine-18 labeling of protein/peptide using the useful 6-fluoronicotinic acid-2,3,5,6-tetrafluorophenyl prosthetic group: A method comparable to direct fluorination. *Journal of labelled compounds & radiopharmaceuticals*, *60*(3), 168–175. https://doi.org/10.1002/jlcr.3487
49. Zhou, Z., McDougald, D., Devoogdt, N., Zalutsky, M. R., & Vaidyanathan, G. (2019). Labeling Single Domain Antibody Fragments with Fluorine-18 Using 2,3,5,6-Tetrafluorophenyl 6-[^{18}F]Fluoronicotinate Resulting in High Tumor-to-Kidney Ratios. *Molecular pharmaceutics*, *16*(1), 214–226. https://doi.org/10.1021/acs.molpharmaceut.8b00951
50. Syvänen, S., Fang, X. T., Faresjö, R., Rokka, J., Lannfelt, L., Olberg, D. E., Eriksson, J., & Sehlin, D. (2020). Fluorine-18-Labeled Antibody Ligands for PET Imaging of Amyloid-β in Brain. *ACS chemical neuroscience*, *11*(24), 4460–4468. https://doi.org/10.1021/acschemneuro.0c00652
51. Piron, S., Verhoeven, J., Vanhove, C., & De Vos, F. (2022). Recent advancements in ^{18}F-labeled PSMA targeting PET radiopharmaceuticals. *Nuclear medicine and biology*, *106-107*, 29–51. https://doi.org/10.1016/j.nucmedbio.2021.12.005
52. Simo, C., Salvador, C., Andreozzi, P., Gomez-Vallejo, V., Romero, G., Dupin, D., Llop, J., & Moya, S. E. (2023). Positron Emission Tomography Studies of the Biodistribution, Translocation, and Fate of Poly Allyl Amine-Based Carriers for Sirna Delivery by

Systemic and Intratumoral Administration. *Small (Weinheim an der Bergstrasse, Germany)*, *19*(48), e2304326. https://doi.org/10.1002/smll.202304326

53. Dillemuth, P., Karskela, T., Ayo, A., Ponkamo, J., Kunnas, J., Rajander, J., Tynninen, O., Roivainen, A., Laakkonen, P., Airaksinen, A. J., & Li, X. G. (2024). Radiosynthesis, structural identification and in vitro tissue binding study of [^{18}F]FNA-S-ACooP, a novel radiopeptide for targeted PET imaging of fatty acid binding protein 3. *EJNMMI radiopharmacy and chemistry*, *9*(1), 16. https://doi.org/10.1186/s41181-024-00245-3
54. Dillemuth, P, Auchynnikava, T, Ayo, A, Kärnä, S, Miner, M, Liljenbäck, H, Lopéz-Picón, F, Roivainen, A, Laakkonen,, P, Airaksinen, A, Li XG (2022). *Radiosynthesis and biological evaluation of [^{18}F]CooP: a brain-homing peptide for imaging glioblastomas using positron emission tomography,* Nuclear Medicine and Biology, 108-109, S18-S19. https://doi.org/10.1016/S0969-8051(22)00082-8
55. Gomes, A. A., Nario, A. P., Lapolli, A. L., Samad, R. E., Bernardes, E. S., & de Rossi, W. (2025). High-efficiency [^{18}F]fluoride pre-concentration using a laser-micromachined anion-exchange micro-cartridge. *EJNMMI radiopharmacy and chemistry*, *10*(1), 11. https://doi.org/10.1186/s41181-025-00334-x
56. Ayo, A., Figueras, E., Schachtsiek, T., Budak, M., Sewald, N., & Laakkonen, P. (2020). Tumor-Targeting Peptides: The Functional Screen of Glioblastoma Homing Peptides to the Target Protein FABP3 (MDGI). *Cancers*, *12*(7), 1836. https://doi.org/10.3390/cancers12071836
57. Hyvönen, M., Enbäck, J., Huhtala, T., Lammi, J., Sihto, H., Weisell, J., Joensuu, H., Rosenthal-Aizman, K., El-Andaloussi, S., Langel, U., Närvänen, A., Bergers, G., & Laakkonen, P. (2014). Novel target for peptide-based imaging and treatment of brain tumors. *Molecular cancer therapeutics*, *13*(4), 996–1007. https://doi.org/10.1158/1535-7163.MCT-13-0684
58. How Does High Performance Liquid Chromatography (HPLC) Work? (2025, May 4). https://www.waters.com/nextgen/fi/en/education/primers/beginner-s-guide-to-liquid-chromatography/how-does-high-performance-liquid-chromatography-work.html?srsltid=AfmBOoroDMHLreU5ck4STx8EQl9XbTtb0tnJmHR_WY1Q5XsiINfSbQpi

59. What is HPLC (High Performance Liquid Chromatography)? (2025, May 4). https://www.waters.com/nextgen/us/en/education/primers/beginner-s-guide-to-liquid-chromatography.html
60. Purification System and Cartridge Selector. (2025, May 4). https://www.biotage.com/purification-system-and-cartridge-selector
61. Mlynárik V. (2017). Introduction to nuclear magnetic resonance. *Analytical biochemistry*, *529*, 4–9. https://doi.org/10.1016/j.ab.2016.05.006
62. Niessen, Wilfried. (2005). LIQUID CHROMATOGRAPHY | Liquid Chromatography–Mass Spectrometry. https://doi.org/10.1016/B0-12-369397-7/00329-0
63. Haskali, M. B., Farnsworth, A. L., Roselt, P. D., & Hutton, C. A. (2020). 4-Nitrophenyl activated esters are superior synthons for indirect radiofluorination of biomolecules. *RSC medicinal chemistry*, *11*(8), 919–922. https://doi.org/10.1039/d0md00140f
64. Jacobson, O., Kiesewetter, D. O., & Chen, X. (2015). Fluorine-18 radiochemistry, labeling strategies and synthetic routes. *Bioconjugate chemistry*, *26*(1), 1–18. https://doi.org/10.1021/bc500475e
65. Cole, E. L., Stewart, M. N., Littich, R., Hoareau, R., & Scott, P. J. (2014). Radiosyntheses using fluorine-18: the art and science of late stage fluorination. *Current topics in medicinal chemistry*, *14*(7), 875–900. https://doi.org/10.2174/1568026614666140202205035
66. Lau, J., Rousseau, E., Kwon, D., Lin, K. S., Bénard, F., & Chen, X. (2020). Insight into the Development of PET Radiopharmaceuticals for Oncology. *Cancers*, *12*(5), 1312. https://doi.org/10.3390/cancers12051312

Appendices

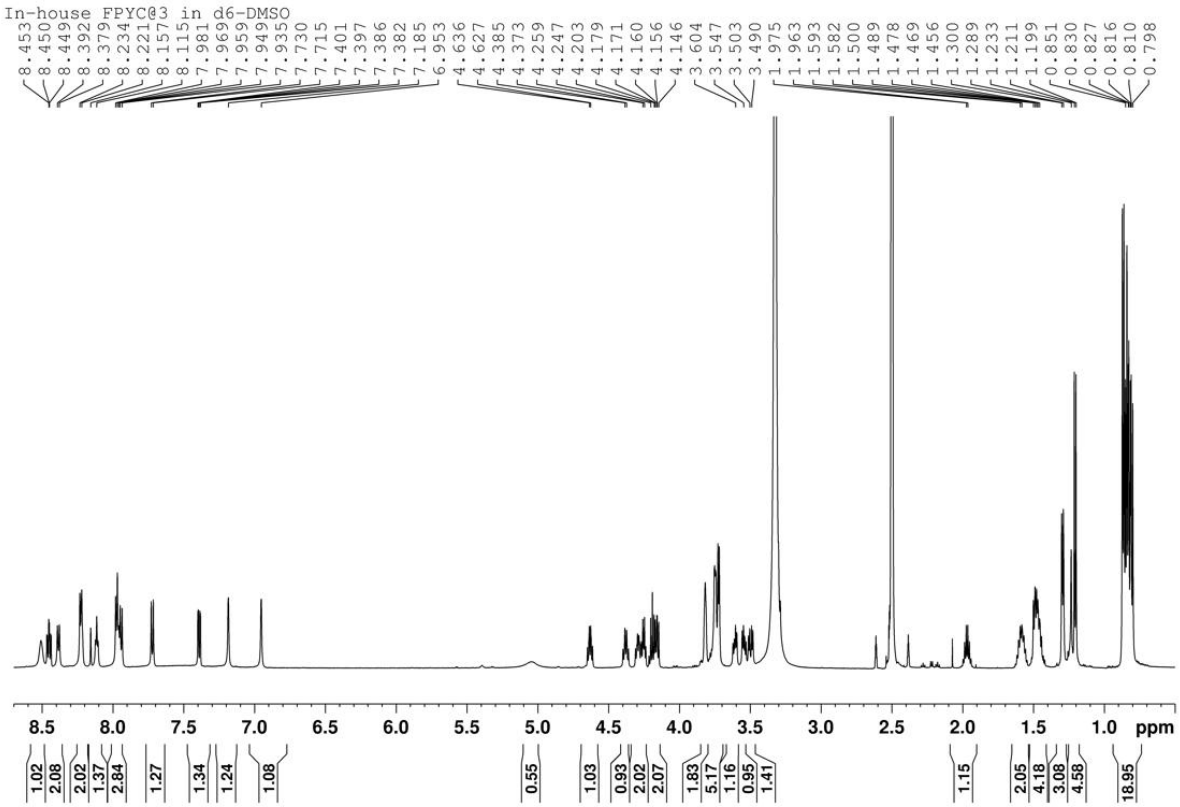

Figure A1. ^{1}H NMR spectrum of in-house made [^{19}F]FNA-*S*-C@3

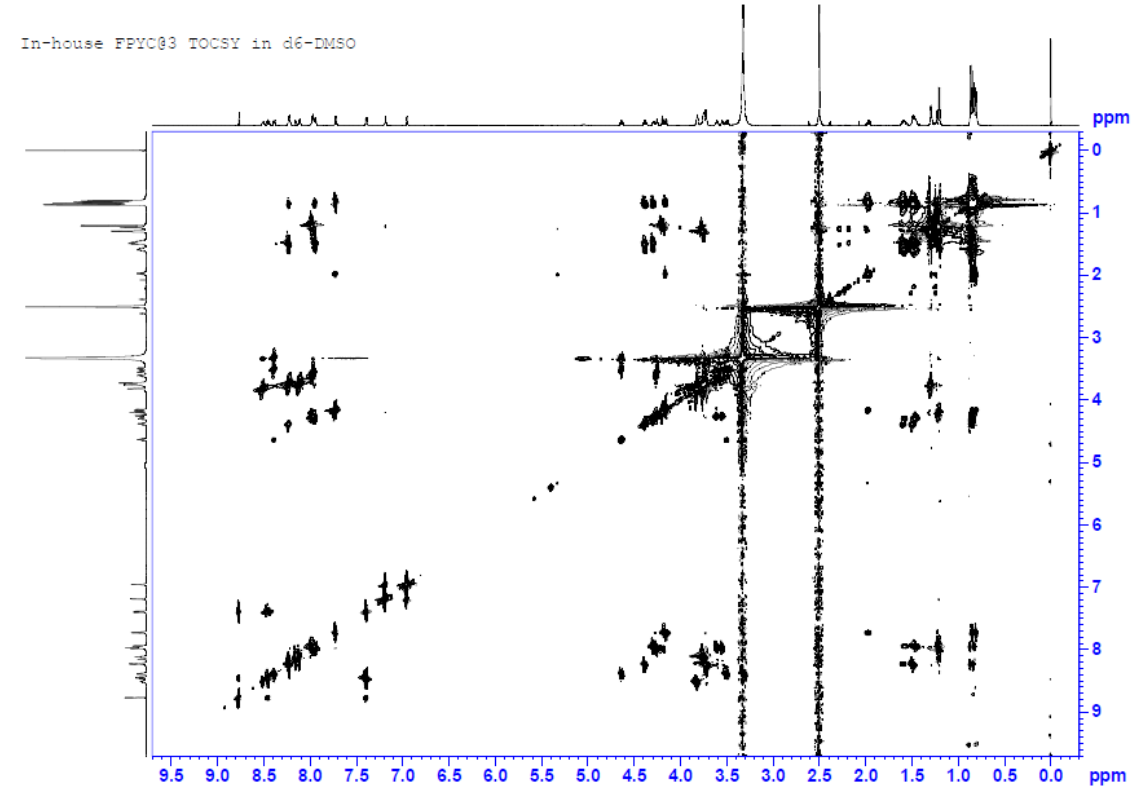

Figure A2. TOCSY spectrum of in-house made [^{19}F]FNA-*S*-C@3

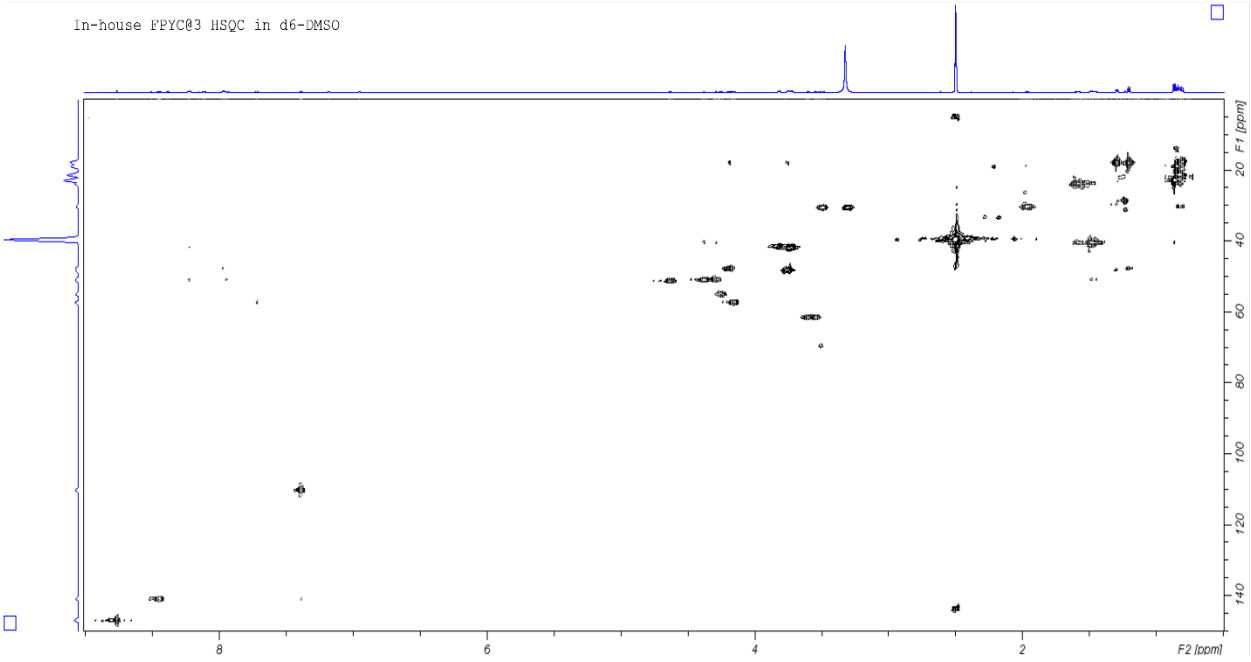

Figure A3. HSQC spectrum of in-house made [^{19}F]FNA-*S*-C@3

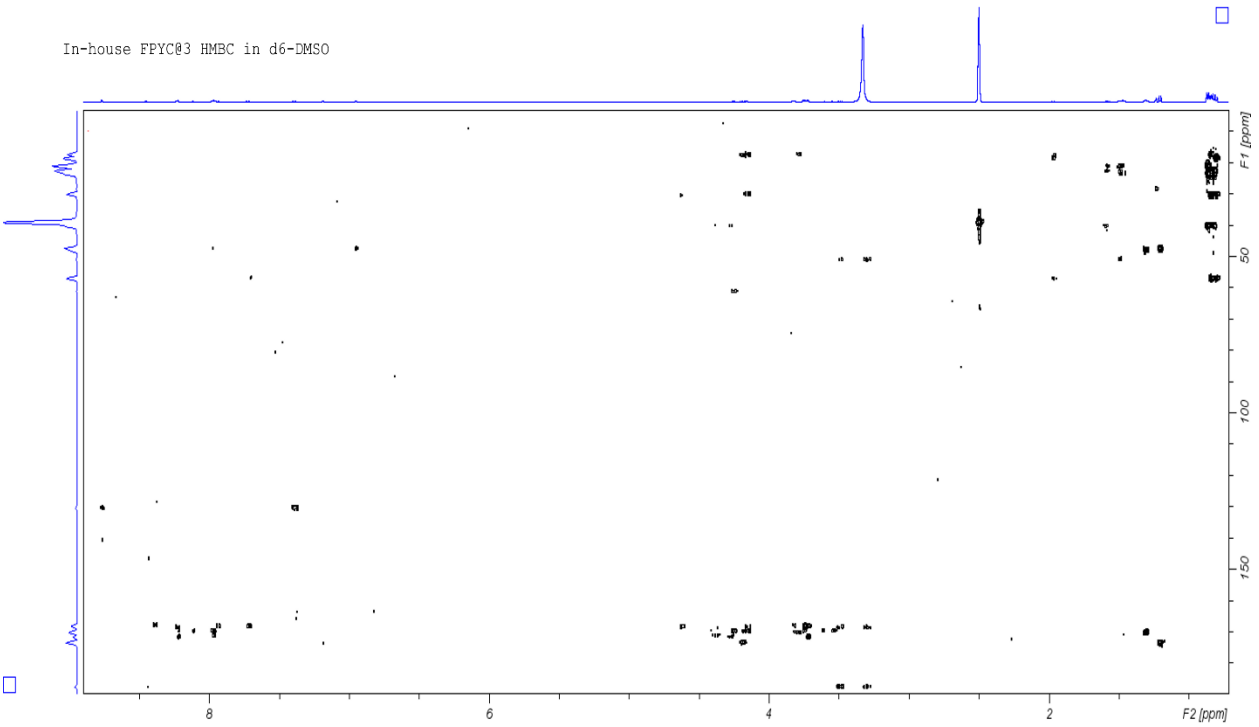

Figure A4. HMBC spectrum of in-house made [^{19}F]FNA-*S*-C@3

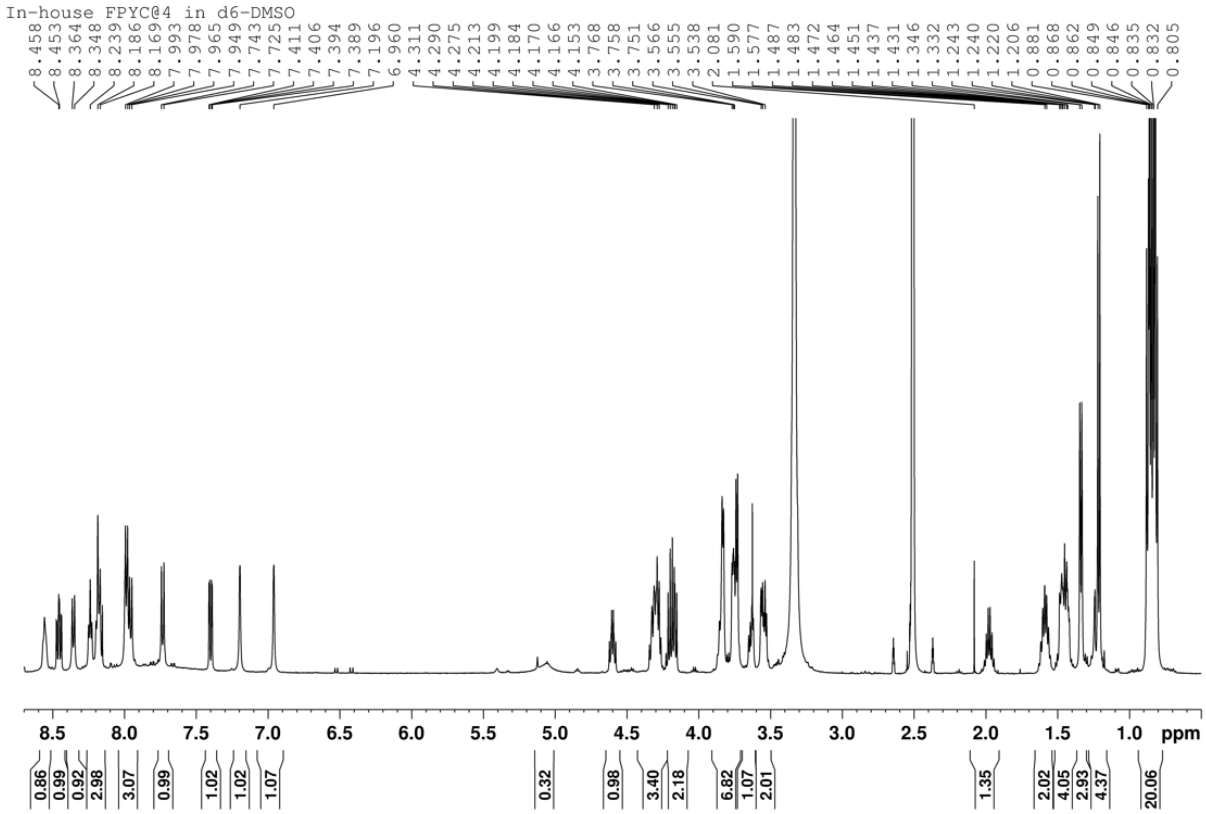

Figure A5. ^{1}H NMR spectrum of in-house made [^{19}F]FNA-*S*-C@4

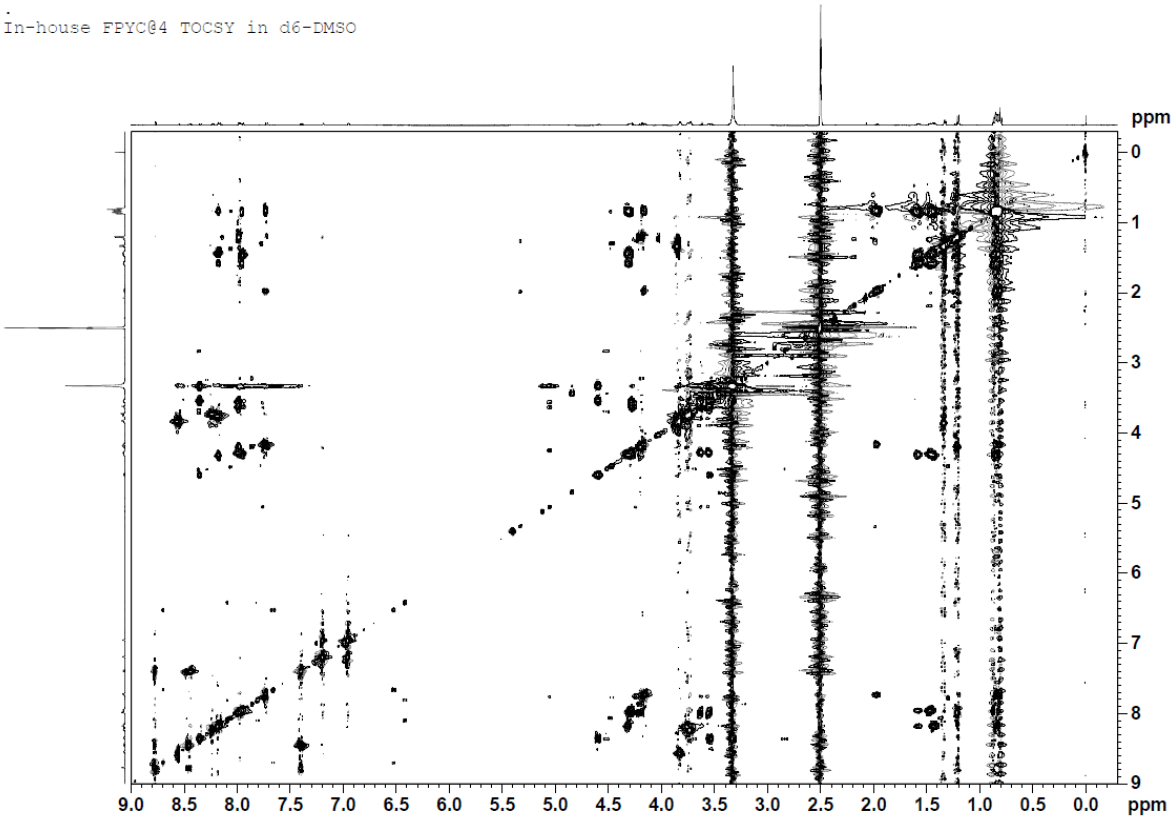

Figure A6. TOCSY spectrum of in-house made [^{19}F]FNA-*S*-C@4

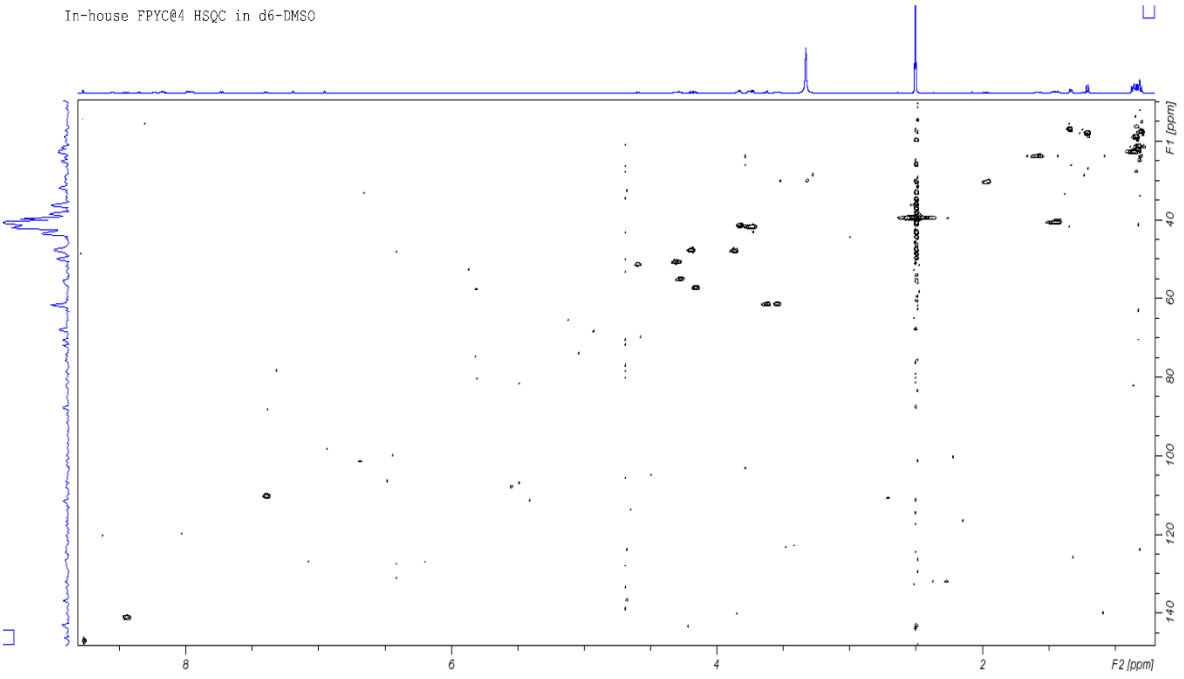

Figure A7. HSQC spectrum of in-house made [^{19}F]FNA-*S*-C@4

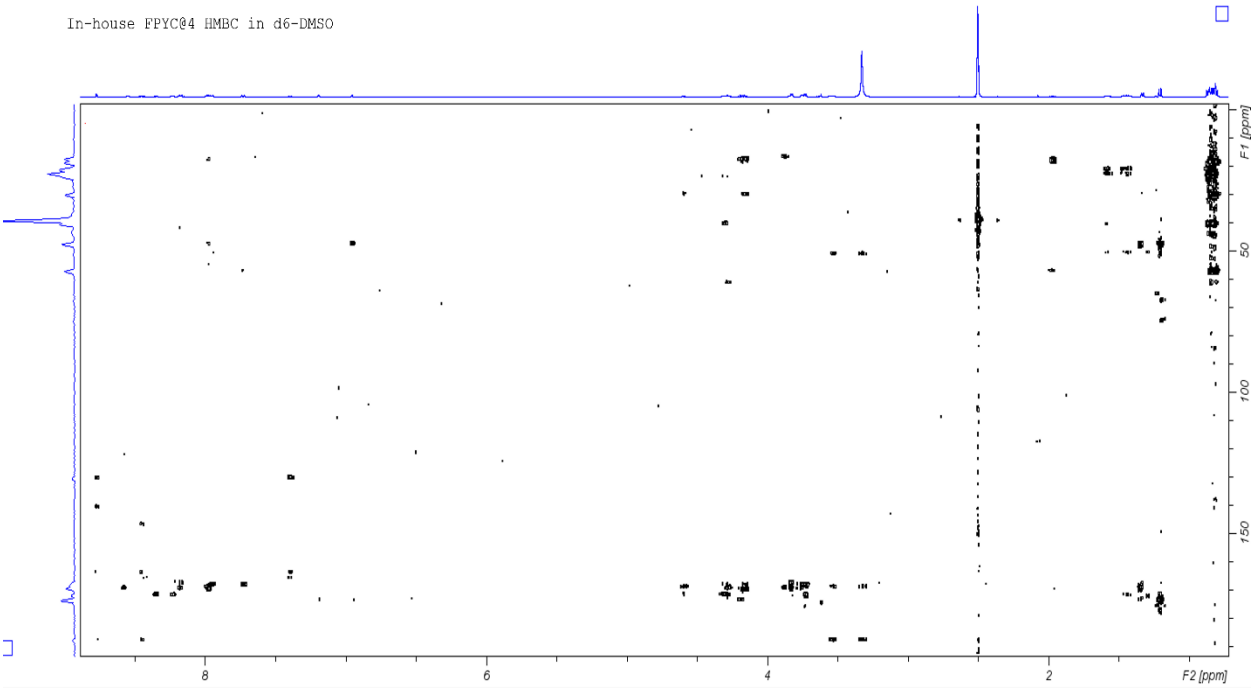

Figure A8. HMBC spectrum of in-house made [^{19}F]FNA-*S*-C@4

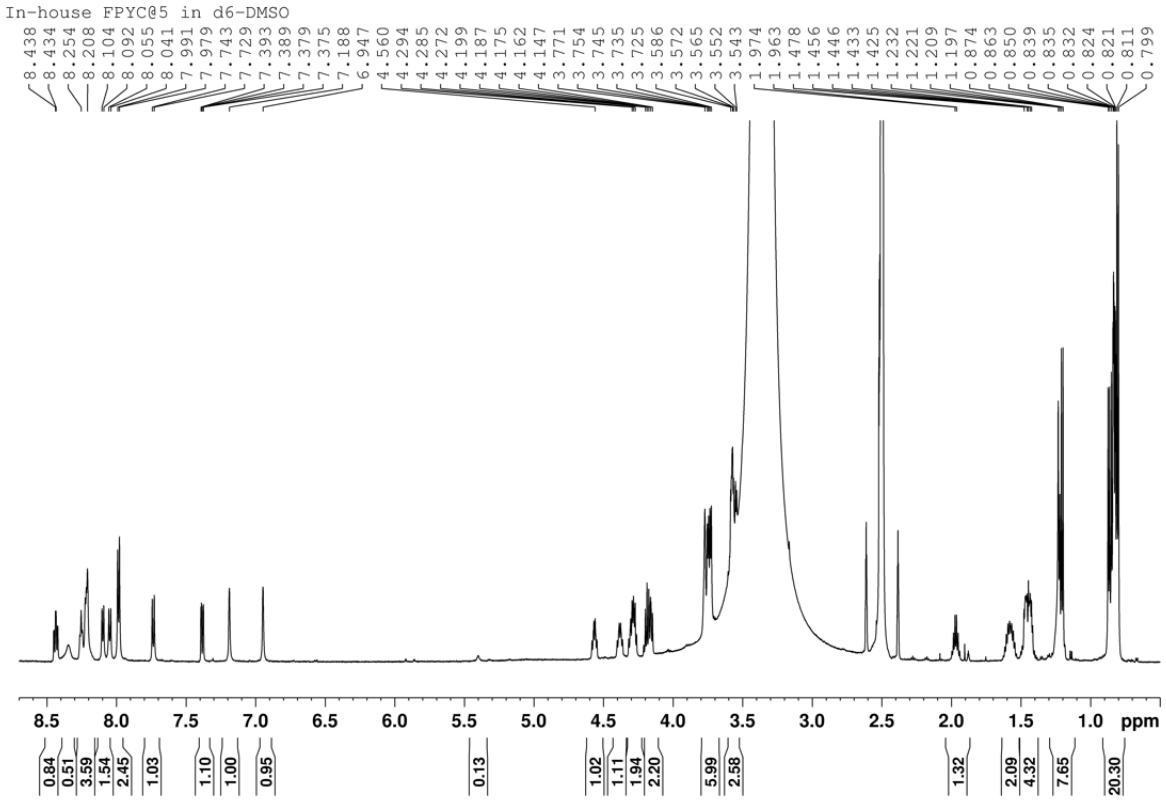

Figure A9. ^{1}H NMR spectrum of in-house made [^{19}F]FNA-*S*-C@5

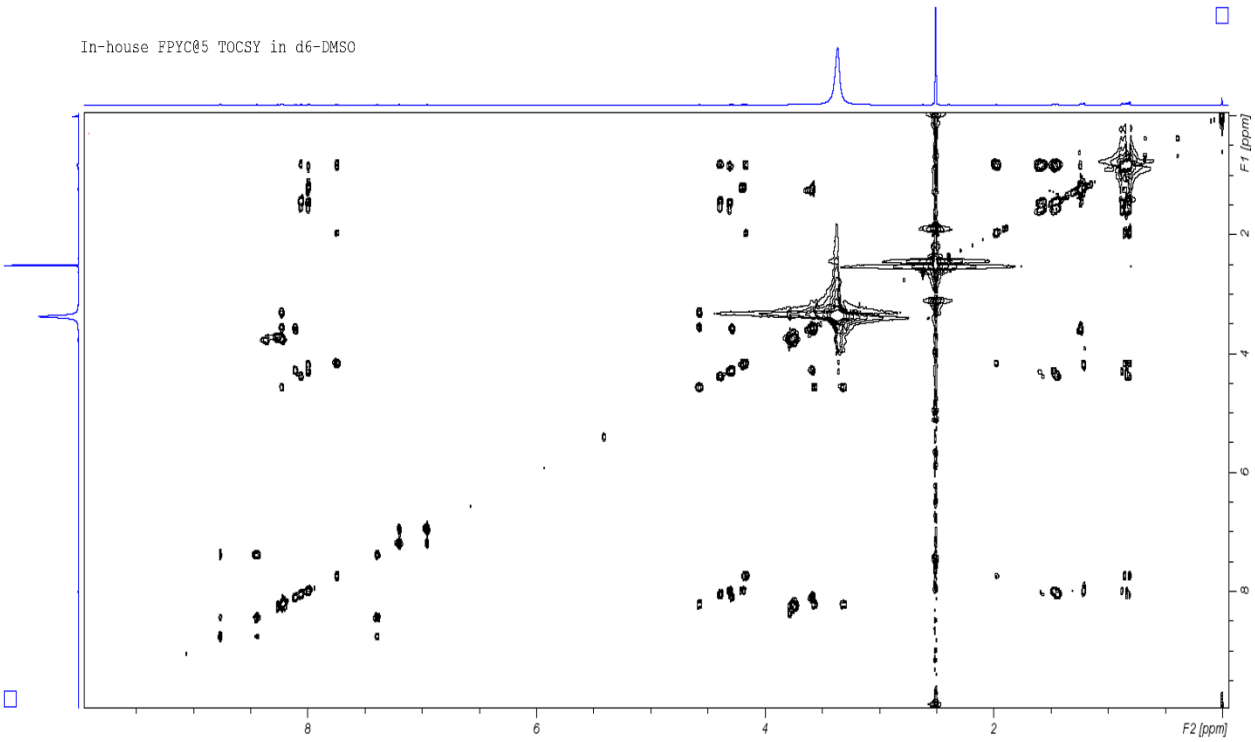

Figure A10. TOCSY spectrum of in-house made [^{19}F]FNA-*S*-C@5

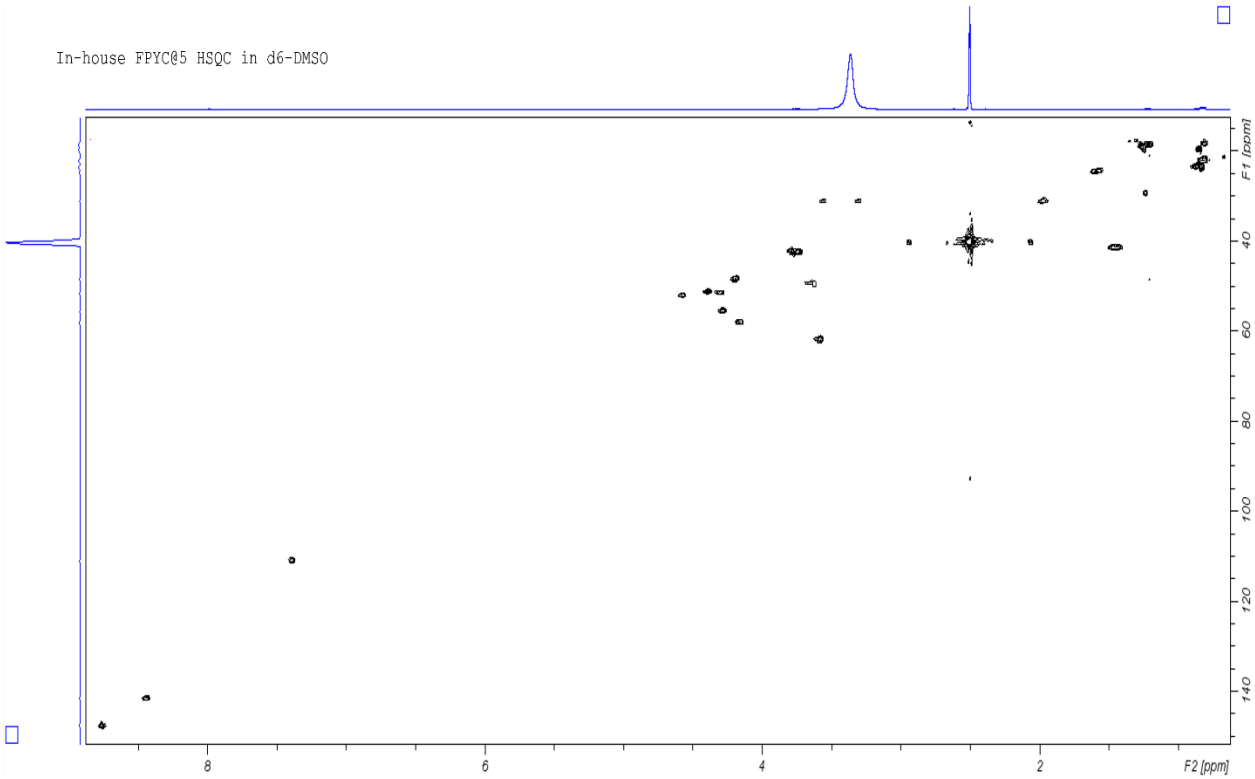

Figure A11. HSQC spectrum of in-house made [^{19}F]FNA-*S*-C@5

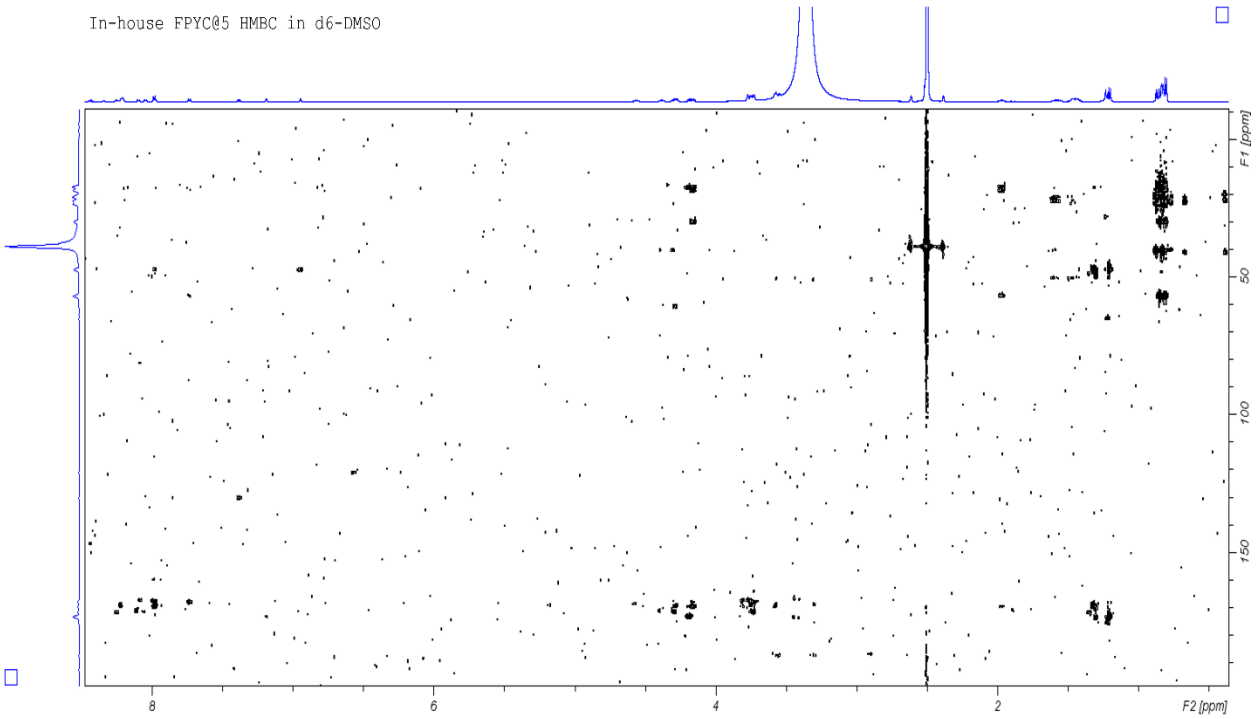

Figure A12. HMBC spectrum of in-house made [^{19}F]FNA-*S*-C@5

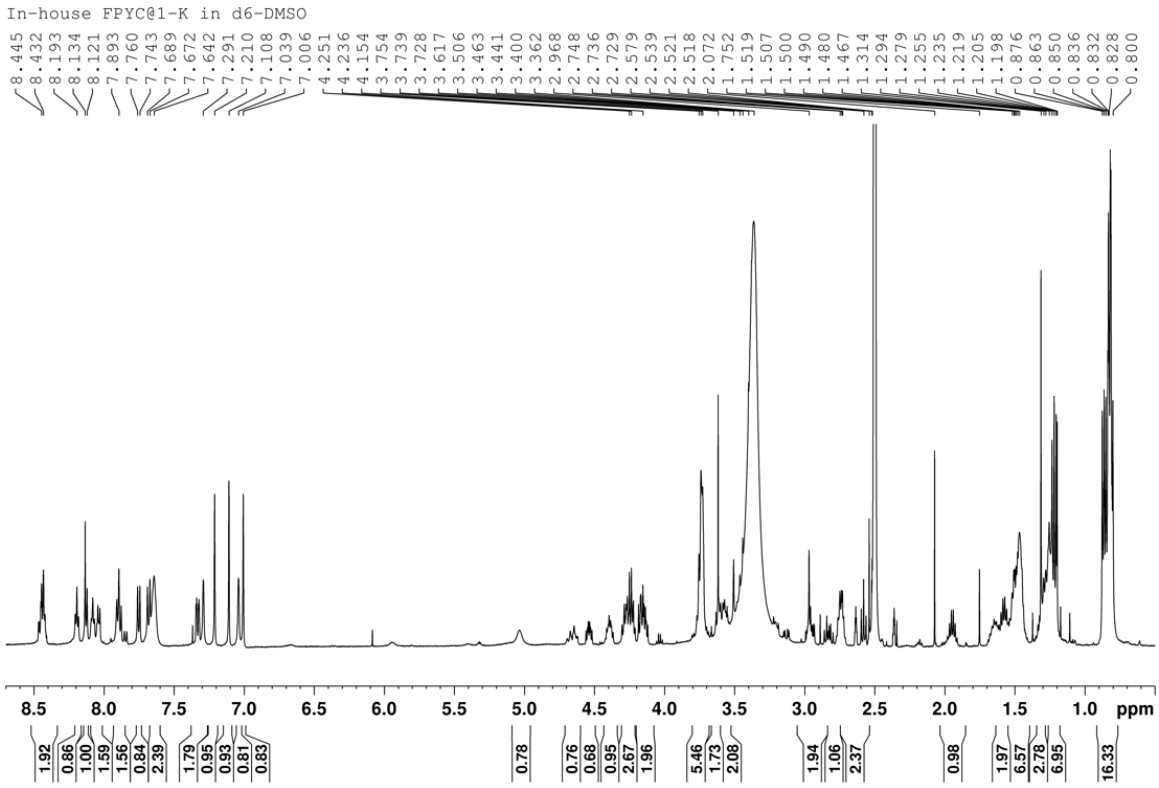

Figure A13. ^{1}H NMR spectrum of in-house made [^{19}F]FNA-*S*-C@1-K

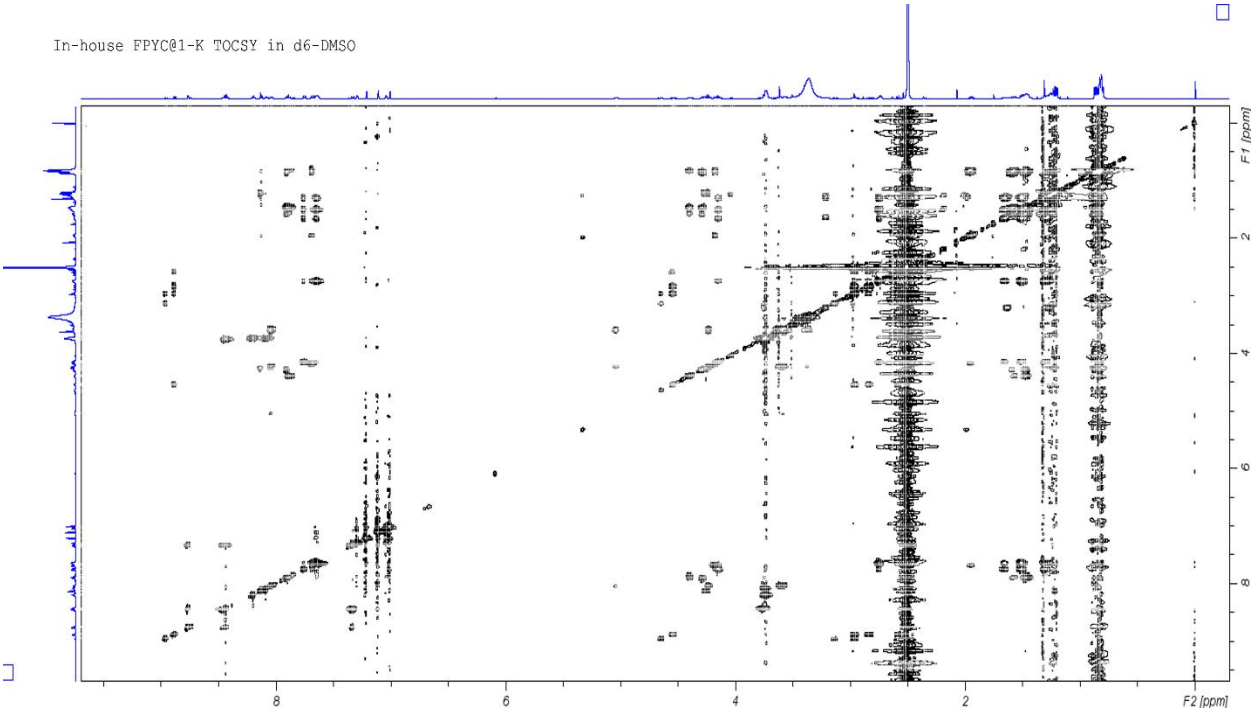

Figure A14. TOCSY spectrum of in-house made [^{19}F]FNA-*S*-C@1-K

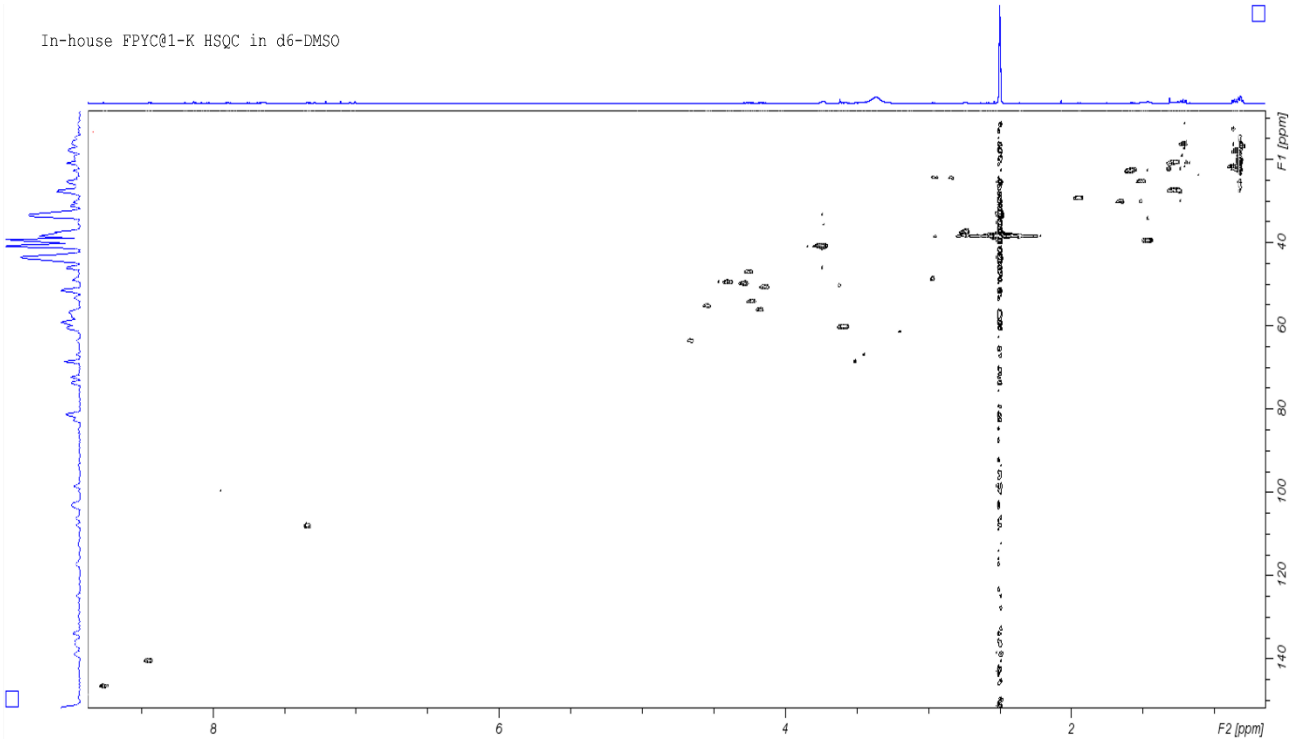

Figure A15. HSQC spectrum of in-house made [^{19}F]FNA-*S*-C@1-K

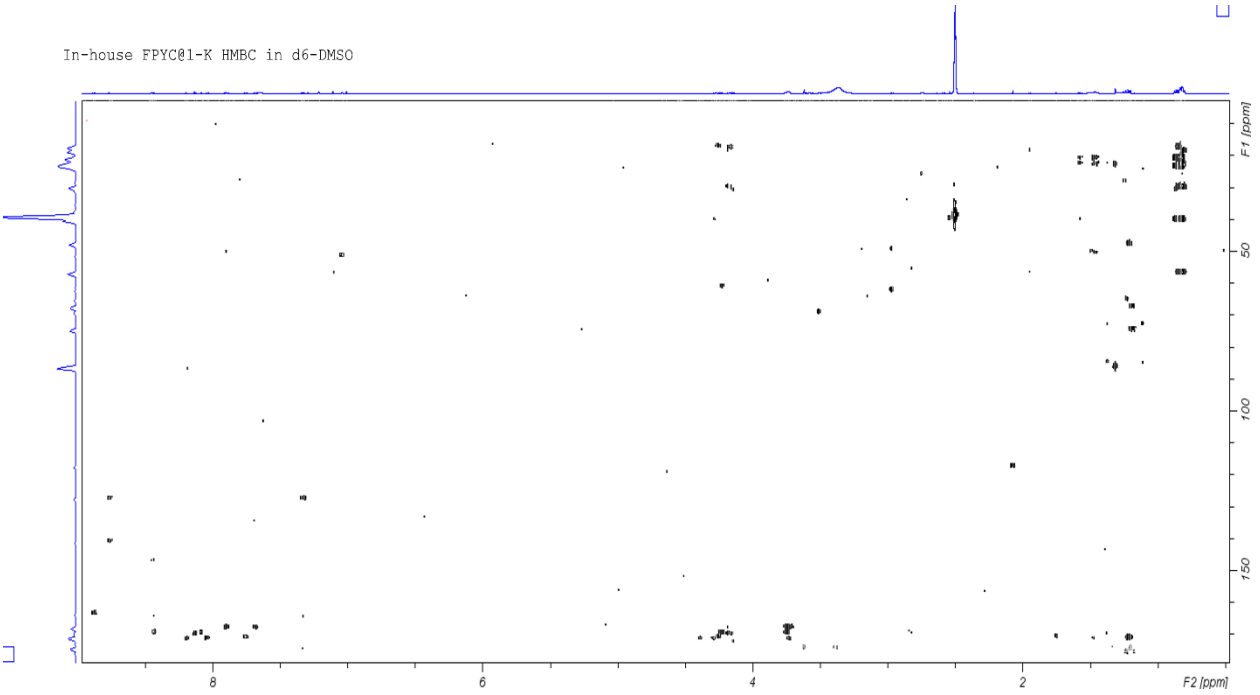

Figure A16. HMBC spectrum of in-house made [^{19}F]FNA-*S*-C@1-K

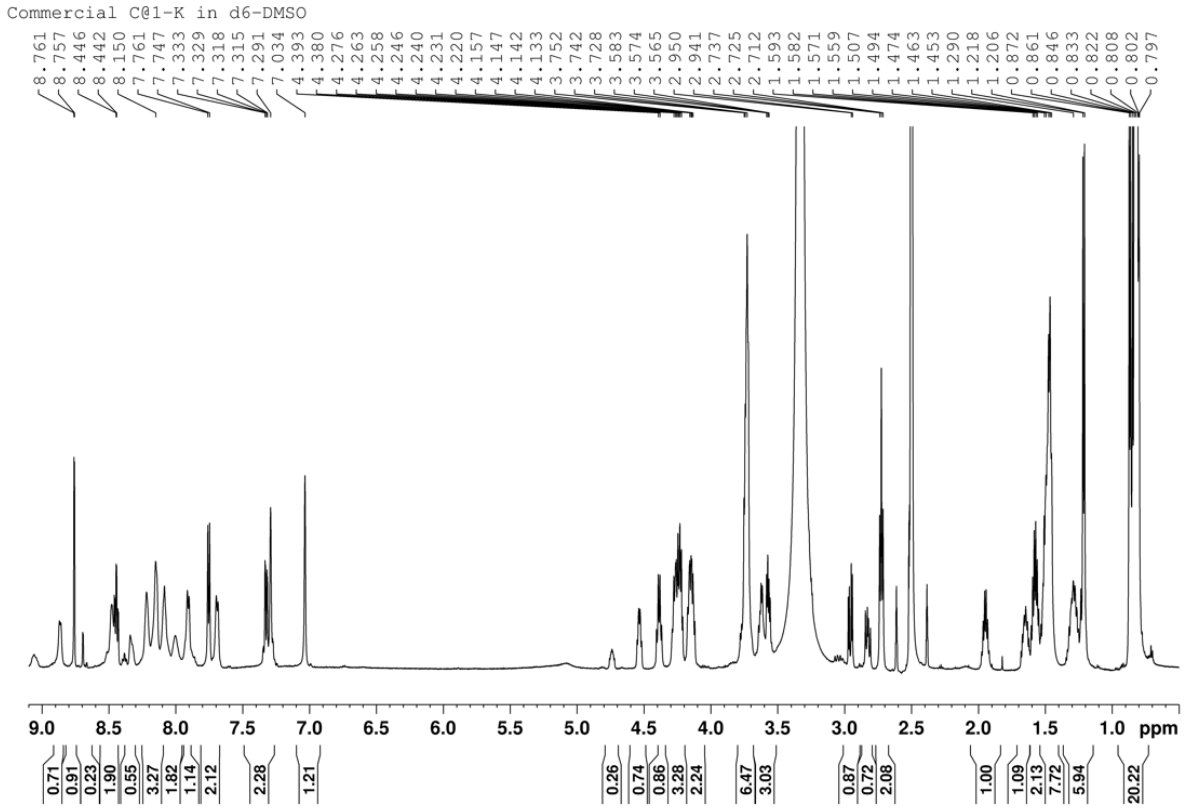

Figure A17. ^{1}H NMR spectrum of commercial [^{19}F]FNA-*S*-C@1-K

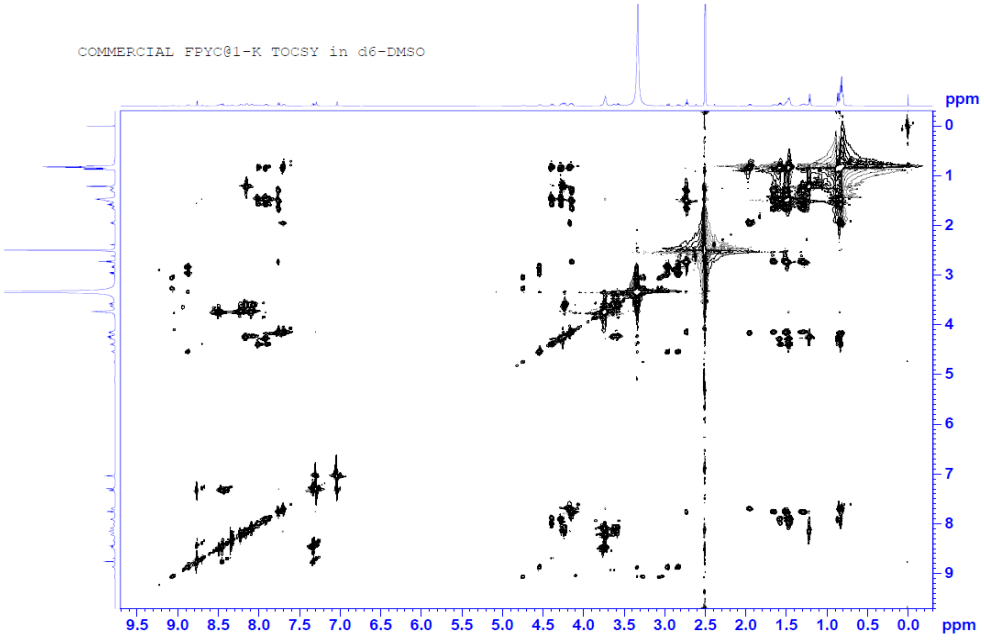

Figure A18. TOCSY spectrum of commercial [^{19}F]FNA-*S*-C@1-K